Today's outline - March 05, 2020

Today's outline - March 05, 2020

- Powder diffraction

Today's outline - March 05, 2020

- Powder diffraction
- Pair distribution function

Today's outline - March 05, 2020

- Powder diffraction
- Pair distribution function
- Bragg & Laue geometries

Today's outline - March 05, 2020

- Powder diffraction
- Pair distribution function
- Bragg & Laue geometries
- Kinematical approach for many layers

Today's outline - March 05, 2020

- Powder diffraction
- Pair distribution function
- Bragg & Laue geometries
- Kinematical approach for many layers
- Dynamical diffraction theory

Today's outline - March 05, 2020

- Powder diffraction
- Pair distribution function
- Bragg & Laue geometries
- Kinematical approach for many layers
- Dynamical diffraction theory
- Characteristics of the Darwin curve

Today's outline - March 05, 2020

- Powder diffraction
- Pair distribution function
- Bragg & Laue geometries
- Kinematical approach for many layers
- Dynamical diffraction theory
- Characteristics of the Darwin curve

No class on Tuesday, March 24, 2020 or Thursday, March 26, 2020

Today's outline - March 05, 2020

- Powder diffraction
- Pair distribution function
- Bragg & Laue geometries
- Kinematical approach for many layers
- Dynamical diffraction theory
- Characteristics of the Darwin curve

No class on Tuesday, March 24, 2020 or Thursday, March 26, 2020

Homework Assignment #04:
Chapter 4: 2, 4, 6, 7, 10
due Tuesday, March 10, 2020

Today's outline - March 05, 2020

- Powder diffraction
- Pair distribution function
- Bragg & Laue geometries
- Kinematical approach for many layers
- Dynamical diffraction theory
- Characteristics of the Darwin curve

No class on Tuesday, March 24, 2020 or Thursday, March 26, 2020

Homework Assignment #04:
Chapter 4: 2, 4, 6, 7, 10
due Tuesday, March 10, 2020

Homework Assignment #05:
Chapter 5: 1, 3, 7, 9, 10
due Thursday, April 02, 2020

Beamline 11BM at the APS

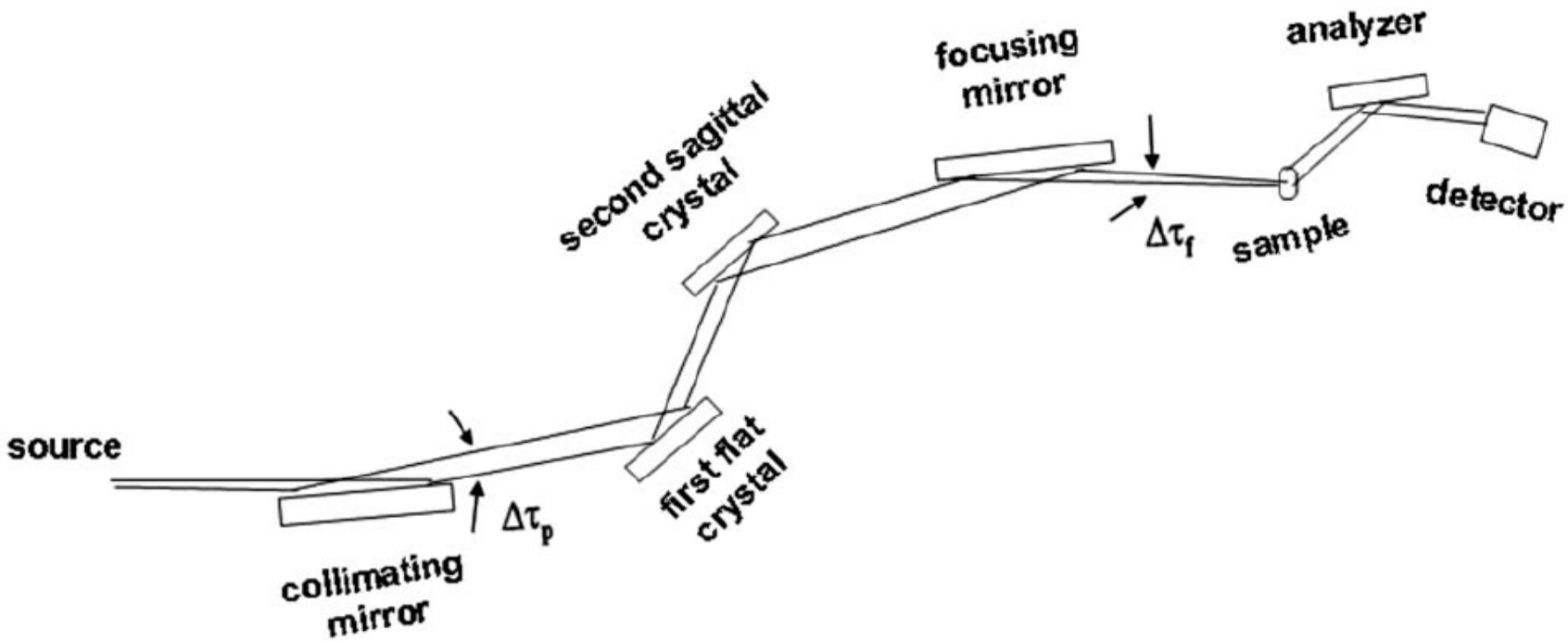

"A dedicated powder diffraction beamline at the Advanced Photon Source: Commissioning and early operational results," J. Wang et al. *Rev. Sci. Instrum.* **79**, 085105 (2008).

Beamline 11BM at the APS

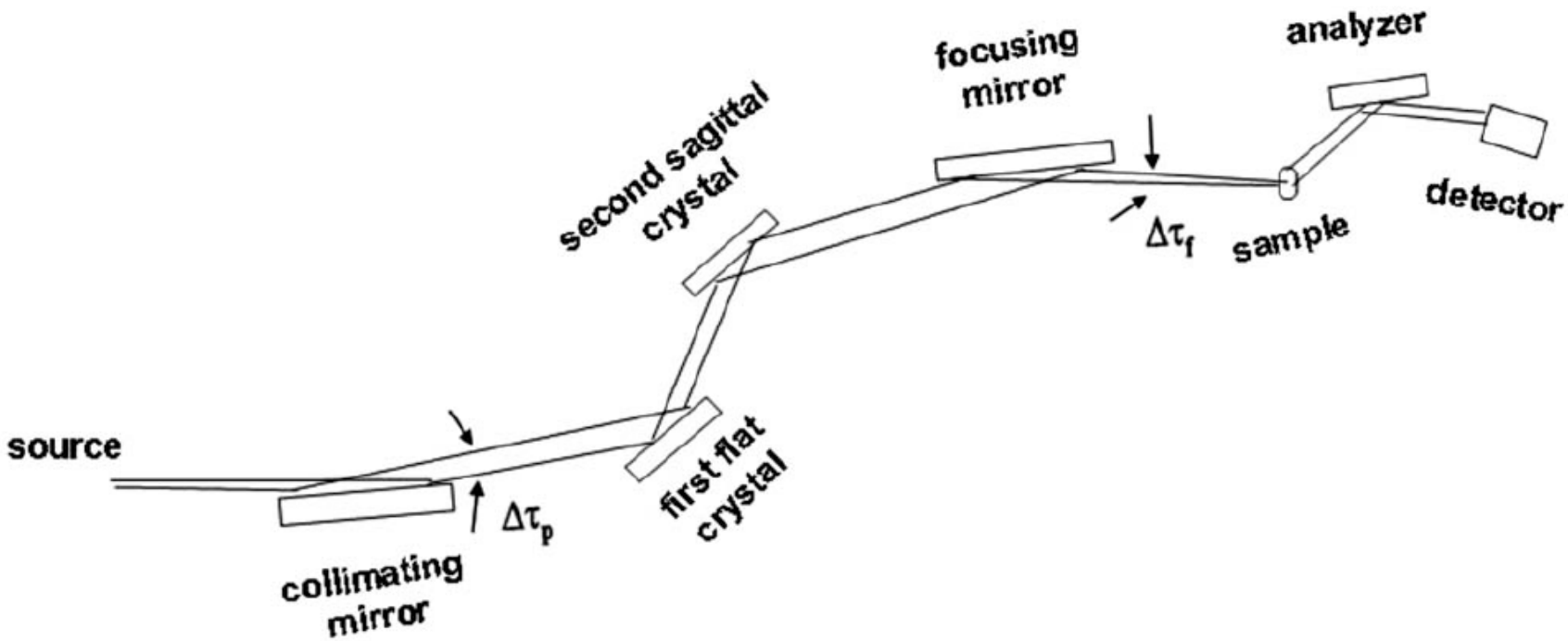

2D detectors have limited angular resolution, for high resolution routine powder diffraction, beamlines such as 11BM are ideal

"A dedicated powder diffraction beamline at the Advanced Photon Source: Commissioning and early operational results," J. Wang et al. *Rev. Sci. Instrum.* **79**, 085105 (2008).

Beamline 11BM at the APS

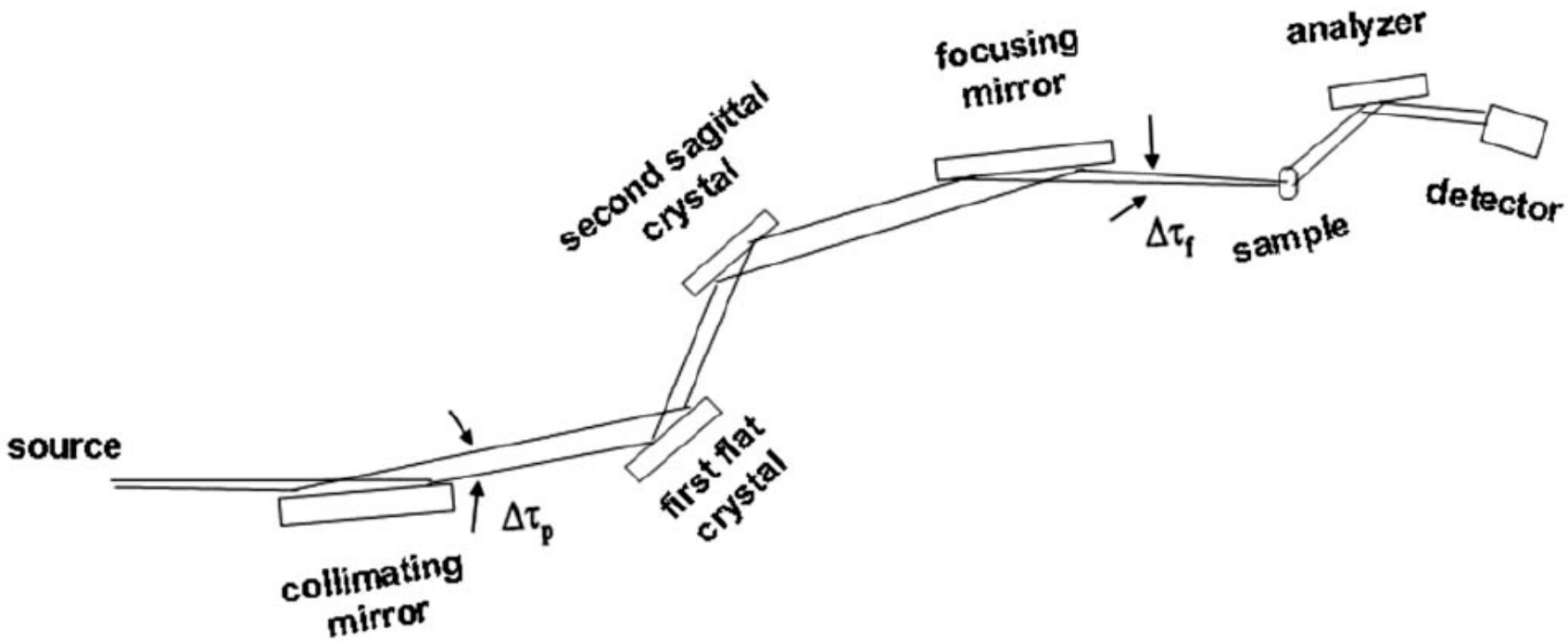

2D detectors have limited angular resolution, for high resolution routine powder diffraction, beamlines such as 11BM are ideal

The initial collimating mirror makes the beam more parallel and then it is focused horizontally and vertically to the sample

"A dedicated powder diffraction beamline at the Advanced Photon Source: Commissioning and early operational results," J. Wang et al. *Rev. Sci. Instrum.* **79**, 085105 (2008).

The high resolution analyzer

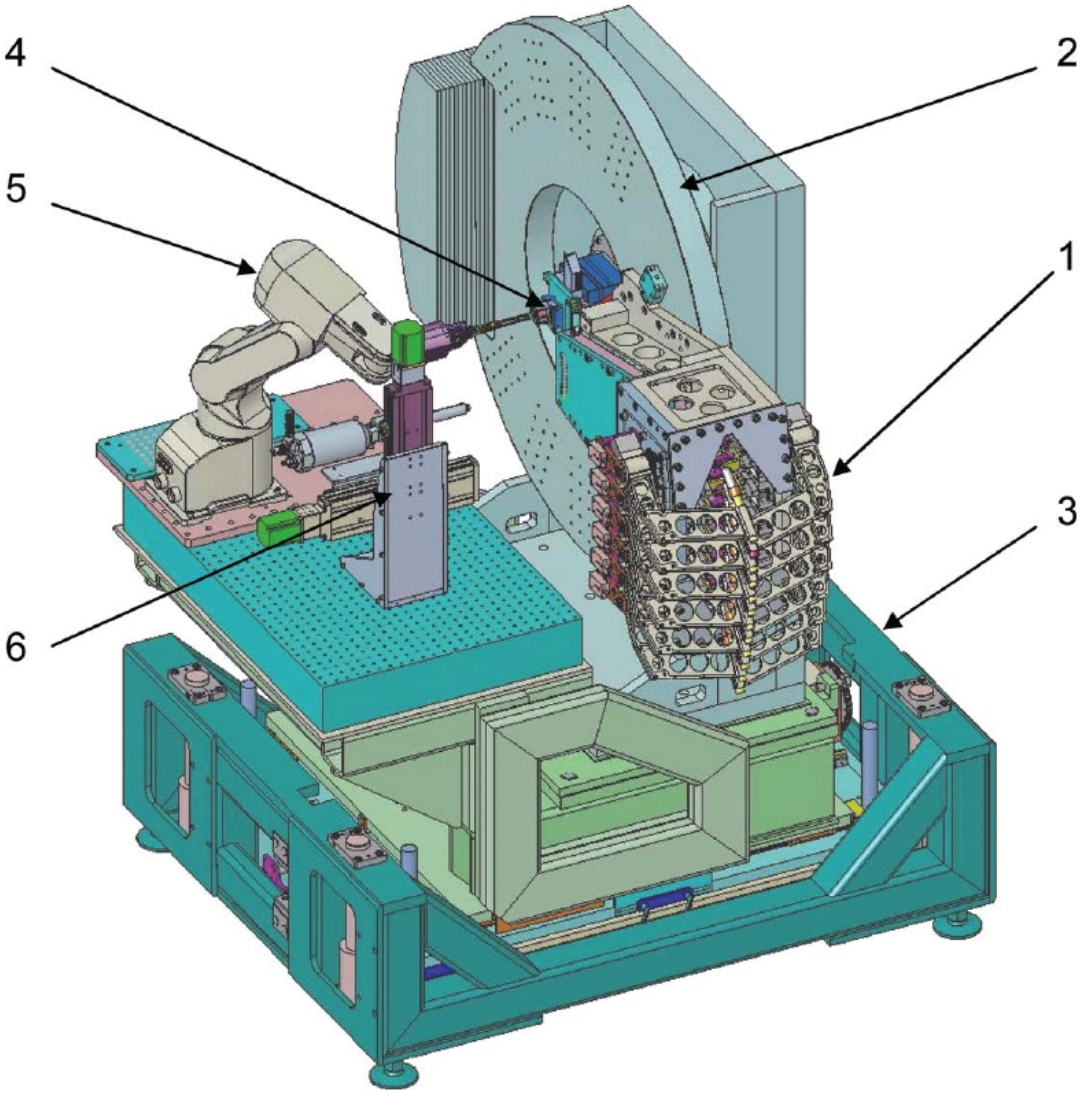

"A twelve-analyzer detector system for high resolution powder diffraction," P.L. Lee et al. *J. Synch. Rad.* **15**, 427-432

The high resolution analyzer

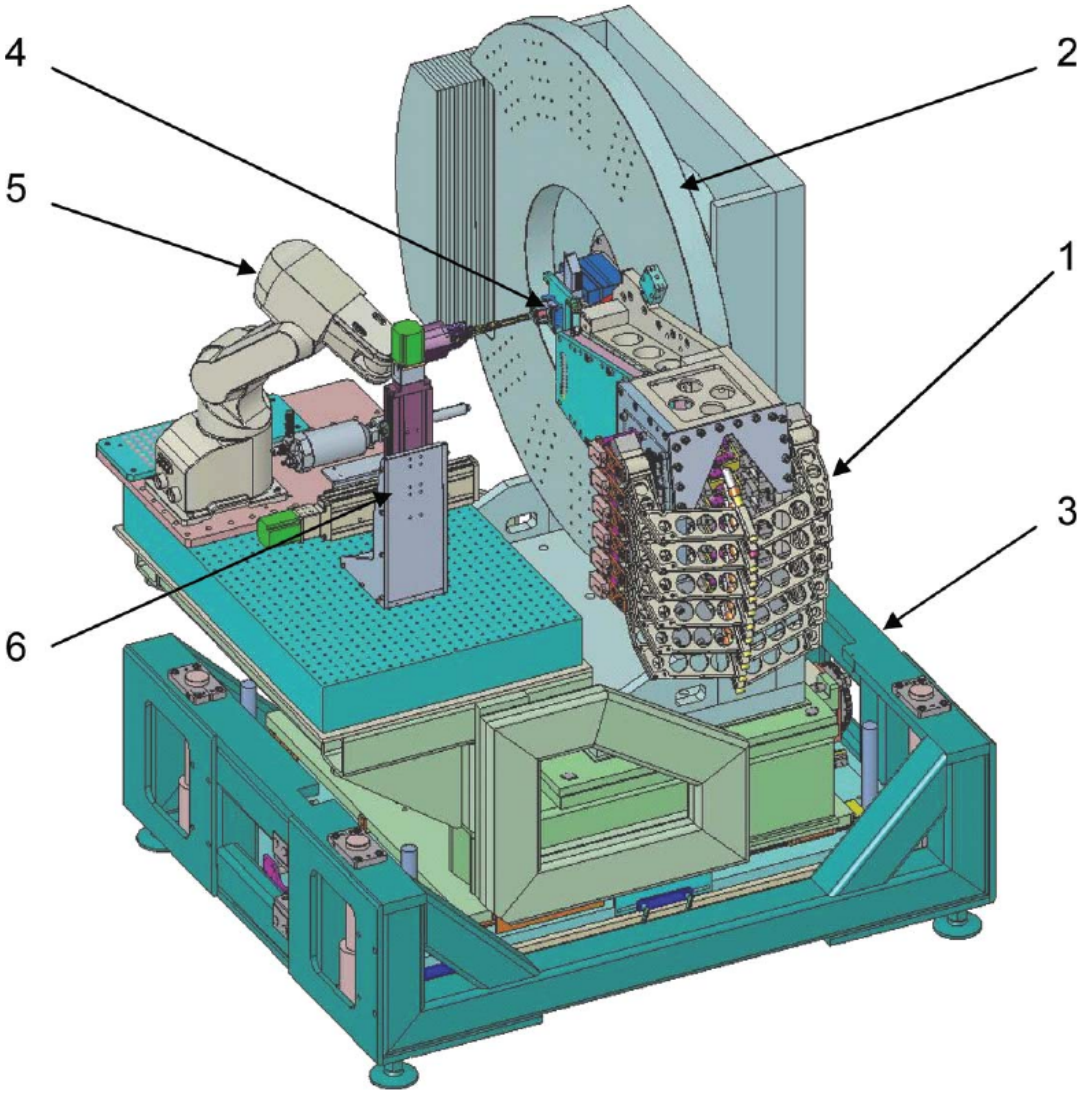

High throughput is obtained using a robot arm to change samples

"A twelve-analyzer detector system for high resolution powder diffraction," P.L. Lee et al. *J. Synch. Rad.* **15**, 427-432

The high resolution analyzer

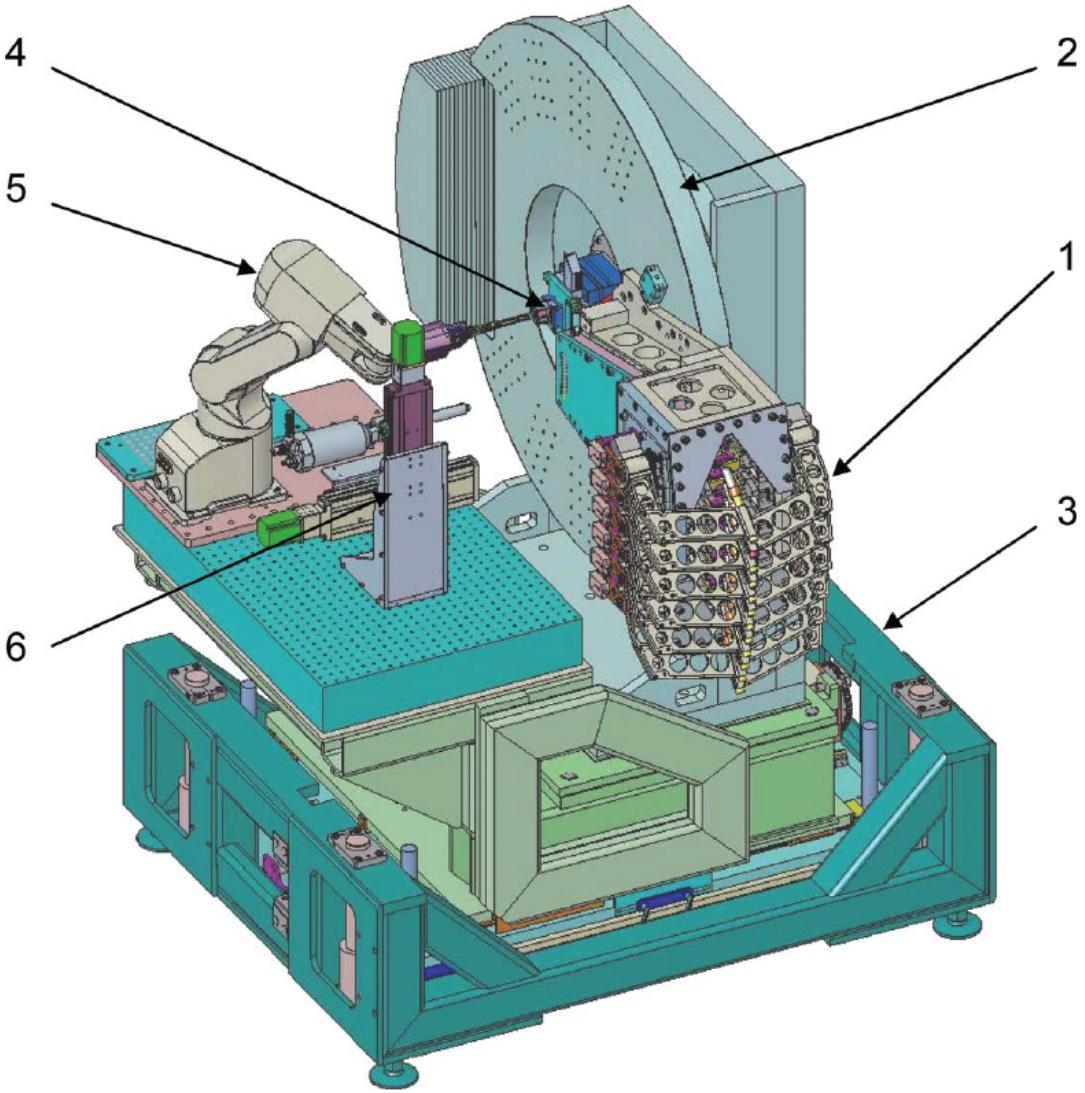

High throughput is obtained using a robot arm to change samples

The sample is mounted on a rotating spindle at the center of the goniometer

"A twelve-analyzer detector system for high resolution powder diffraction," P.L. Lee et al. *J. Synch. Rad.* **15**, 427-432

The high resolution analyzer

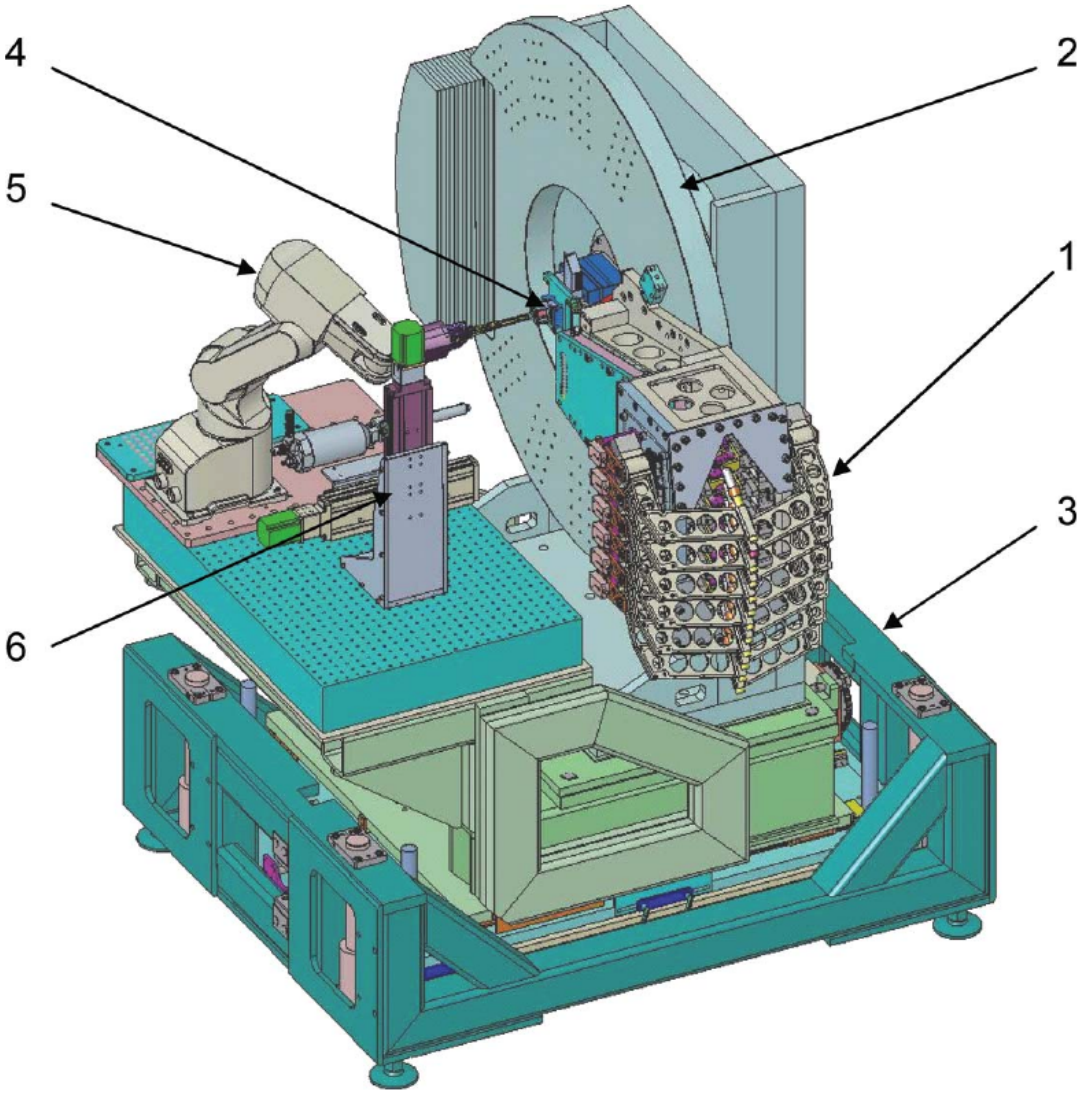

High throughput is obtained using a robot arm to change samples

The sample is mounted on a rotating spindle at the center of the goniometer

High resolution is achieved with a 12 crystal analyzer system which is rotated on the main circle of the goniometer

"A twelve-analyzer detector system for high resolution powder diffraction," P.L. Lee et al. *J. Synch. Rad.* **15**, 427-432

The high resolution analyzer

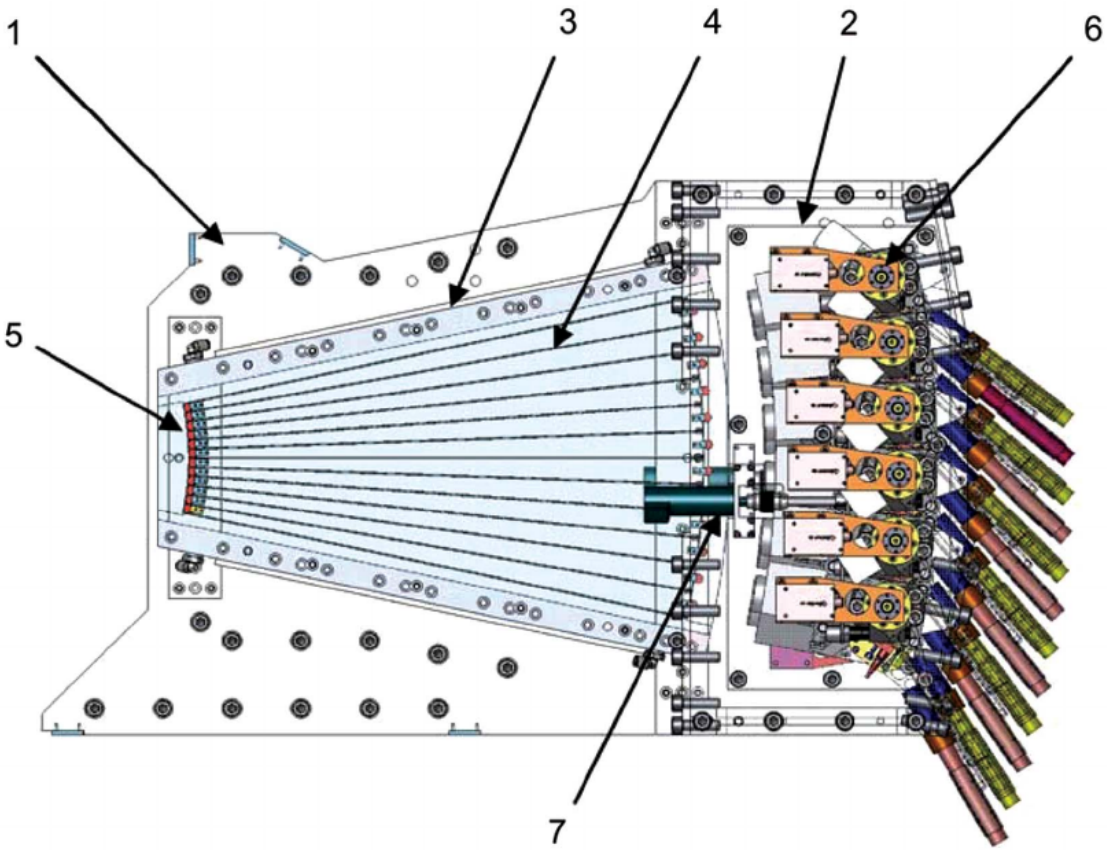

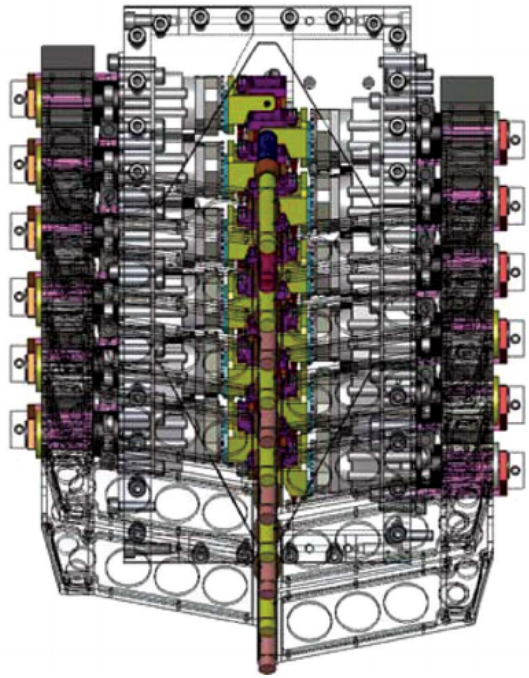

"A twelve-analyzer detector system for high resolution powder diffraction," P.L. Lee et al. *J. Synch. Rad.* **15**, 427-432

The high resolution analyzer

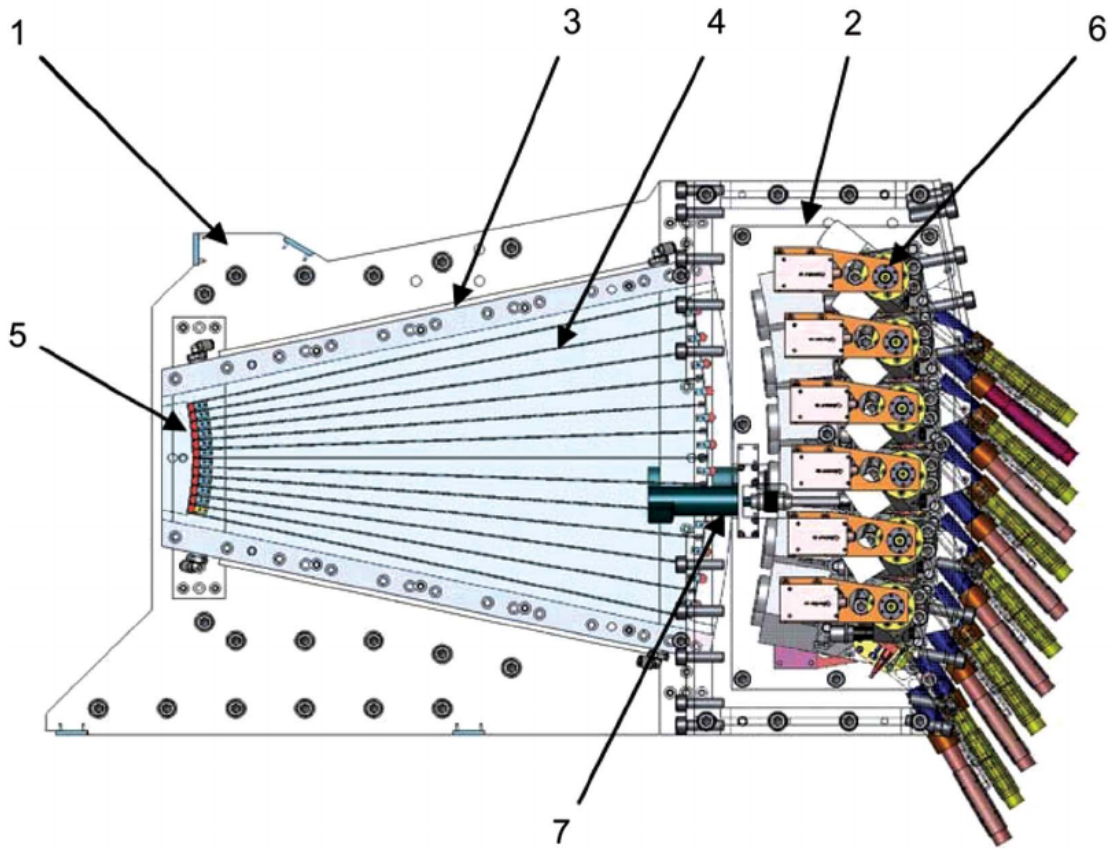

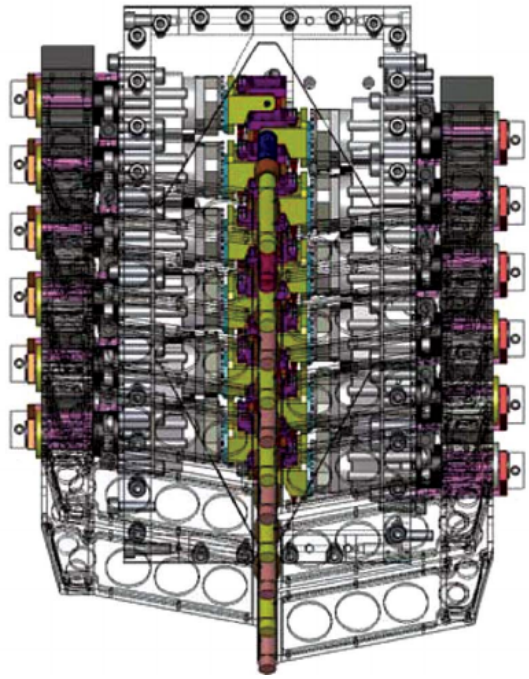

Each of the 12 analyzer crystals is tuned to the desired scattering energy and as the entire assembly is scanned, all twelve banks are collecting data and then are merged

"A twelve-analyzer detector system for high resolution powder diffraction," P.L. Lee et al. *J. Synch. Rad.* **15**, 427-432

The analyzer and robot arm

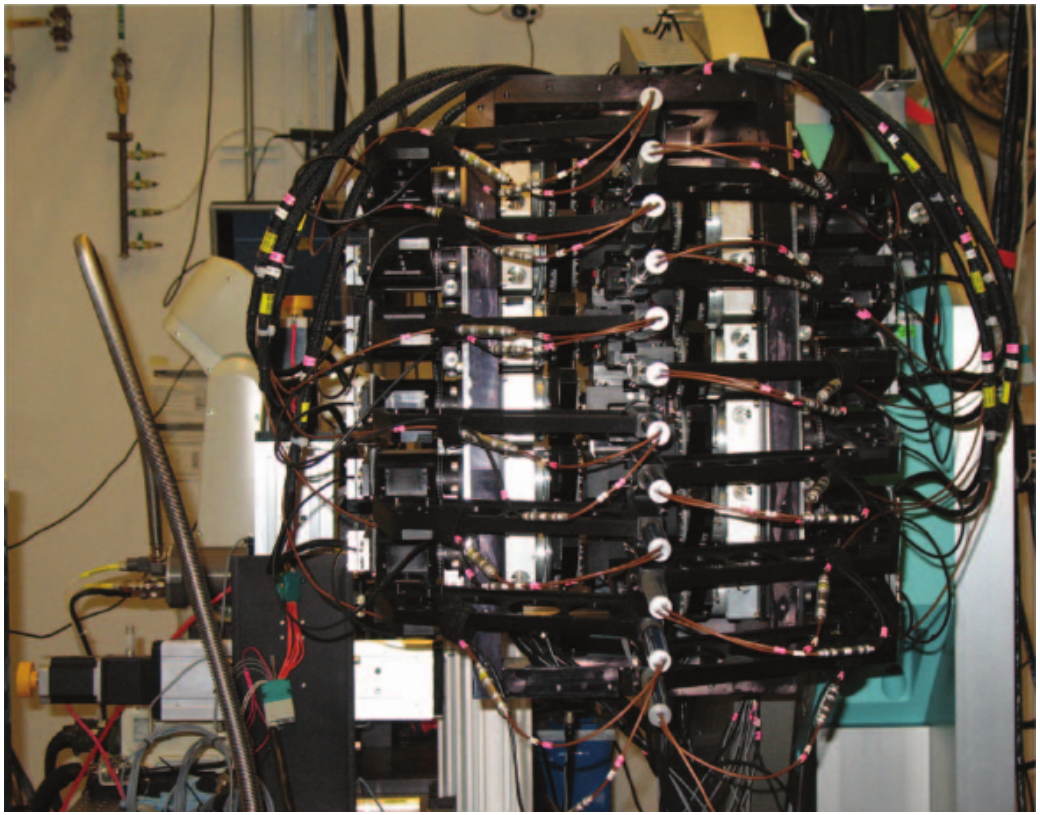

"A twelve-analyzer detector system for high resolution powder diffraction," P.L. Lee et al. *J. Synch. Rad.* **15**, 427-432

The analyzer and robot arm

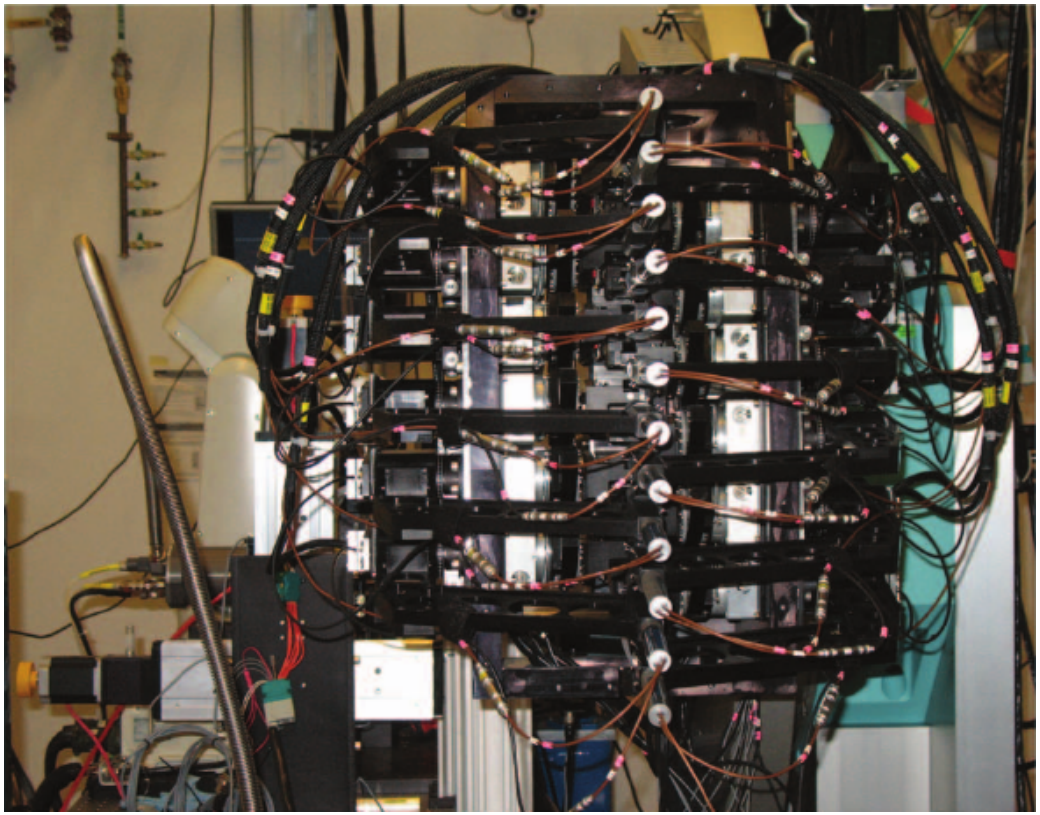

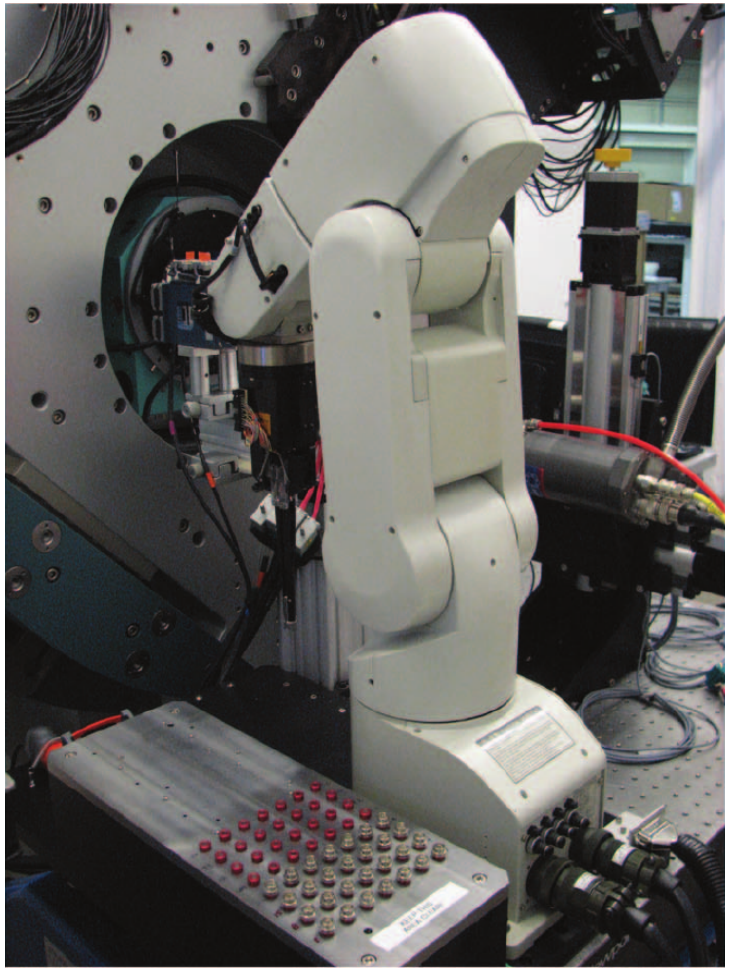

Samples are in Kapton capillaries and magnetic bases for remote mounting

"A twelve-analyzer detector system for high resolution powder diffraction," P.L. Lee et al. *J. Synch. Rad.* **15**, 427-432

Data from high resolution LaB_6 standard

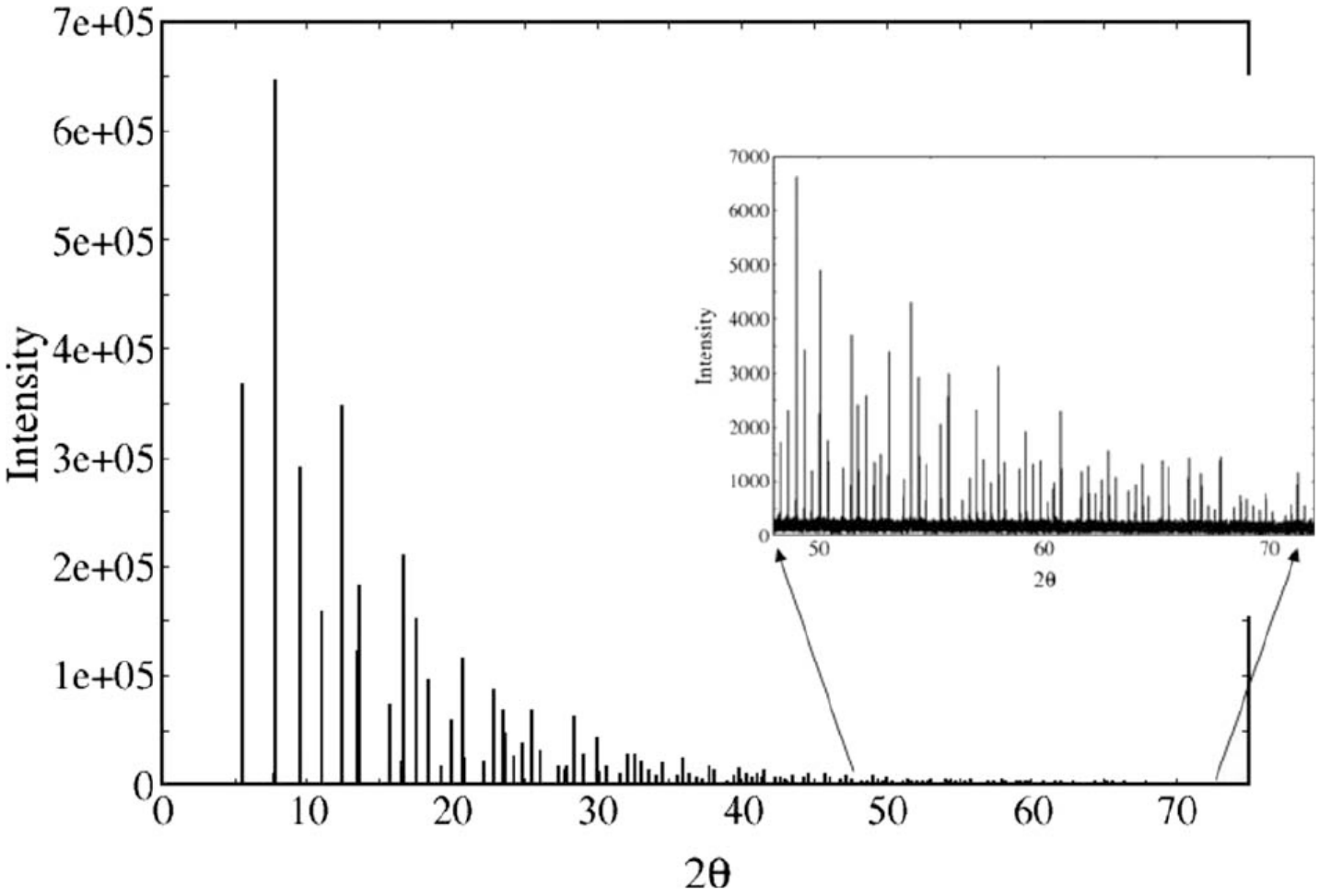

"A dedicated powder diffraction beamline at the Advanced Photon Source: Commissioning and early operational results," J. Wang et al. *Rev. Sci. Instrum.* **79**, 085105 (2008).

Data from high resolution LaB_6 standard

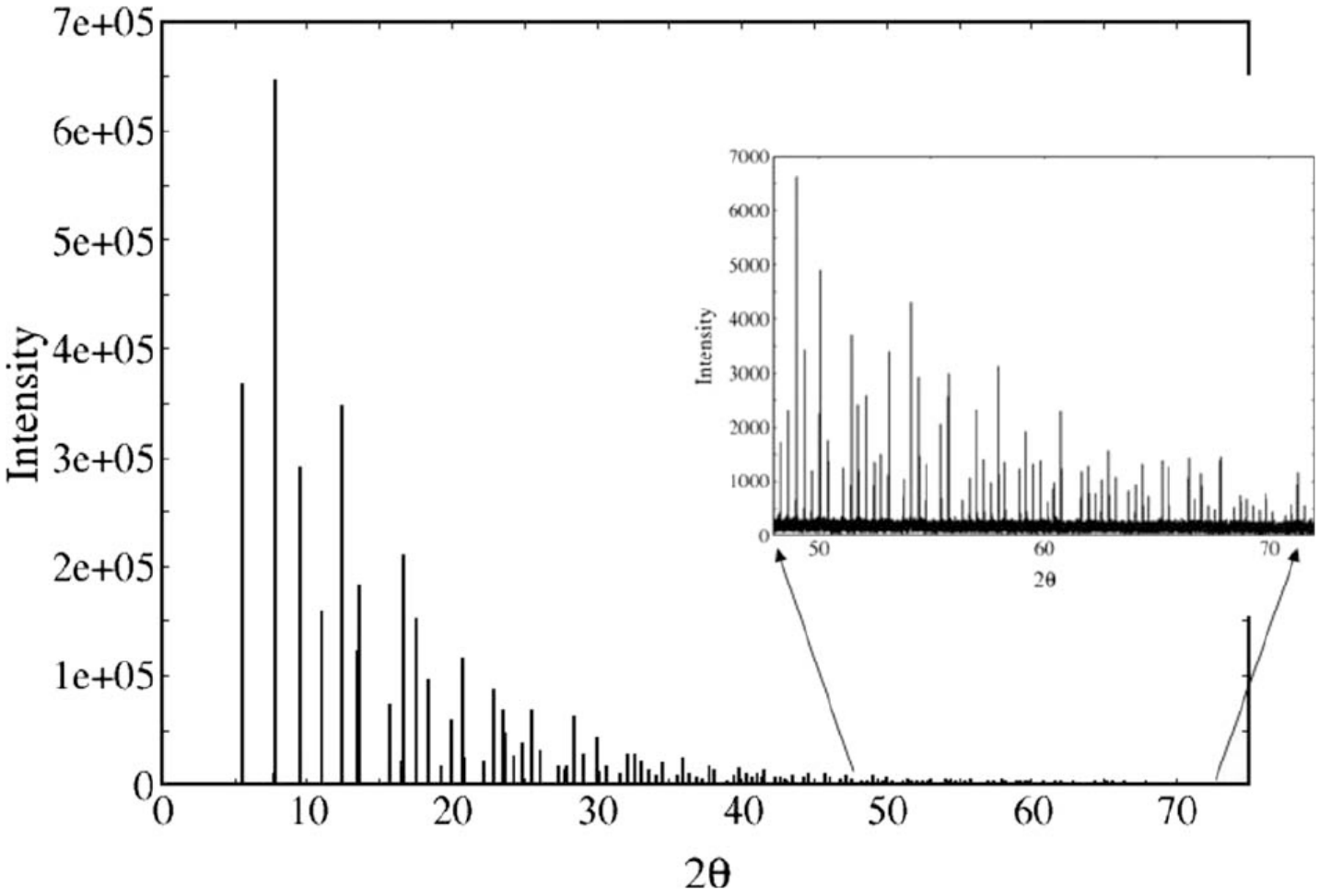

High resolution data with high count rates can be obtained out to very high angles with a wavelength of $\lambda \approx 0.5$Å.

"A dedicated powder diffraction beamline at the Advanced Photon Source: Commissioning and early operational results," J. Wang et al. *Rev. Sci. Instrum.* **79**, 085105 (2008).

Refinement of SiO_2 and Al_2O_3

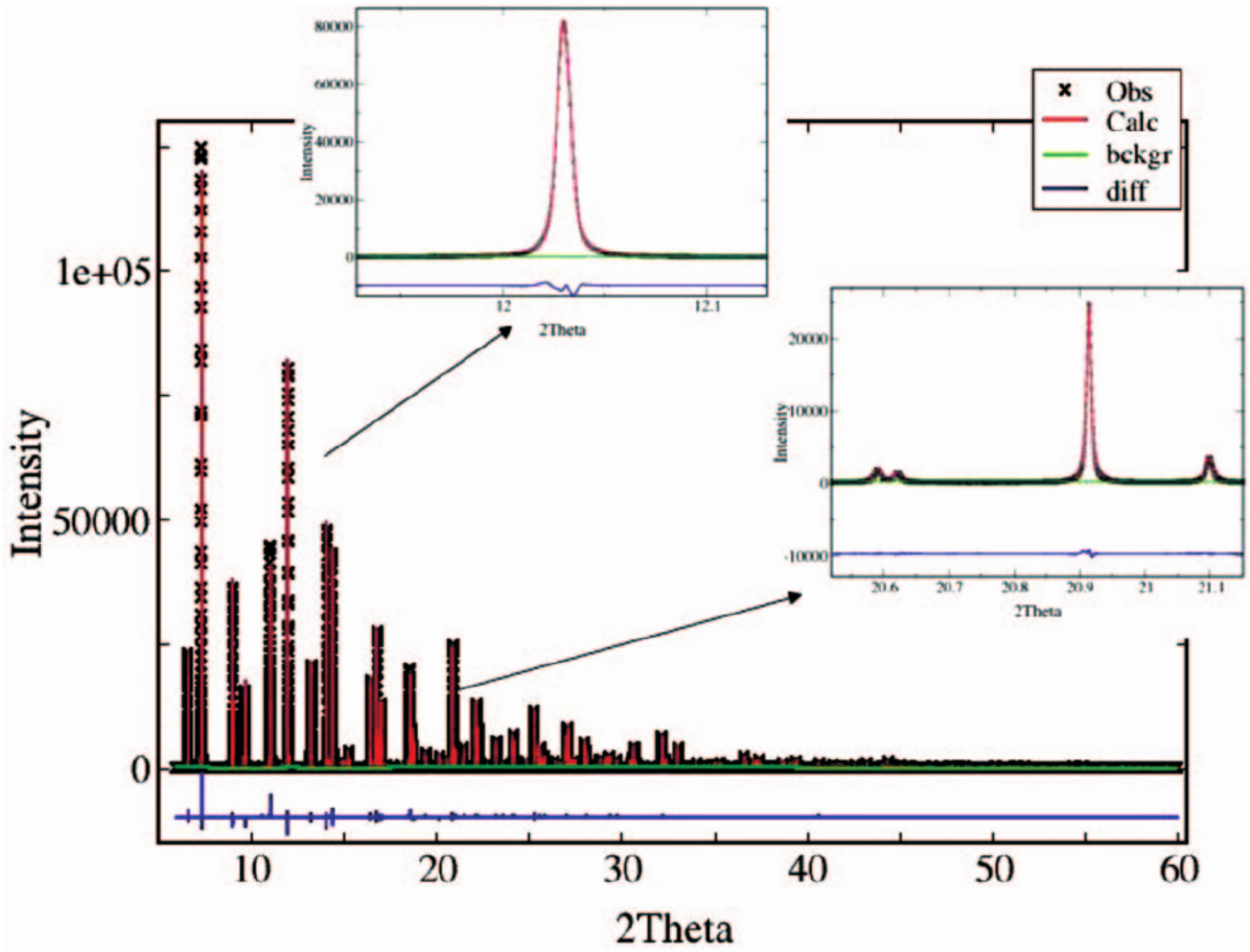

"A dedicated powder diffraction beamline at the Advanced Photon Source: Commissioning and early operational results," J. Wang et al. *Rev. Sci. Instrum.* **79**, 085105 (2008).

CaO-CaO_2 reaction kinetics

CaO is a possible material to be used for carbon sequestration

A. Biasin, C.U. Segre, G. Salviulo, F. Zorzi, and M. Strumendo, *Chemical Eng. Sci.* **127**, 13-24 (2015)

CaO-CaO_2 reaction kinetics

CaO is a possible material to be used for carbon sequestration

CaO will absorb CO_2 at temperatures as low as 450°C forming $CaCO_3$ and can be regenerated by calcination at temperatures above 700°C

A. Biasin, C.U. Segre, G. Salviulo, F. Zorzi, and M. Strumendo, *Chemical Eng. Sci.* **127**, 13-24 (2015)

CaO-CaO_2 reaction kinetics

CaO is a possible material to be used for carbon sequestration

CaO will absorb CO_2 at temperatures as low as 450°C forming $CaCO_3$ and can be regenerated by calcination at temperatures above 700°C

It is important to understand the fundamental reaction kinetics of thse processes in order to be able to design carbon sequestration procedures.

A. Biasin, C.U. Segre, G. Salviulo, F. Zorzi, and M. Strumendo, *Chemical Eng. Sci.* **127**, 13-24 (2015)

CaO-CaO_2 reaction kinetics

CaO is a possible material to be used for carbon sequestration

CaO will absorb CO_2 at temperatures as low as 450°C forming $CaCO_3$ and can be regenerated by calcination at temperatures above 700°C

It is important to understand the fundamental reaction kinetics of thse processes in order to be able to design carbon sequestration procedures.

Measurements heretofore have been performed in TGA systems which have fundamental mass flow limitations. These experiments were performed at Sector 17-BM of the APS. Samples were loaded in quartz capillaries and a 2D area detector was used to take snaps at up to 0.25s/frame.

A. Biasin, C.U. Segre, G. Salviulo, F. Zorzi, and M. Strumendo, *Chemical Eng. Sci.* **127**, 13-24 (2015)

CaO-CaO_2 reaction kinetics

CaO is a possible material to be used for carbon sequestration

CaO will absorb CO_2 at temperatures as low as 450°C forming $CaCO_3$ and can be regenerated by calcination at temperatures above 700°C

It is important to understand the fundamental reaction kinetics of thse processes in order to be able to design carbon sequestration procedures.

Measurements heretofore have been performed in TGA systems which have fundamental mass flow limitations. These experiments were performed at Sector 17-BM of the APS. Samples were loaded in quartz capillaries and a 2D area detector was used to take snaps at up to 0.25s/frame.

Rietveld refinement was used to measure the lattice parameters, crystallite sizes and phase fractions during carbonation and calcination cycles

A. Biasin, C.U. Segre, G. Salviulo, F. Zorzi, and M. Strumendo, *Chemical Eng. Sci.* **127**, 13-24 (2015)

Typical diffraciton pattern

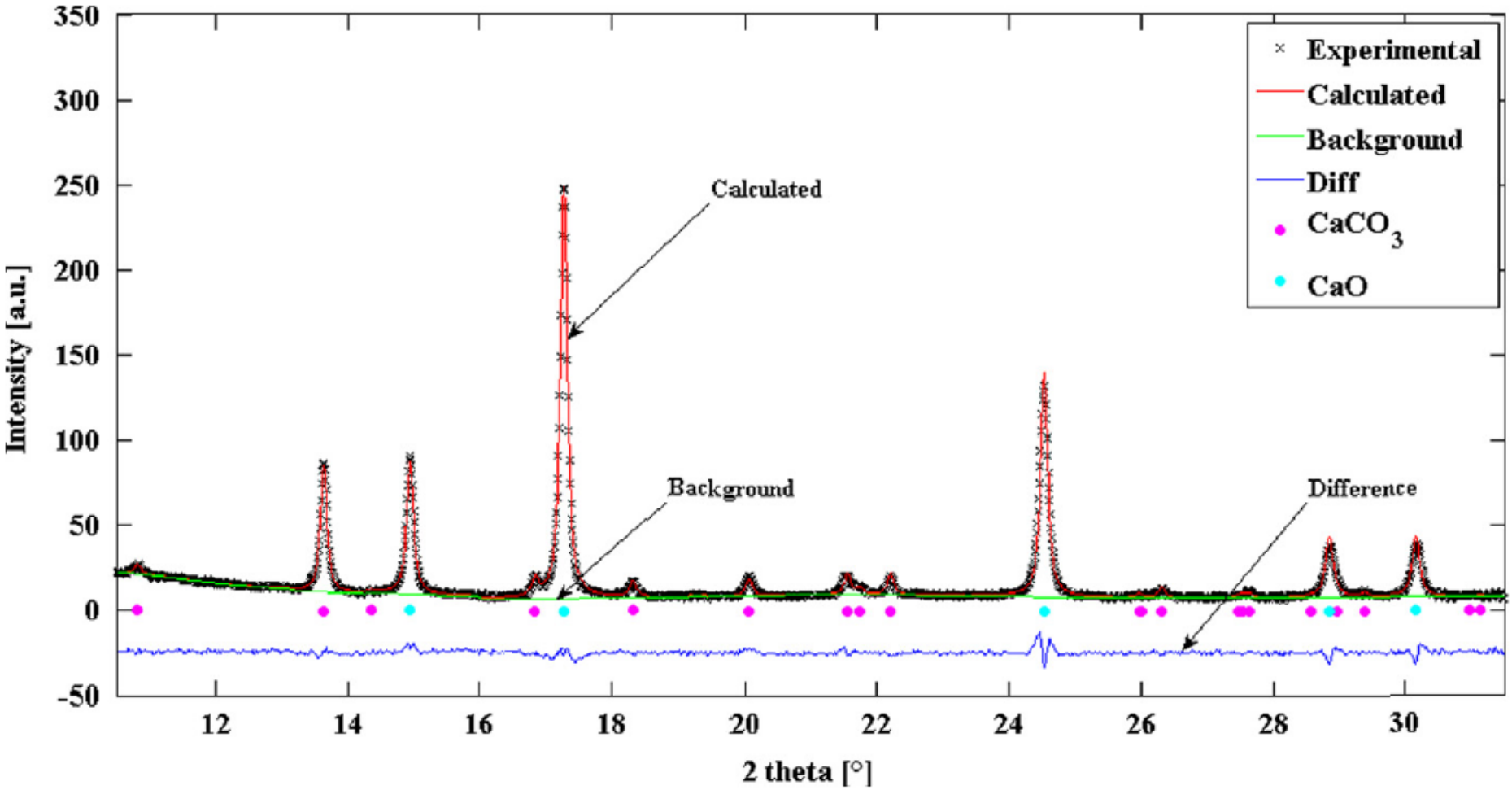

A. Biasin, C.U. Segre, G. Salviulo, F. Zorzi, and M. Strumendo, *Chemical Eng. Sci.* **127**, 13-24 (2015)

Final conversion fraction

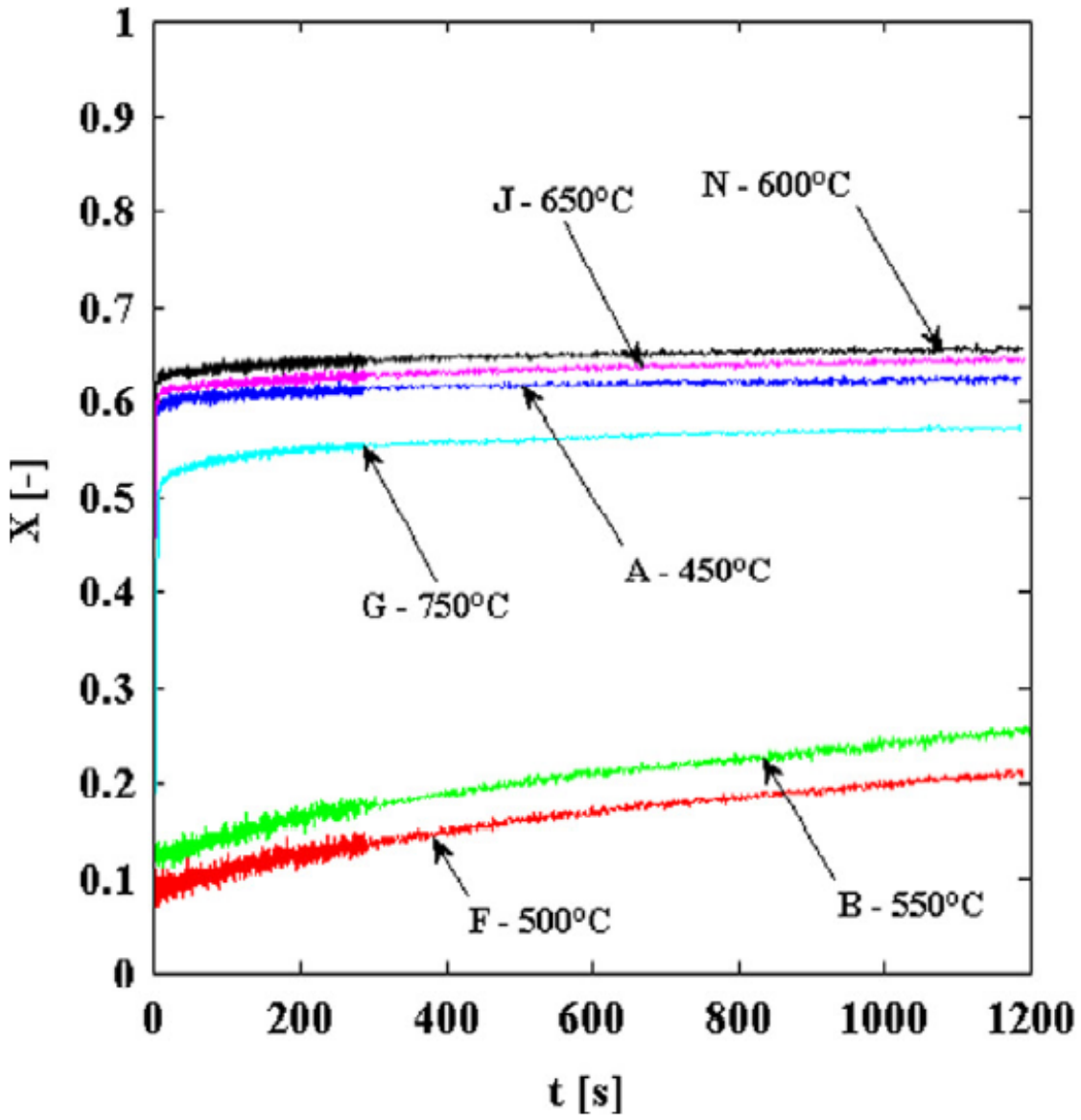

A. Biasin, C.U. Segre, G. Salviulo, F. Zorzi, and M. Strumendo, *Chemical Eng. Sci.* **127**, 13-24 (2015)

Final conversion fraction

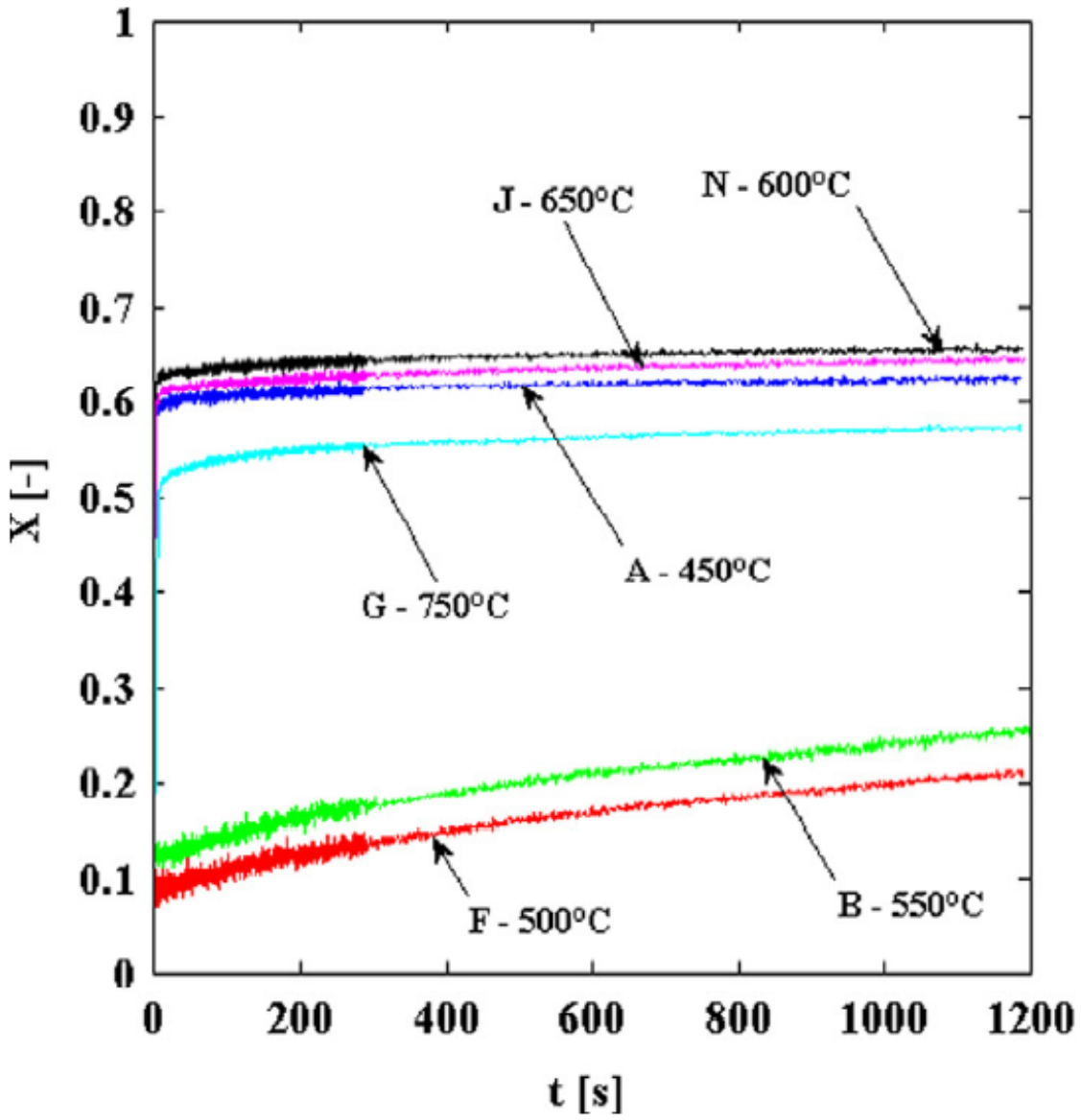

Final conversion fraction depends on temperature but also some other parameter (what?)

A. Biasin, C.U. Segre, G. Salviulo, F. Zorzi, and M. Strumendo, *Chemical Eng. Sci.* **127**, 13-24 (2015)

Final conversion fraction

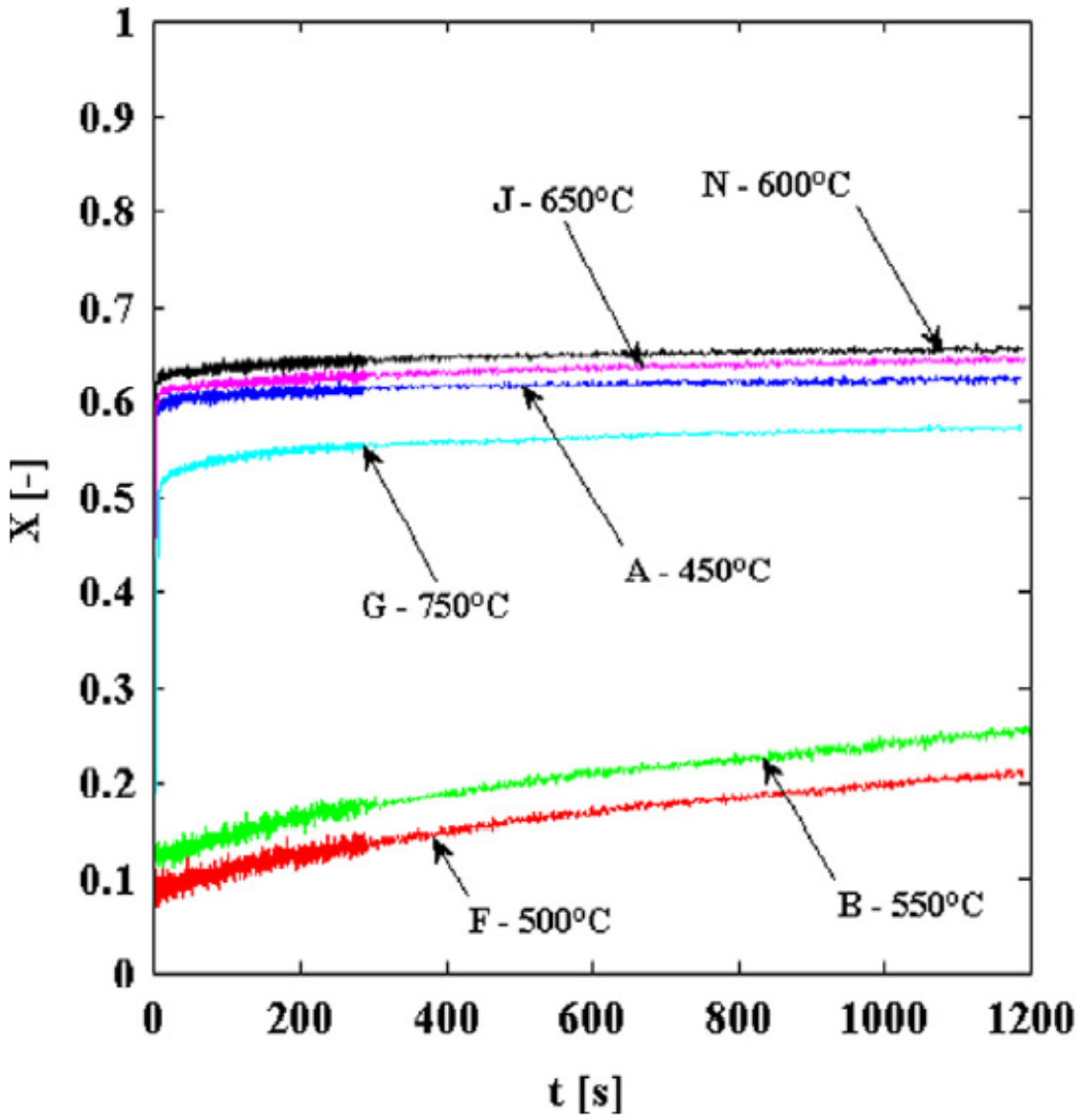

Final conversion fraction depends on temperature but also some other parameter (what?)

Remember that these powders have only been seived to a particular grain size, what about the internal structure?

A. Biasin, C.U. Segre, G. Salviulo, F. Zorzi, and M. Strumendo, *Chemical Eng. Sci.* **127**, 13-24 (2015)

CaO-CaO_2 reaction kinetics

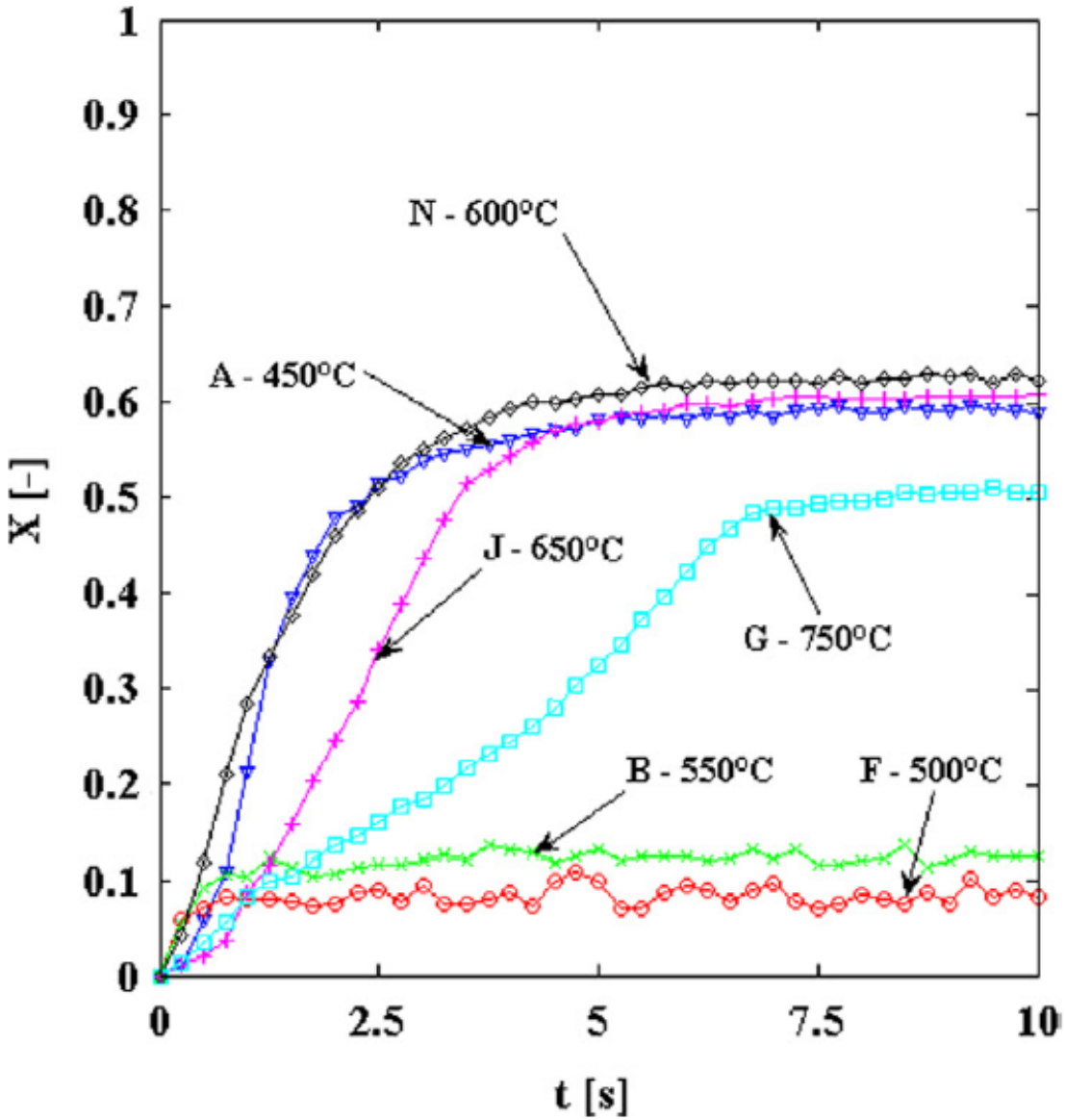

A. Biasin, C.U. Segre, G. Salviulo, F. Zorzi, and M. Strumendo, *Chemical Eng. Sci.* **127**, 13-24 (2015)

CaO-CaO_2 reaction kinetics

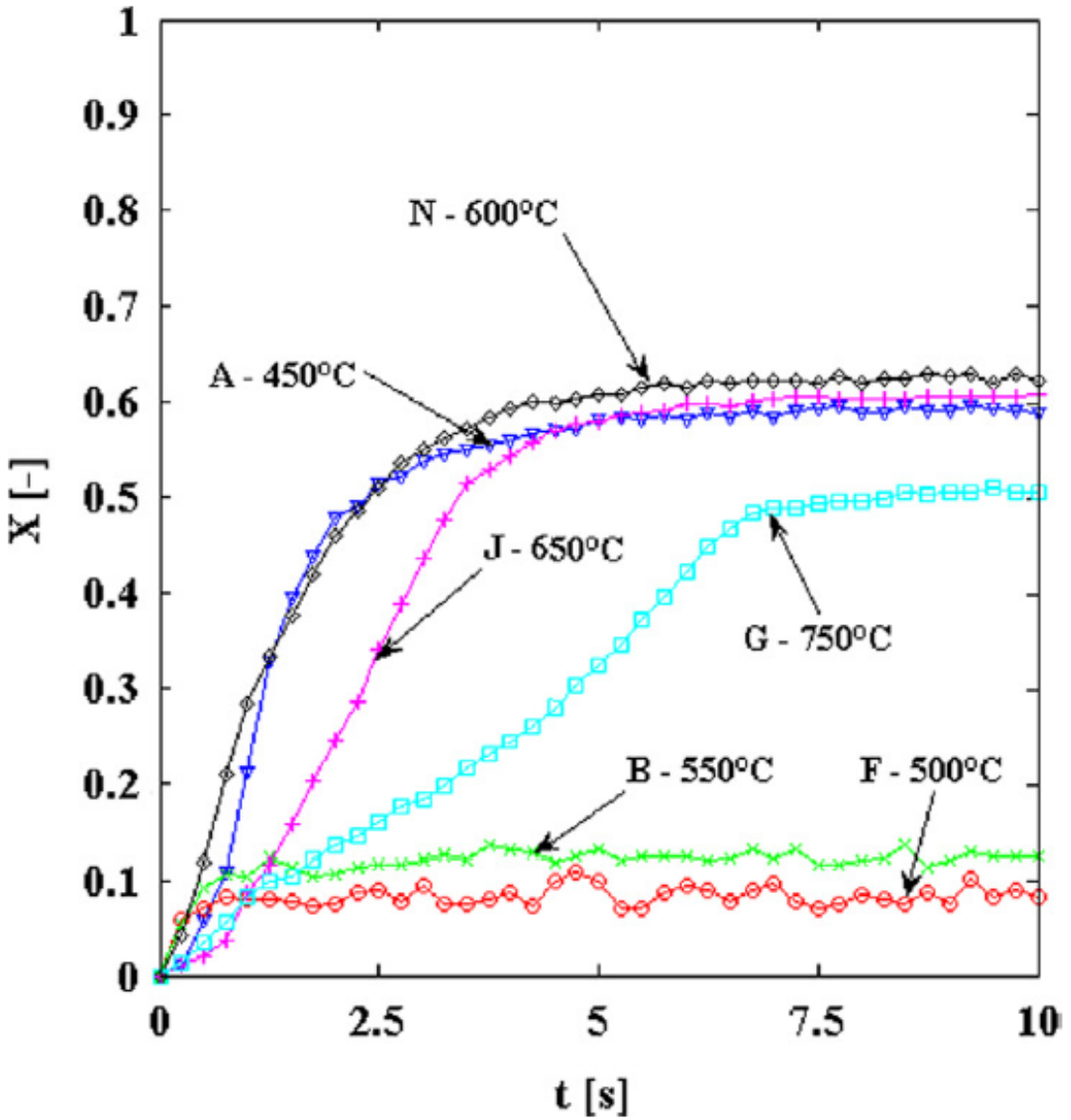

Because of the high speed of the 2D detector, it is possible to look at the conversion reaction at unprecedented time scales

A. Biasin, C.U. Segre, G. Salviulo, F. Zorzi, and M. Strumendo, *Chemical Eng. Sci.* **127**, 13-24 (2015)

CaO-CaO_2 reaction kinetics

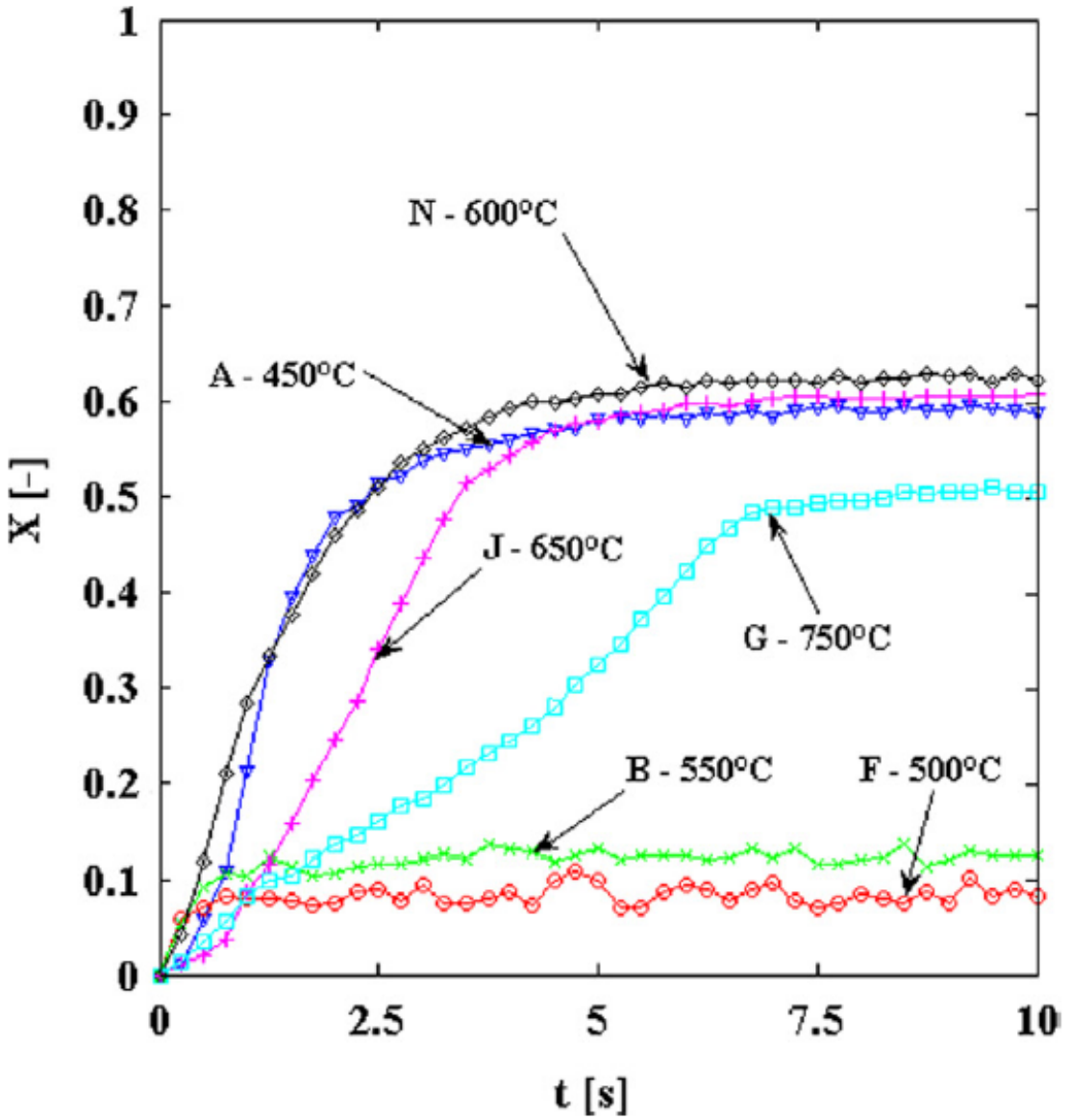

Because of the high speed of the 2D detector, it is possible to look at the conversion reaction at unprecedented time scales

Reaction kinetics much faster, $1/\tau = 0.28$ s^{-1}, than previously observed with TGA measurements

A. Biasin, C.U. Segre, G. Salviulo, F. Zorzi, and M. Strumendo, *Chemical Eng. Sci.* **127**, 13-24 (2015)

CaO-CaO_2 reaction kinetics

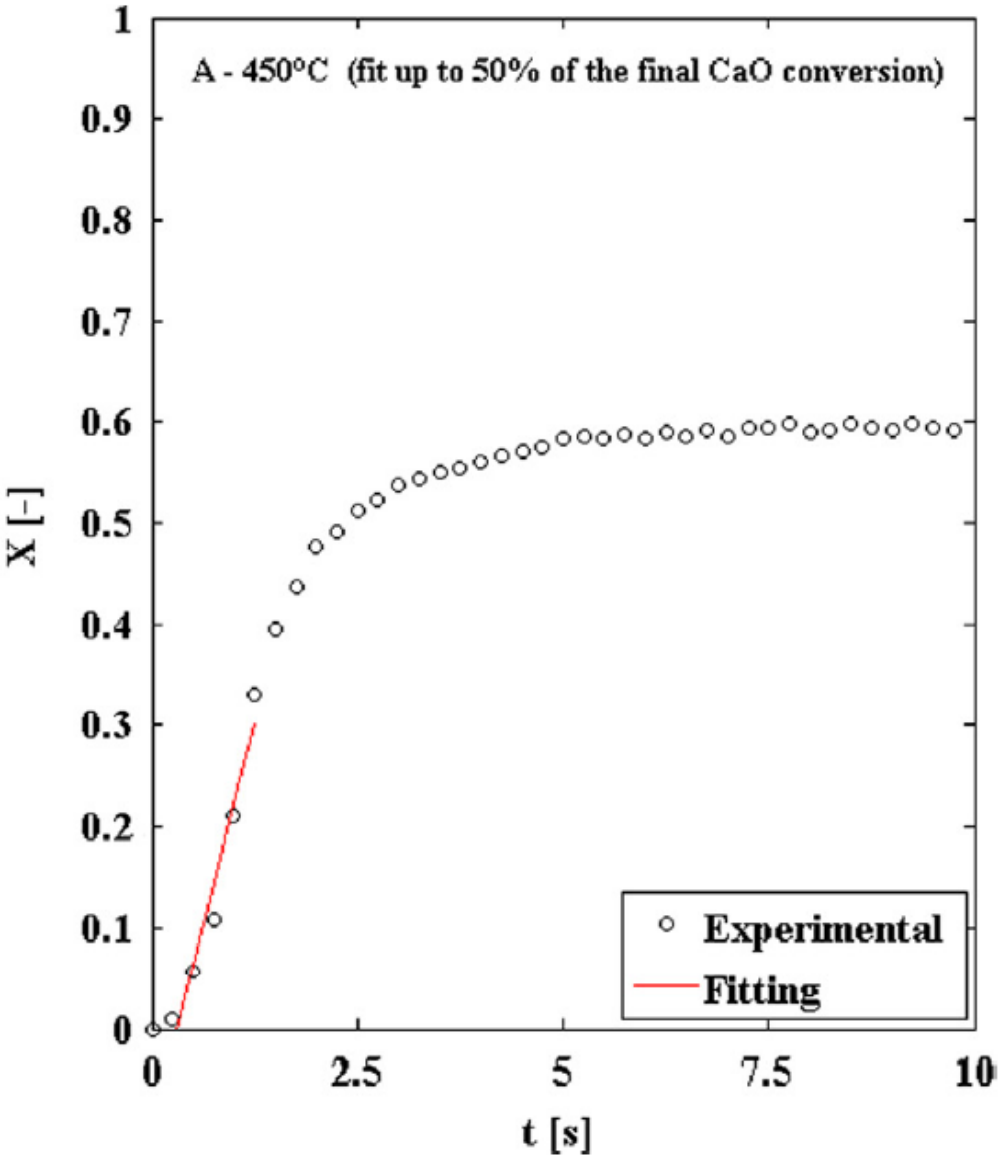

A. Biasin, C.U. Segre, G. Salviulo, F. Zorzi, and M. Strumendo, *Chemical Eng. Sci.* **127**, 13-24 (2015)

CaO-CaO_2 reaction kinetics

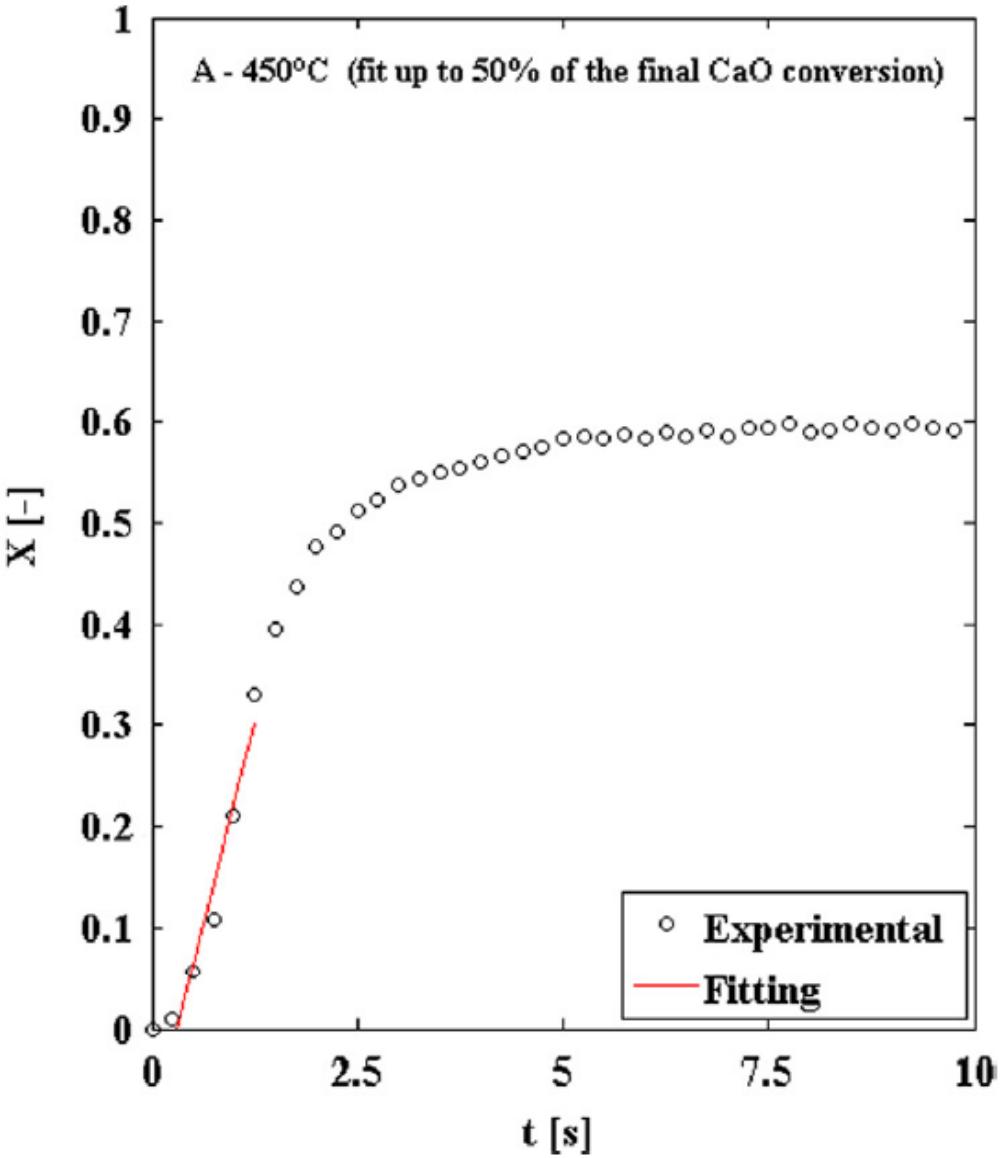

The rates of conversion are determined by fitting the initial (up to 50%) slope of the phase fraction as a function of time with a straight line

A. Biasin, C.U. Segre, G. Salviulo, F. Zorzi, and M. Strumendo, *Chemical Eng. Sci.* **127**, 13-24 (2015)

CaO-CaO_2 reaction kinetics

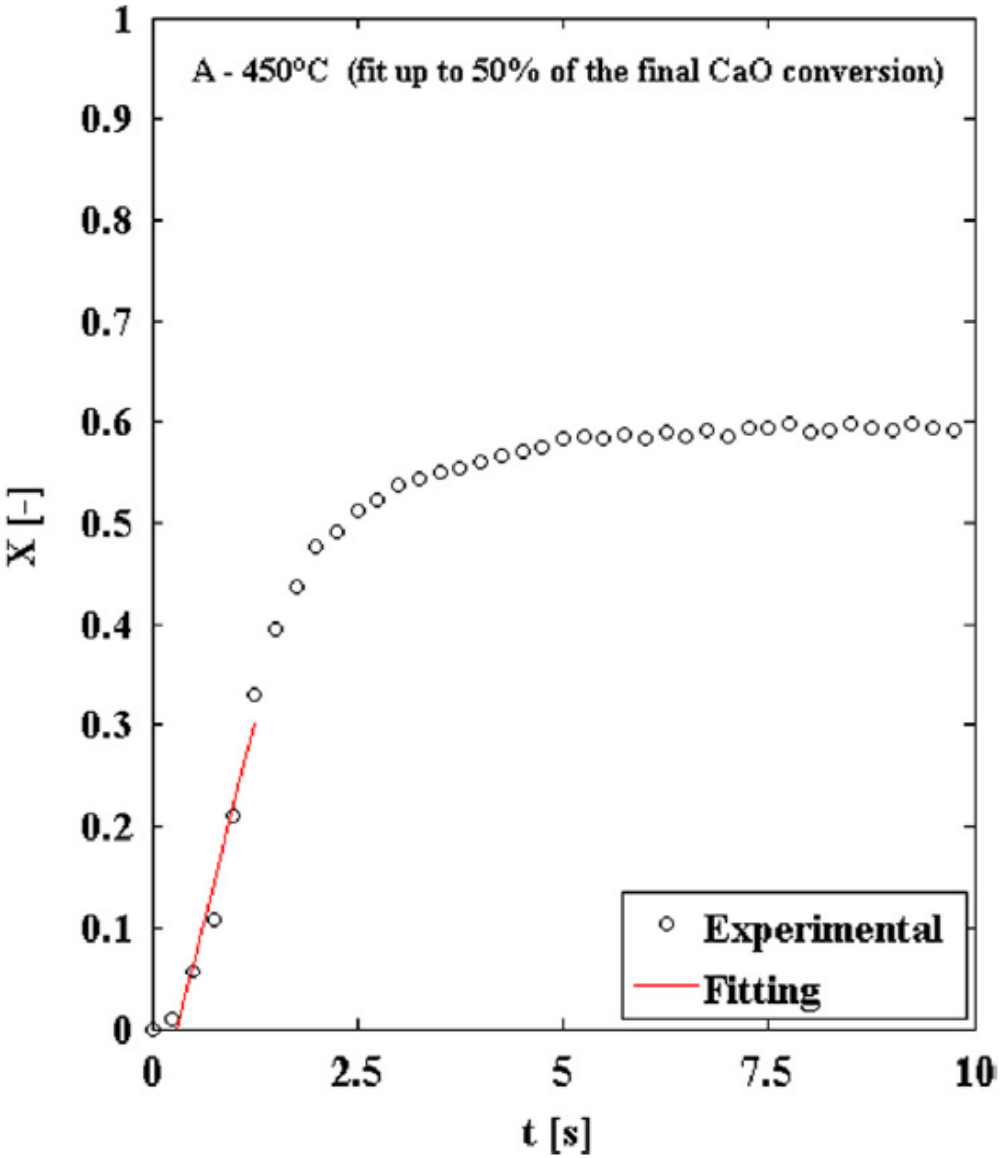

The rates of conversion are determined by fitting the initial (up to 50%) slope of the phase fraction as a function of time with a straight line

These data are then plotted versus the initial CaO crystallite size as determined by Rietveld refinements

A. Biasin, C.U. Segre, G. Salviulo, F. Zorzi, and M. Strumendo, *Chemical Eng. Sci.* **127**, 13-24 (2015)

CaO-CaO_2 reaction kinetics

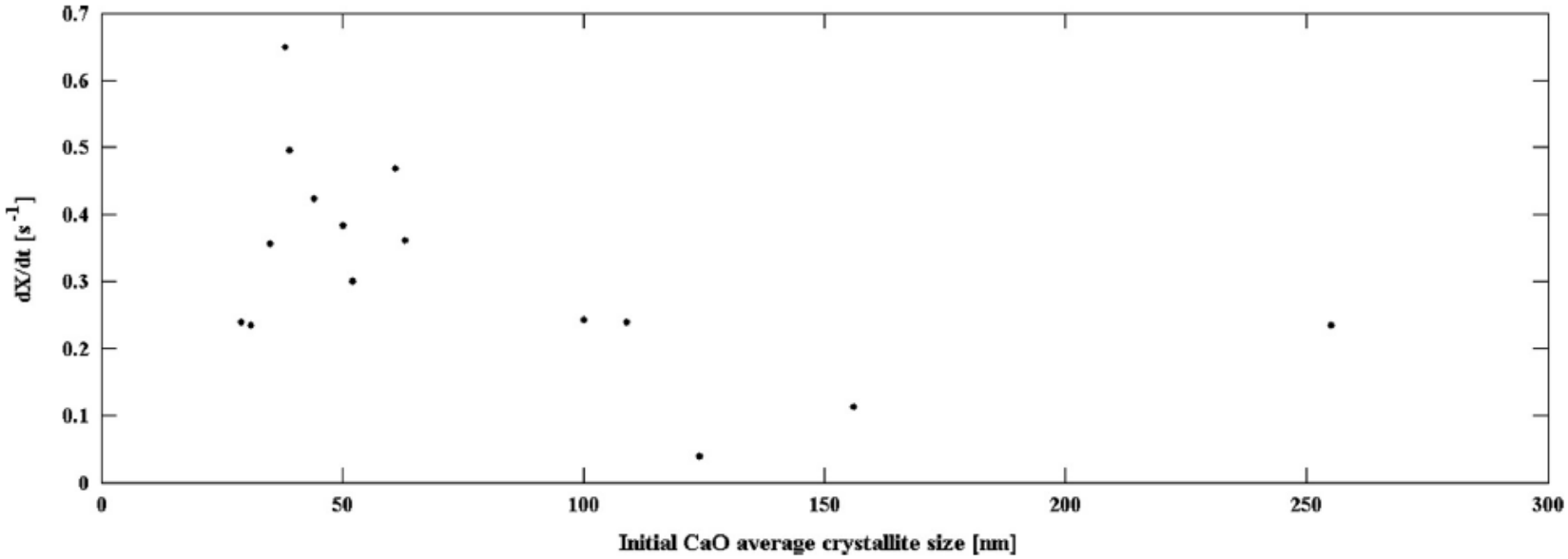

Initial crystallite size is one of the determining factors in inital rate of conversion and fraction converted.

CaO crystallite size can be related to porosity which is key to the conversion process.

A. Biasin, C.U. Segre, G. Salviulo, F. Zorzi, and M. Strumendo, *Chemical Eng. Sci.* **127**, 13-24 (2015)

Pair distribution function

By treating powder diffraction patterns using total scattering methods it is possible to study disorder in crystalline materials as well as nanocrystalline materials

Pair distribution function

By treating powder diffraction patterns using total scattering methods it is possible to study disorder in crystalline materials as well as nanocrystalline materials

The theoretical approach is identical to that for short range order and SAXS, starting with the total scattered intensity from a multi-atomic system

Pair distribution function

By treating powder diffraction patterns using total scattering methods it is possible to study disorder in crystalline materials as well as nanocrystalline materials

The theoretical approach is identical to that for short range order and SAXS, starting with the total scattered intensity from a multi-atomic system

$$I(\vec{Q}) = \sum_n f_n(\vec{Q}) e^{i\vec{Q}\cdot\vec{r_n}} \sum_m f_m^*(\vec{Q}) e^{-i\vec{Q}\cdot\vec{r_m}}$$

Pair distribution function

By treating powder diffraction patterns using total scattering methods it is possible to study disorder in crystalline materials as well as nanocrystalline materials

The theoretical approach is identical to that for short range order and SAXS, starting with the total scattered intensity from a multi-atomic system

$$I(\vec{Q}) = \sum_n f_n(\vec{Q}) e^{i\vec{Q}\cdot\vec{r_n}} \sum_m f_m^*(\vec{Q}) e^{-i\vec{Q}\cdot\vec{r_m}} = \sum_{n,m} f_n(\vec{Q}) f_m^*(\vec{Q}) e^{i\vec{Q}\cdot(\vec{r_n}-\vec{r_m})}$$

Pair distribution function

By treating powder diffraction patterns using total scattering methods it is possible to study disorder in crystalline materials as well as nanocrystalline materials

The theoretical approach is identical to that for short range order and SAXS, starting with the total scattered intensity from a multi-atomic system

$$I(\vec{Q}) = \sum_n f_n(\vec{Q}) e^{i\vec{Q}\cdot\vec{r_n}} \sum_m f_m^*(\vec{Q}) e^{-i\vec{Q}\cdot\vec{r_m}} = \sum_{n,m} f_n(\vec{Q}) f_m^*(\vec{Q}) e^{i\vec{Q}\cdot(\vec{r_n}-\vec{r_m})}$$

$$= N\langle f(\vec{Q})^2\rangle + \sum_{n,m\neq n} f_m(\vec{Q}) f_n^*(\vec{Q}) e^{i\vec{Q}\cdot(\vec{r_n}-\vec{r_m})}$$

Pair distribution function

By treating powder diffraction patterns using total scattering methods it is possible to study disorder in crystalline materials as well as nanocrystalline materials

The theoretical approach is identical to that for short range order and SAXS, starting with the total scattered intensity from a multi-atomic system

$$I(\vec{Q}) = \sum_n f_n(\vec{Q}) e^{i\vec{Q}\cdot\vec{r_n}} \sum_m f_m^*(\vec{Q}) e^{-i\vec{Q}\cdot\vec{r_m}} = \sum_{n,m} f_n(\vec{Q}) f_m^*(\vec{Q}) e^{i\vec{Q}\cdot(\vec{r_n}-\vec{r_m})}$$

$$= N\langle f(\vec{Q})^2\rangle + \sum_{n,m\neq n} f_m(\vec{Q}) f_n^*(\vec{Q}) e^{i\vec{Q}\cdot(\vec{r_n}-\vec{r_m})} = N\langle f(\vec{Q})^2\rangle + I_d(\vec{Q})$$

Pair distribution function

By treating powder diffraction patterns using total scattering methods it is possible to study disorder in crystalline materials as well as nanocrystalline materials

The theoretical approach is identical to that for short range order and SAXS, starting with the total scattered intensity from a multi-atomic system

$$I(\vec{Q}) = \sum_n f_n(\vec{Q}) e^{i\vec{Q}\cdot\vec{r_n}} \sum_m f_m^*(\vec{Q}) e^{-i\vec{Q}\cdot\vec{r_m}} = \sum_{n,m} f_n(\vec{Q}) f_m^*(\vec{Q}) e^{i\vec{Q}\cdot(\vec{r_n}-\vec{r_m})}$$

$$= N\langle f(\vec{Q})^2\rangle + \sum_{n,m\neq n} f_m(\vec{Q}) f_n^*(\vec{Q}) e^{i\vec{Q}\cdot(\vec{r_n}-\vec{r_m})} = N\langle f(\vec{Q})^2\rangle + I_d(\vec{Q})$$

where the first term is simply the self-scattering from all the atoms in the sample and we define the discrete scattering intensity, $I_d(\vec{Q})$, as:

Pair distribution function

By treating powder diffraction patterns using total scattering methods it is possible to study disorder in crystalline materials as well as nanocrystalline materials

The theoretical approach is identical to that for short range order and SAXS, starting with the total scattered intensity from a multi-atomic system

$$I(\vec{Q}) = \sum_n f_n(\vec{Q}) e^{i\vec{Q}\cdot\vec{r_n}} \sum_m f_m^*(\vec{Q}) e^{-i\vec{Q}\cdot\vec{r_m}} = \sum_{n,m} f_n(\vec{Q}) f_m^*(\vec{Q}) e^{i\vec{Q}\cdot(\vec{r_n}-\vec{r_m})}$$

$$= N\langle f(\vec{Q})^2\rangle + \sum_{n,m\neq n} f_m(\vec{Q}) f_n^*(\vec{Q}) e^{i\vec{Q}\cdot(\vec{r_n}-\vec{r_m})} = N\langle f(\vec{Q})^2\rangle + I_d(\vec{Q})$$

where the first term is simply the self-scattering from all the atoms in the sample and we define the discrete scattering intensity, $I_d(\vec{Q})$, as:

$$I_d(\vec{Q}) = I_c(\vec{Q}) - N\langle f(\vec{Q})^2\rangle = \sum_{n,m\neq n} f_m(\vec{Q}) f_n^*(\vec{Q}) e^{i\vec{Q}\cdot(\vec{r_n}-\vec{r_m})}$$

Scattering factor

The total scattering structure function, $S(\vec{Q})$ is given in terms of the discrete scattering intensity

Scattering factor

The total scattering structure function, $S(\vec{Q})$ is given in terms of the discrete scattering intensity

$$S(\vec{Q}) - 1 = \frac{I_d(\vec{Q})}{N\langle f \rangle^2}$$

Scattering factor

The total scattering structure function, $S(\vec{Q})$ is given in terms of the discrete scattering intensity

$$S(\vec{Q}) - 1 = \frac{I_d(\vec{Q})}{N\langle f \rangle^2} = \frac{1}{N\langle f \rangle^2} \sum_{n,m \neq n} f_m(\vec{Q}) f_n^*(\vec{Q}) e^{i\vec{Q}\cdot(\vec{r_n} - \vec{r_m})}$$

where $\langle f \rangle$ is the sample averaged scattering power

Scattering factor

The total scattering structure function, $S(\vec{Q})$ is given in terms of the discrete scattering intensity

$$S(\vec{Q}) - 1 = \frac{I_d(\vec{Q})}{N\langle f \rangle^2} = \frac{1}{N\langle f \rangle^2} \sum_{n,m \neq n} f_m(\vec{Q}) f_n^*(\vec{Q}) e^{i\vec{Q}\cdot(\vec{r_n} - \vec{r_m})}$$

where $\langle f \rangle$ is the sample averaged scattering power

if $\vec{Q}$ is taken to be in the $\hat{z}$ direction and the sample is assumed to be isotropic, angular averaging gives

Scattering factor

The total scattering structure function, $S(\vec{Q})$ is given in terms of the discrete scattering intensity

$$S(\vec{Q}) - 1 = \frac{I_d(\vec{Q})}{N\langle f \rangle^2} = \frac{1}{N\langle f \rangle^2} \sum_{n,m \neq n} f_m(\vec{Q}) f_n^*(\vec{Q}) e^{i\vec{Q}\cdot(\vec{r_n} - \vec{r_m})}$$

where $\langle f \rangle$ is the sample averaged scattering power

if $\vec{Q}$ is taken to be in the $\hat{z}$ direction and the sample is assumed to be isotropic, angular averaging gives

$$S(Q) - 1 = \frac{1}{N\langle f \rangle^2} \sum_{n,m \neq n} f_m(Q) f_n^*(Q) \frac{\sin Q r_{mn}}{Q r_{mn}}$$

Scattering factor

The total scattering structure function, $S(\vec{Q})$ is given in terms of the discrete scattering intensity

$$S(\vec{Q}) - 1 = \frac{I_d(\vec{Q})}{N\langle f \rangle^2} = \frac{1}{N\langle f \rangle^2} \sum_{n,m \neq n} f_m(\vec{Q}) f_n^*(\vec{Q}) e^{i\vec{Q}\cdot(\vec{r_n} - \vec{r_m})}$$

where $\langle f \rangle$ is the sample averaged scattering power

if $\vec{Q}$ is taken to be in the $\hat{z}$ direction and the sample is assumed to be isotropic, angular averaging gives

$$S(Q) - 1 = \frac{1}{N\langle f \rangle^2} \sum_{n,m \neq n} f_m(Q) f_n^*(Q) \frac{\sin Q r_{mn}}{Q r_{mn}}$$

and the reduced total scattering structure function, $F(Q)$ is

Scattering factor

The total scattering structure function, $S(\vec{Q})$ is given in terms of the discrete scattering intensity

$$S(\vec{Q}) - 1 = \frac{I_d(\vec{Q})}{N\langle f \rangle^2} = \frac{1}{N\langle f \rangle^2} \sum_{n,m \neq n} f_m(\vec{Q}) f_n^*(\vec{Q}) e^{i\vec{Q}\cdot(\vec{r_n} - \vec{r_m})}$$

where $\langle f \rangle$ is the sample averaged scattering power

if $\vec{Q}$ is taken to be in the $\hat{z}$ direction and the sample is assumed to be isotropic, angular averaging gives

$$S(Q) - 1 = \frac{1}{N\langle f \rangle^2} \sum_{n,m \neq n} f_m(Q) f_n^*(Q) \frac{\sin Q r_{mn}}{Q r_{mn}}$$

and the reduced total scattering structure function, $F(Q)$ is

$$F(Q) = Q[S(Q) - 1]$$

Scattering factor

The total scattering structure function, $S(\vec{Q})$ is given in terms of the discrete scattering intensity

$$S(\vec{Q}) - 1 = \frac{I_d(\vec{Q})}{N\langle f \rangle^2} = \frac{1}{N\langle f \rangle^2} \sum_{n,m \neq n} f_m(\vec{Q}) f_n^*(\vec{Q}) e^{i\vec{Q}\cdot(\vec{r_n} - \vec{r_m})}$$

where $\langle f \rangle$ is the sample averaged scattering power

if $\vec{Q}$ is taken to be in the $\hat{z}$ direction and the sample is assumed to be isotropic, angular averaging gives

$$S(Q) - 1 = \frac{1}{N\langle f \rangle^2} \sum_{n,m \neq n} f_m(Q) f_n^*(Q) \frac{\sin Qr_{mn}}{Qr_{mn}}$$

and the reduced total scattering structure function, $F(Q)$ is

$$F(Q) = Q[S(Q) - 1] = \frac{1}{N\langle f \rangle^2} \sum_{n,m \neq n} f_m(Q) f_n^*(Q) \frac{\sin Qr_{mn}}{r_{mn}}$$

PDF modeling

$$F(Q) = Q[S(Q) - 1] = \frac{1}{N\langle f \rangle^2} \sum_{n,m \neq n} f_m(Q) f_n^*(Q) \frac{\sin Q r_{mn}}{r_{mn}}$$

PDF modeling

$$F(Q) = Q[S(Q) - 1] = \frac{1}{N\langle f \rangle^2} \sum_{n,m \neq n} f_m(Q) f_n^*(Q) \frac{\sin Q r_{mn}}{r_{mn}}$$

The experimental pair distribution function, $G(r)$ is computed by taking the sine-Fourier transform

PDF modeling

$$F(Q) = Q[S(Q) - 1] = \frac{1}{N\langle f \rangle^2} \sum_{n,m \neq n} f_m(Q) f_n^*(Q) \frac{\sin Qr_{mn}}{r_{mn}}$$

The experimental pair distribution function, $G(r)$ is computed by taking the sine-Fourier transform

$$G(r) = \frac{2}{\pi} \int_{Q_{min}}^{Q_{max}} F(Q) \sin Qr \, dQ$$

PDF modeling

$$F(Q) = Q[S(Q) - 1] = \frac{1}{N\langle f \rangle^2} \sum_{n,m \neq n} f_m(Q) f_n^*(Q) \frac{\sin Qr_{mn}}{r_{mn}}$$

The experimental pair distribution function, $G(r)$ is computed by taking the sine-Fourier transform

$$G(r) = \frac{2}{\pi} \int_{Q_{min}}^{Q_{max}} F(Q) \sin Qr \, dQ$$

but $G(r)$ can be calculated from a known structural model

PDF modeling

$$F(Q) = Q[S(Q) - 1] = \frac{1}{N\langle f \rangle^2} \sum_{n,m \neq n} f_m(Q) f_n^*(Q) \frac{\sin Qr_{mn}}{r_{mn}}$$

The experimental pair distribution function, $G(r)$ is computed by taking the sine-Fourier transform

$$G(r) = \frac{2}{\pi} \int_{Q_{min}}^{Q_{max}} F(Q) \sin Qr \, dQ$$

but $G(r)$ can be calculated from a known structural model

$$G(r) = 4\pi r[\rho(r) - \rho_0],$$

PDF modeling

$$F(Q) = Q[S(Q) - 1] = \frac{1}{N\langle f \rangle^2} \sum_{n,m \neq n} f_m(Q) f_n^*(Q) \frac{\sin Q r_{mn}}{r_{mn}}$$

The experimental pair distribution function, $G(r)$ is computed by taking the sine-Fourier transform

$$G(r) = \frac{2}{\pi} \int_{Q_{min}}^{Q_{max}} F(Q) \sin Qr \, dQ$$

but $G(r)$ can be calculated from a known structural model

$$G(r) = 4\pi r[\rho(r) - \rho_0], \qquad \rho(r) = \frac{1}{4\pi r^2 N\langle f \rangle^2} \sum_{n,m \neq n} Z_m Z_n \delta(r - r_{mn})$$

PDF modeling

$$F(Q) = Q[S(Q) - 1] = \frac{1}{N\langle f \rangle^2} \sum_{n,m \neq n} f_m(Q) f_n^*(Q) \frac{\sin Qr_{mn}}{r_{mn}}$$

The experimental pair distribution function, $G(r)$ is computed by taking the sine-Fourier transform

$$G(r) = \frac{2}{\pi} \int_{Q_{min}}^{Q_{max}} F(Q) \sin Qr \, dQ$$

but $G(r)$ can be calculated from a known structural model

$$G(r) = 4\pi r[\rho(r) - \rho_0], \qquad \rho(r) = \frac{1}{4\pi r^2 N\langle f \rangle^2} \sum_{n,m \neq n} Z_m Z_n \delta(r - r_{mn})$$

where ρ_0 is the atomic number density, $\rho(r)$ is the atomic pair density, and r_{mn} is the distance between atoms m and n

PDF modeling

$$F(Q) = Q[S(Q) - 1] = \frac{1}{N\langle f \rangle^2} \sum_{n,m \neq n} f_m(Q) f_n^*(Q) \frac{\sin Q r_{mn}}{r_{mn}}$$

The experimental pair distribution function, $G(r)$ is computed by taking the sine-Fourier transform

$$G(r) = \frac{2}{\pi} \int_{Q_{min}}^{Q_{max}} F(Q) \sin Qr \, dQ$$

but $G(r)$ can be calculated from a known structural model

$$G(r) = 4\pi r[\rho(r) - \rho_0], \qquad \rho(r) = \frac{1}{4\pi r^2 N\langle f \rangle^2} \sum_{n,m \neq n} Z_m Z_n \delta(r - r_{mn})$$

where ρ_0 is the atomic number density, $\rho(r)$ is the atomic pair density, and r_{mn} is the distance between atoms m and n

So what does the pair distribution function look like in practice?

PDF processing: $F(Q)$

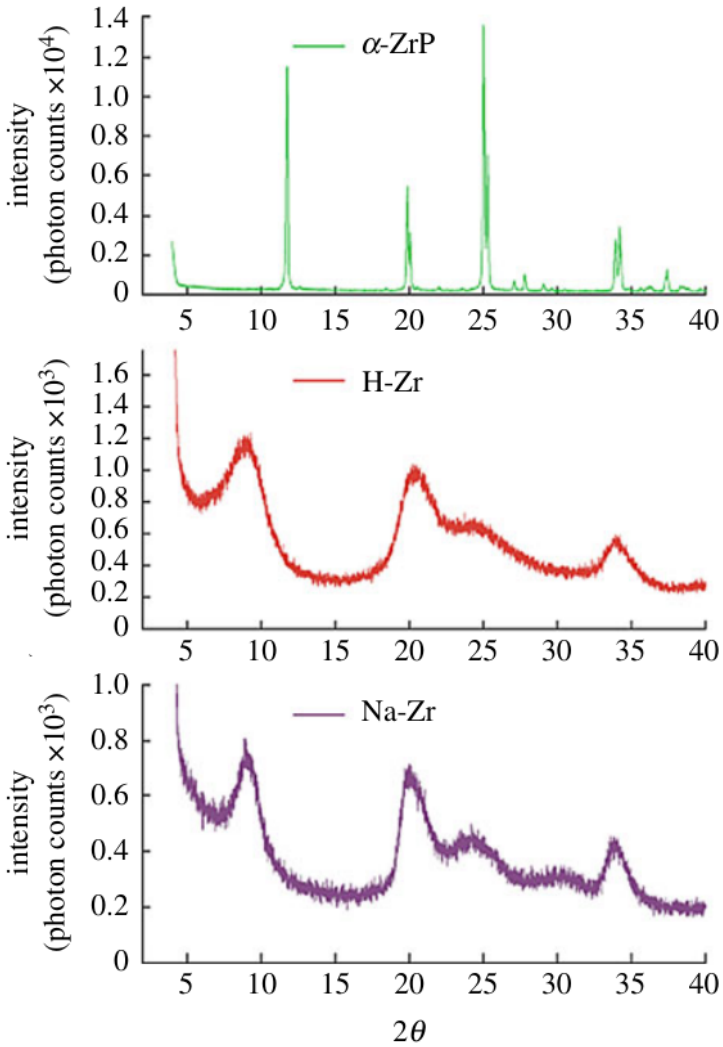

PDF processing: $F(Q)$

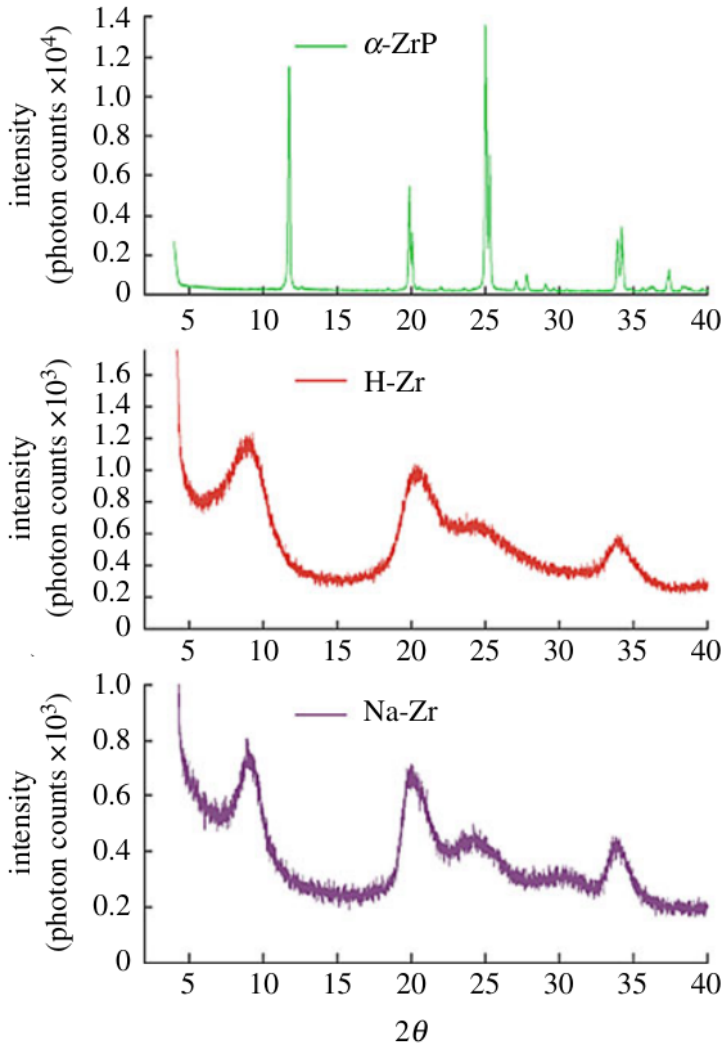

The broad peaks of nanoparticle systems still contains information once processed into the reduced total scattering function

PDF processing: $F(Q)$

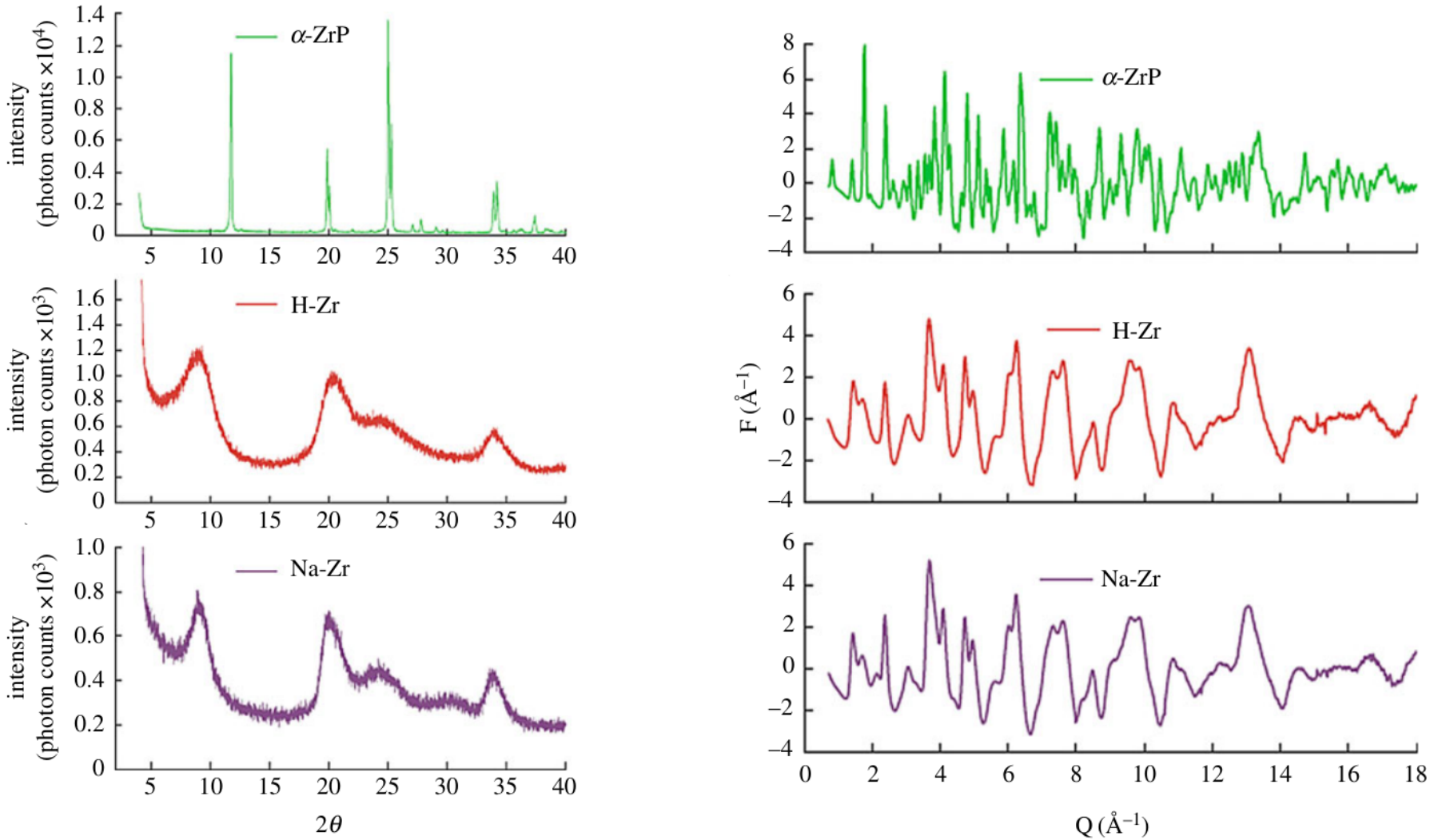

The broad peaks of nanoparticle systems still contains information once processed into the reduced total scattering function

PDF processing: $G(r)$

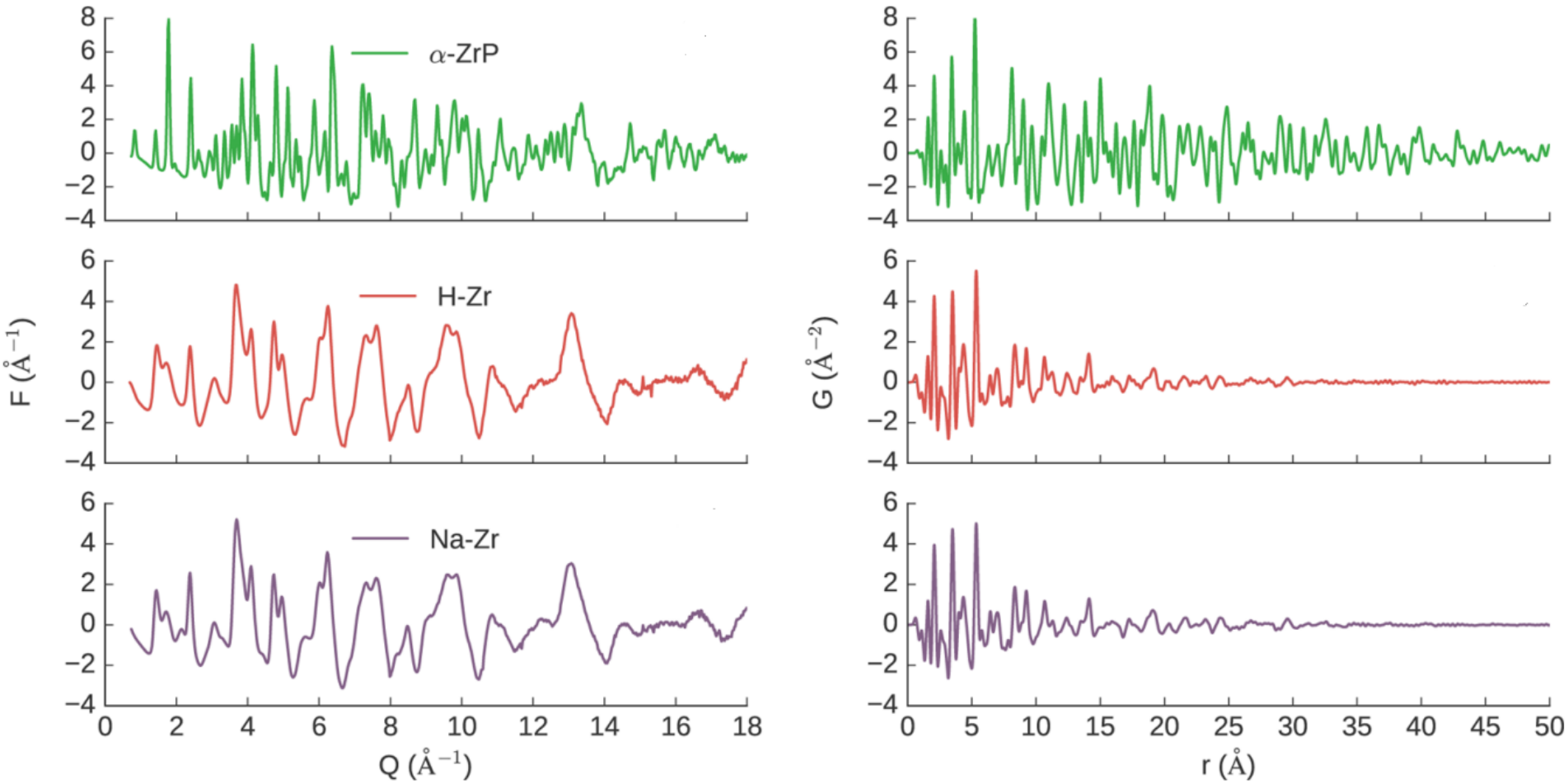

"Local environment of terbium(III) ions in layered nanocrystalline zirconium(IV) phosphate – phosphate ion exchange materials," M.W. Terban, et al. *Inorg. Chem.* **56**, 8837-8846 (2017).

PDF processing: $G(r)$

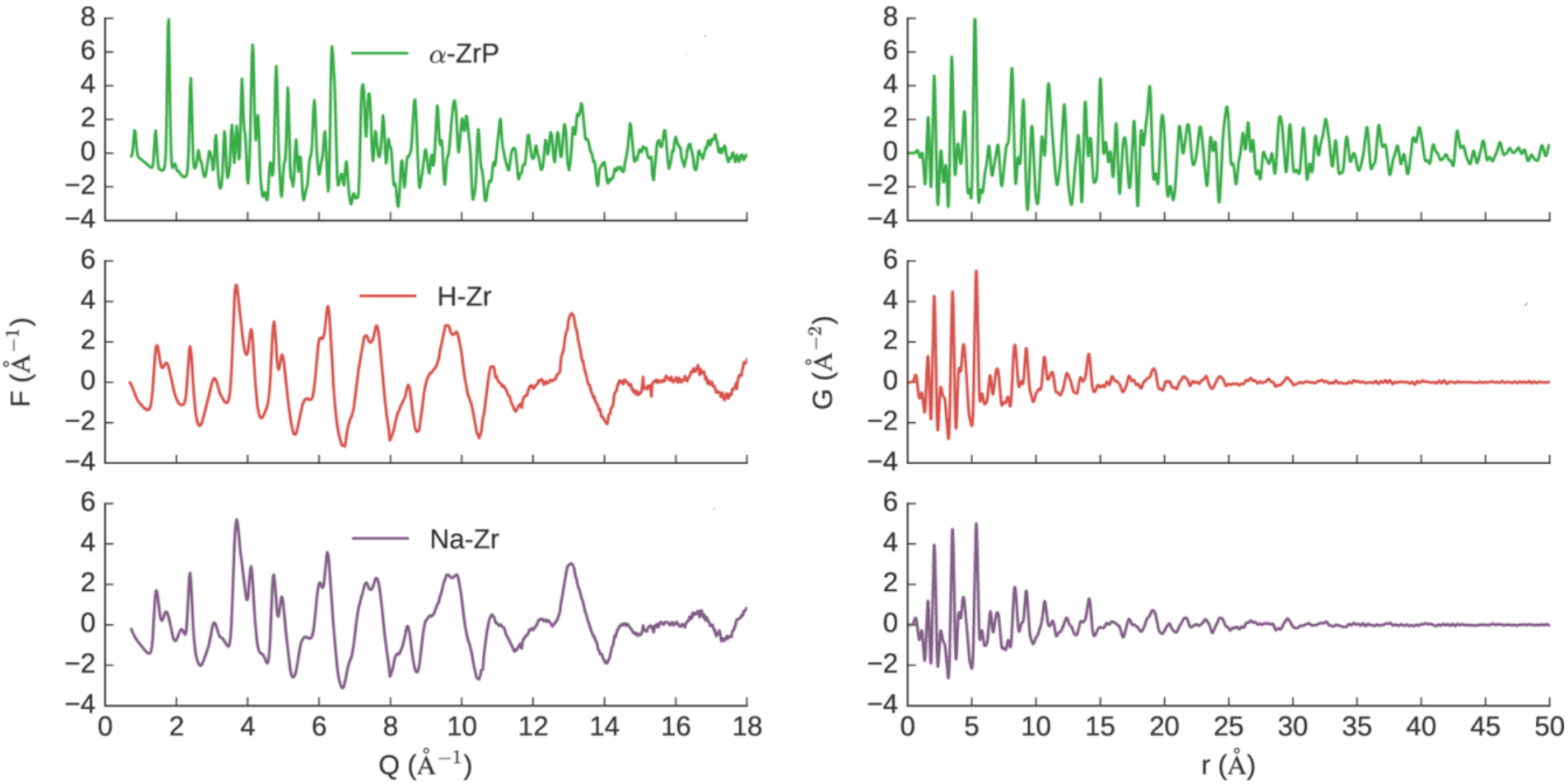

When Fourier transformed, the significant differences in crystalline and nanoparticulate samples are obvious

"Local environment of terbium(III) ions in layered nanocrystalline zirconium(IV) phosphate – phosphate ion exchange materials," M.W. Terban, et al. *Inorg. Chem.* **56**, 8837-8846 (2017).

PDF structure of CdSe nanoparticles

The goal of this study was to compare the PDF structures of CdSe nanoparticles of various sizes with the results obtained from traditional analysis of optical data and electron microscopy

"Quantitative size-dependent structure and strain determination of CdSe nanoparticles using atomic pair distribution function analysis," A.S. Masadeh, et al. *Phys. Rev. B* **76**, 115413 (2007).

PDF structure of CdSe nanoparticles

The goal of this study was to compare the PDF structures of CdSe nanoparticles of various sizes with the results obtained from traditional analysis of optical data and electron microscopy

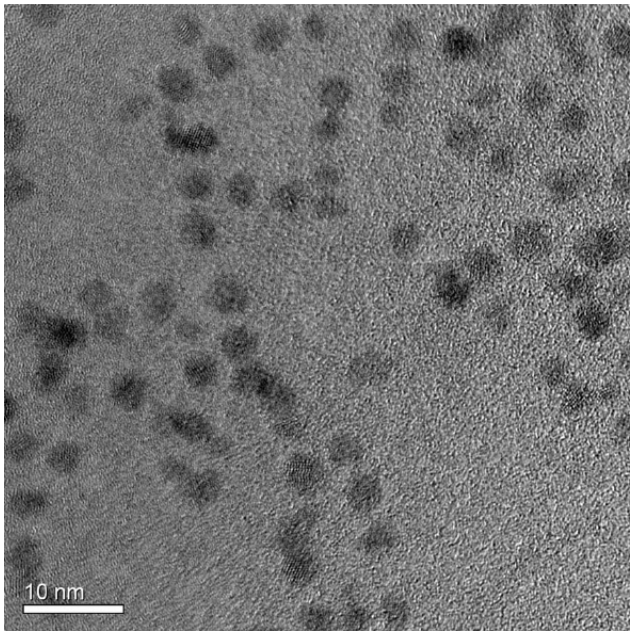

Nanoparticles of of three different sizes were obtained by changing the nucleation time from 1200 s (left)

"Quantitative size-dependent structure and strain determination of CdSe nanoparticles using atomic pair distribution function analysis," A.S. Masadeh, et al. *Phys. Rev. B* **76**, 115413 (2007).

PDF structure of CdSe nanoparticles

The goal of this study was to compare the PDF structures of CdSe nanoparticles of various sizes with the results obtained from traditional analysis of optical data and electron microscopy

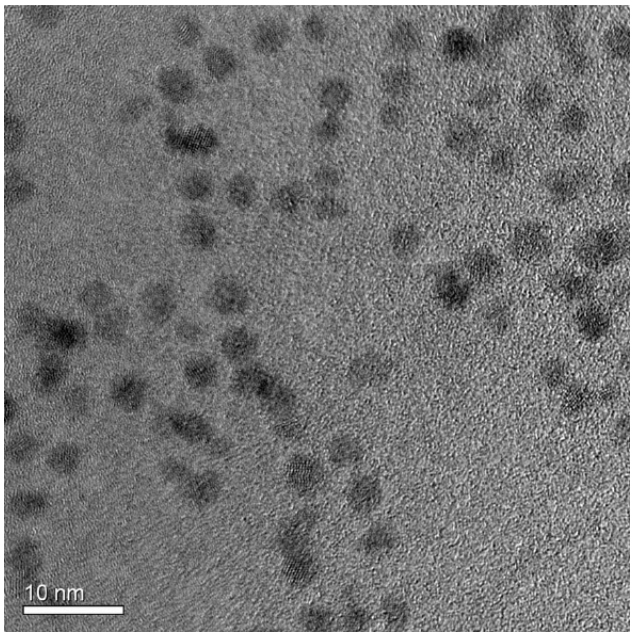

Nanoparticles of of three different sizes were obtained by changing the nucleation time from 1200 s (left) to 15 s (right) during synthesis

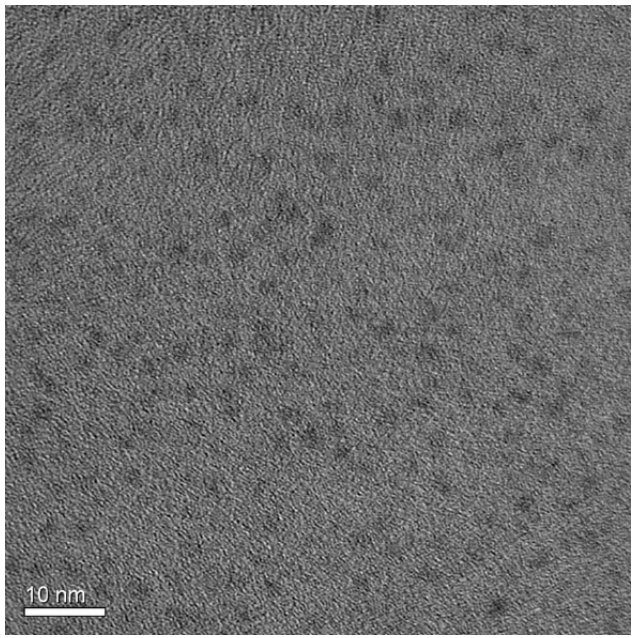

"Quantitative size-dependent structure and strain determination of CdSe nanoparticles using atomic pair distribution function analysis," A.S. Masadeh, et al. *Phys. Rev. B* **76**, 115413 (2007).

PDF structure of CdSe nanoparticles

The goal of this study was to compare the PDF structures of CdSe nanoparticles of various sizes with the results obtained from traditional analysis of optical data and electron microscopy

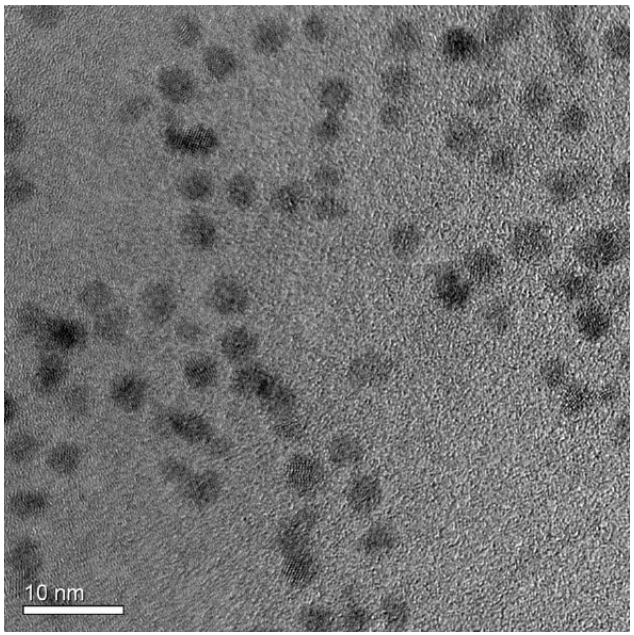

Nanoparticles of of three different sizes were obtained by changing the nucleation time from 1200 s (left) to 15 s (right) during synthesis

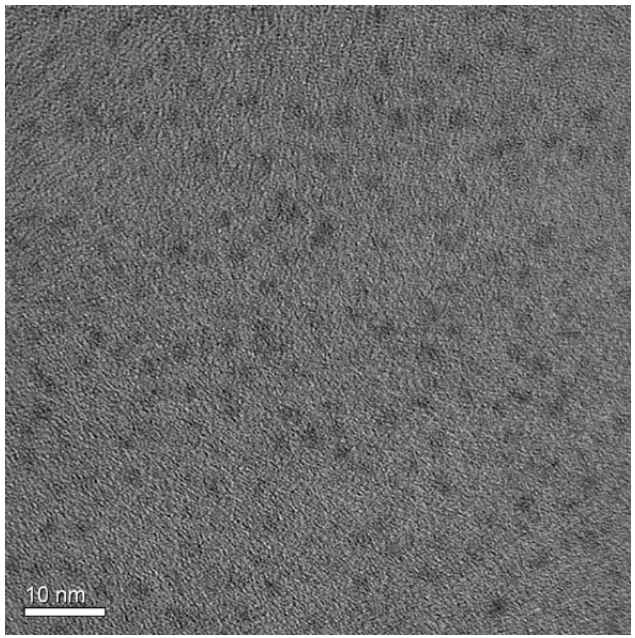

Optical absorbance and fluorescence indicates that the particle sizes range from 3.5 nm to 2.0 nm

"Quantitative size-dependent structure and strain determination of CdSe nanoparticles using atomic pair distribution function analysis," A.S. Masadeh, et al. *Phys. Rev. B* **76**, 115413 (2007).

PDF data collection

Diffraction data were collected at APS beamline 6-IDD with incident 87 keV x-rays on a 2D image plate detector

"Quantitative size-dependent structure and strain determination of CdSe nanoparticles using atomic pair distribution function analysis," A.S. Masadeh, et al. *Phys. Rev. B* **76**, 115413 (2007).

PDF data collection

Diffraction data were collected at APS beamline 6-IDD with incident 87 keV x-rays on a 2D image plate detector

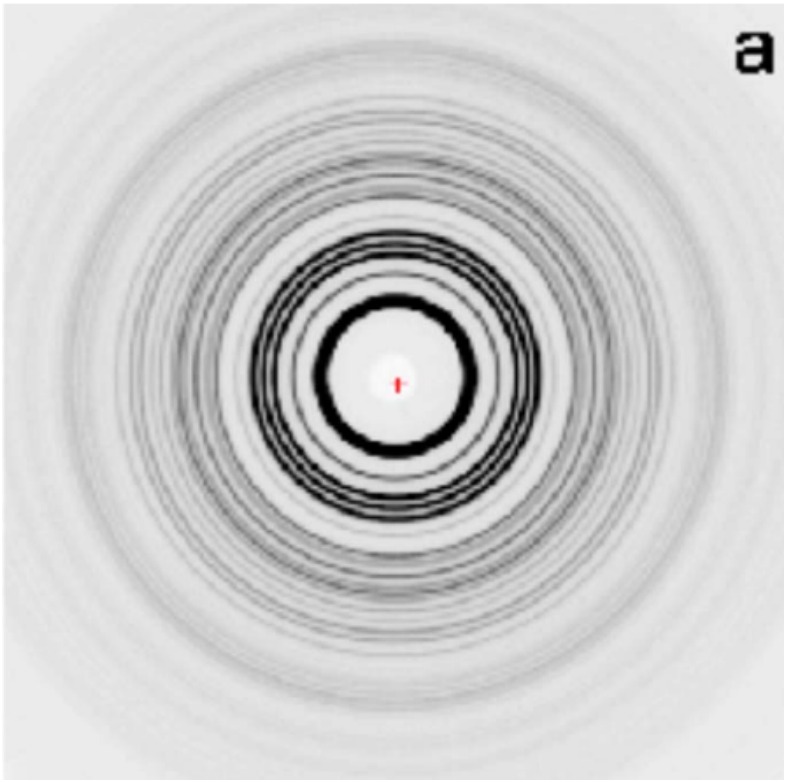

Data were collected on bulk CdSe (left)

"Quantitative size-dependent structure and strain determination of CdSe nanoparticles using atomic pair distribution function analysis," A.S. Masadeh, et al. *Phys. Rev. B* **76**, 115413 (2007).

PDF data collection

Diffraction data were collected at APS beamline 6-IDD with incident 87 keV x-rays on a 2D image plate detector

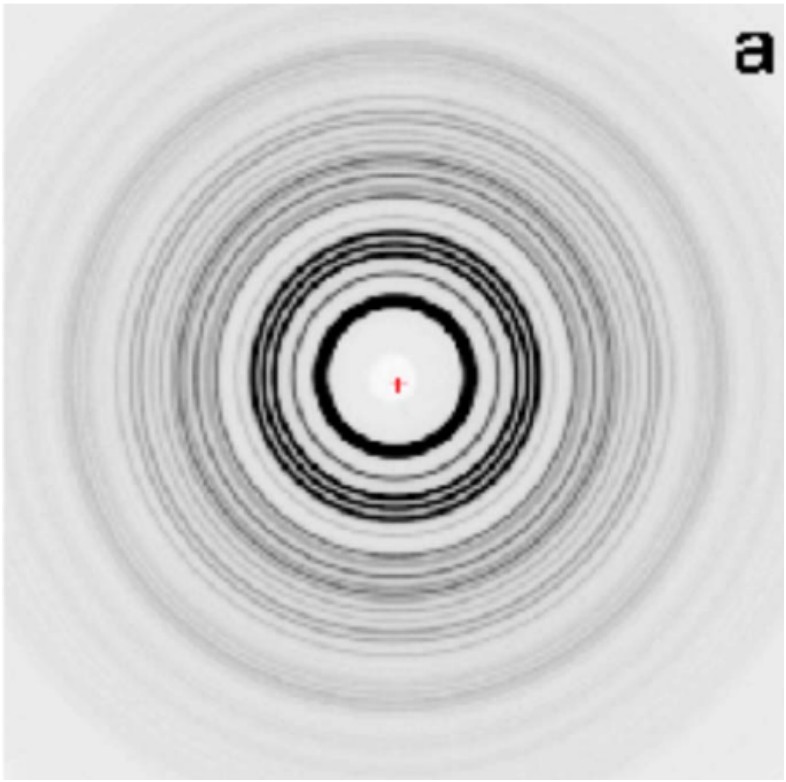

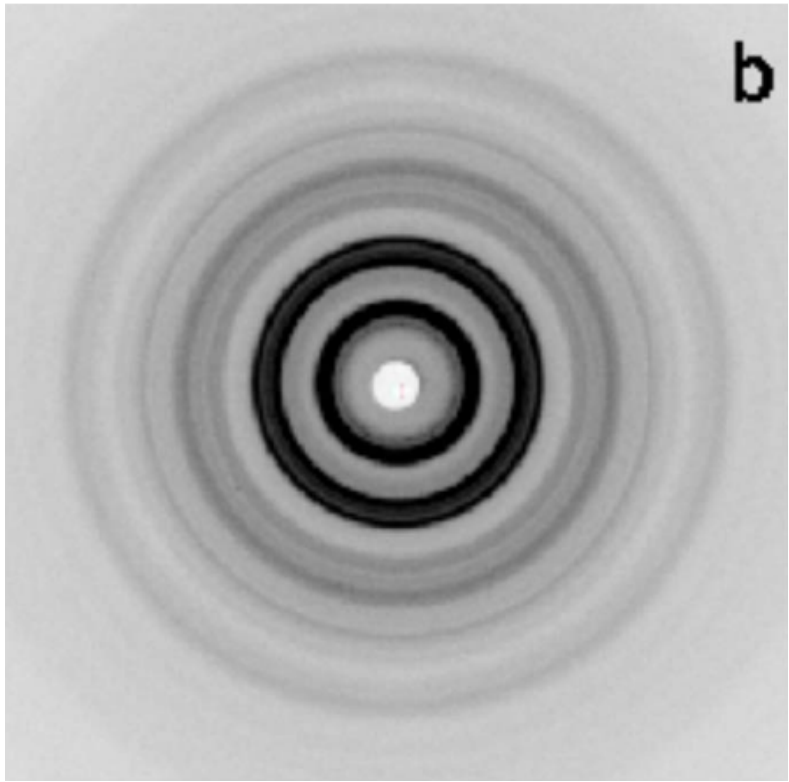

Data were collected on bulk CdSe (left) and the CdSe nanoparticles (right) then azimuthally integrated to get the powder pattern

"Quantitative size-dependent structure and strain determination of CdSe nanoparticles using atomic pair distribution function analysis," A.S. Masadeh, et al. *Phys. Rev. B* **76**, 115413 (2007).

$F(Q)$ and $G(r)$

The data for bulk and nanoparticle samples was processed to obtain $F(Q)$ and $G(r)$ in preparation for structural modeling

"Quantitative size-dependent structure and strain determination of CdSe nanoparticles using atomic pair distribution function analysis," A.S. Masadeh, et al. *Phys. Rev. B* **76**, 115413 (2007).

$F(Q)$ and $G(r)$

The data for bulk and nanoparticle samples was processed to obtain $F(Q)$ and $G(r)$ in preparation for structural modeling

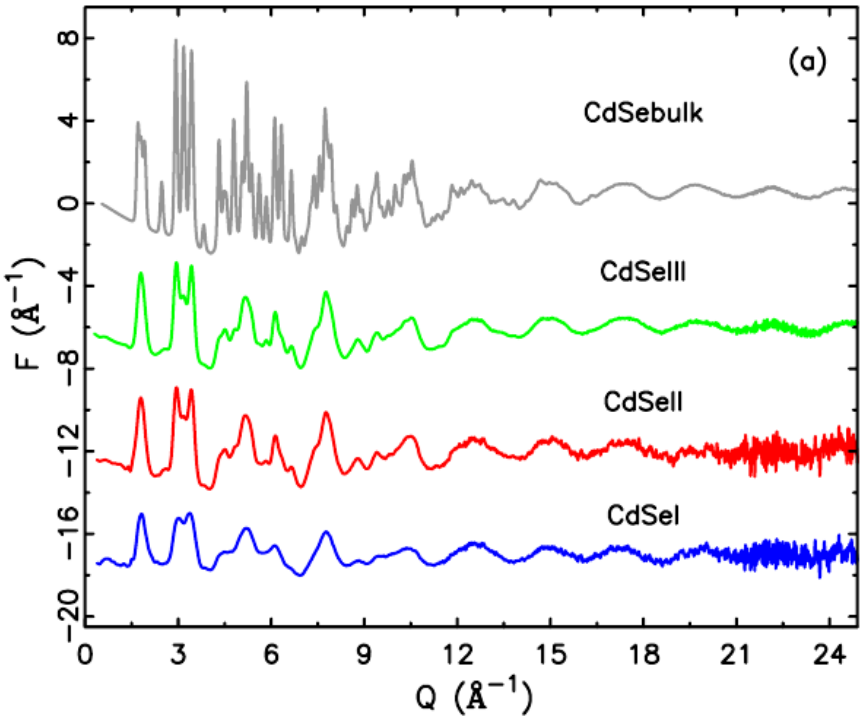

"Quantitative size-dependent structure and strain determination of CdSe nanoparticles using atomic pair distribution function analysis," A.S. Masadeh, et al. *Phys. Rev. B* **76**, 115413 (2007).

$F(Q)$ and $G(r)$

The data for bulk and nanoparticle samples was processed to obtain $F(Q)$ and $G(r)$ in preparation for structural modeling

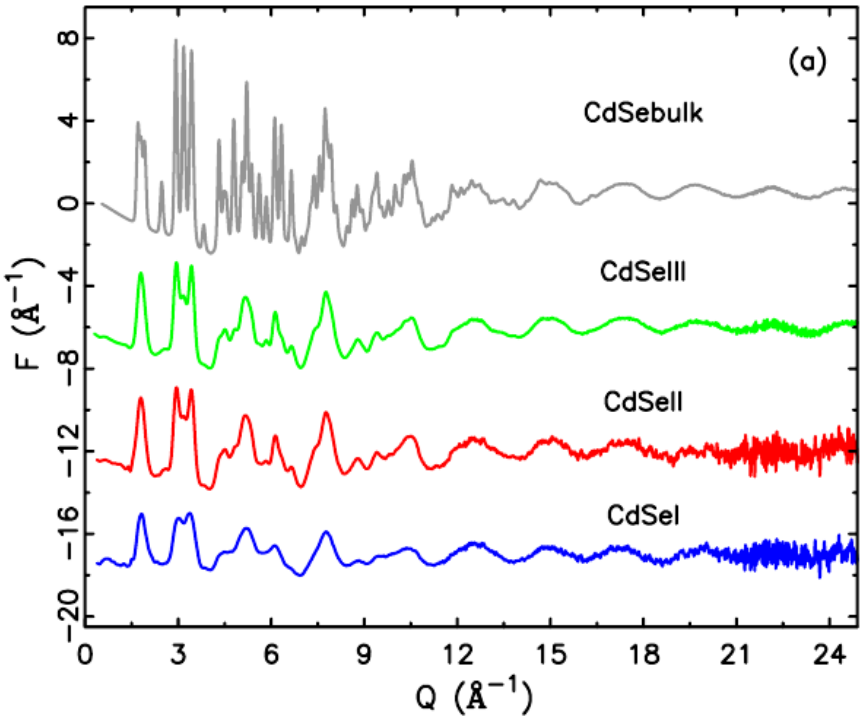

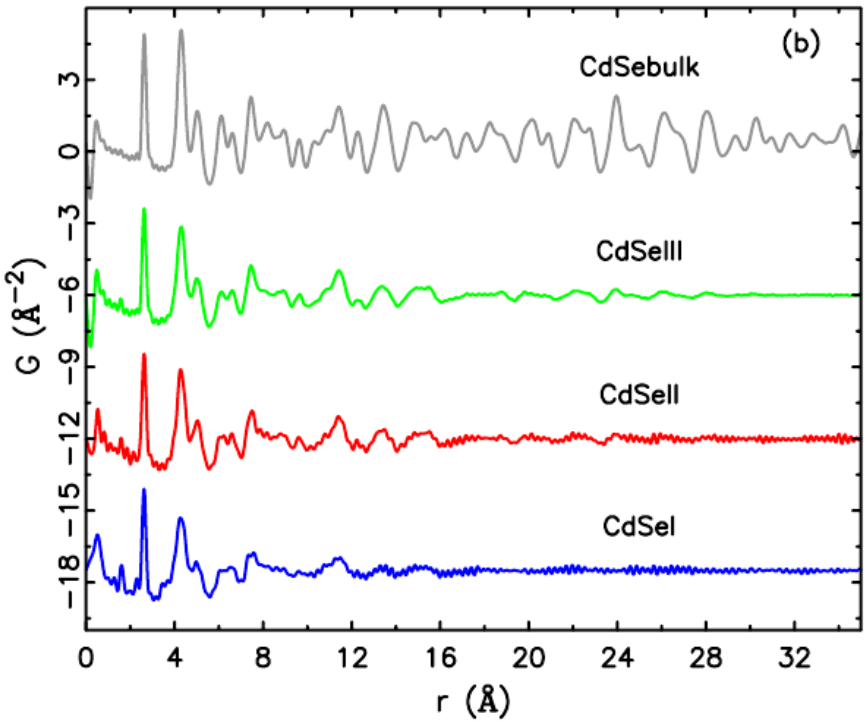

"Quantitative size-dependent structure and strain determination of CdSe nanoparticles using atomic pair distribution function analysis," A.S. Masadeh, et al. *Phys. Rev. B* **76**, 115413 (2007).

$F(Q)$ and $G(r)$

The data for bulk and nanoparticle samples was processed to obtain $F(Q)$ and $G(r)$ in preparation for structural modeling

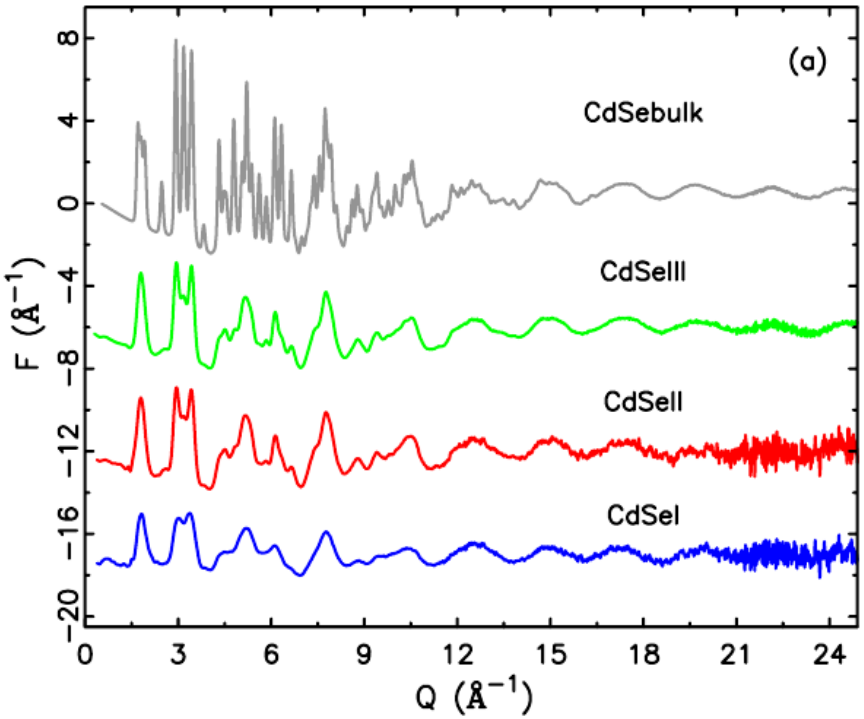

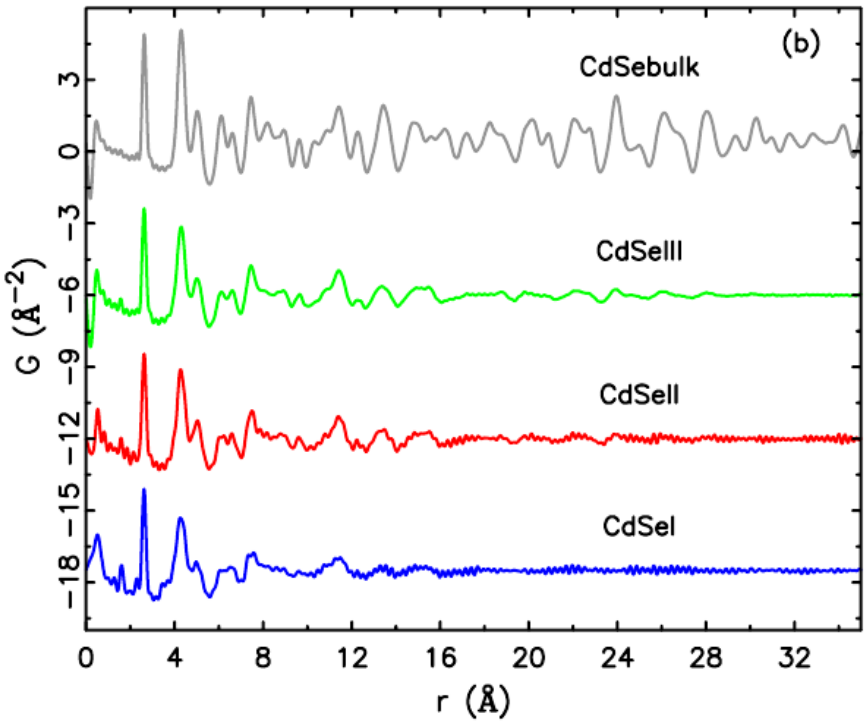

The particle size progression shows in the range over which the $G(r)$ has distinct peak structure

"Quantitative size-dependent structure and strain determination of CdSe nanoparticles using atomic pair distribution function analysis," A.S. Masadeh, et al. *Phys. Rev. B* **76**, 115413 (2007).

Initial modeling

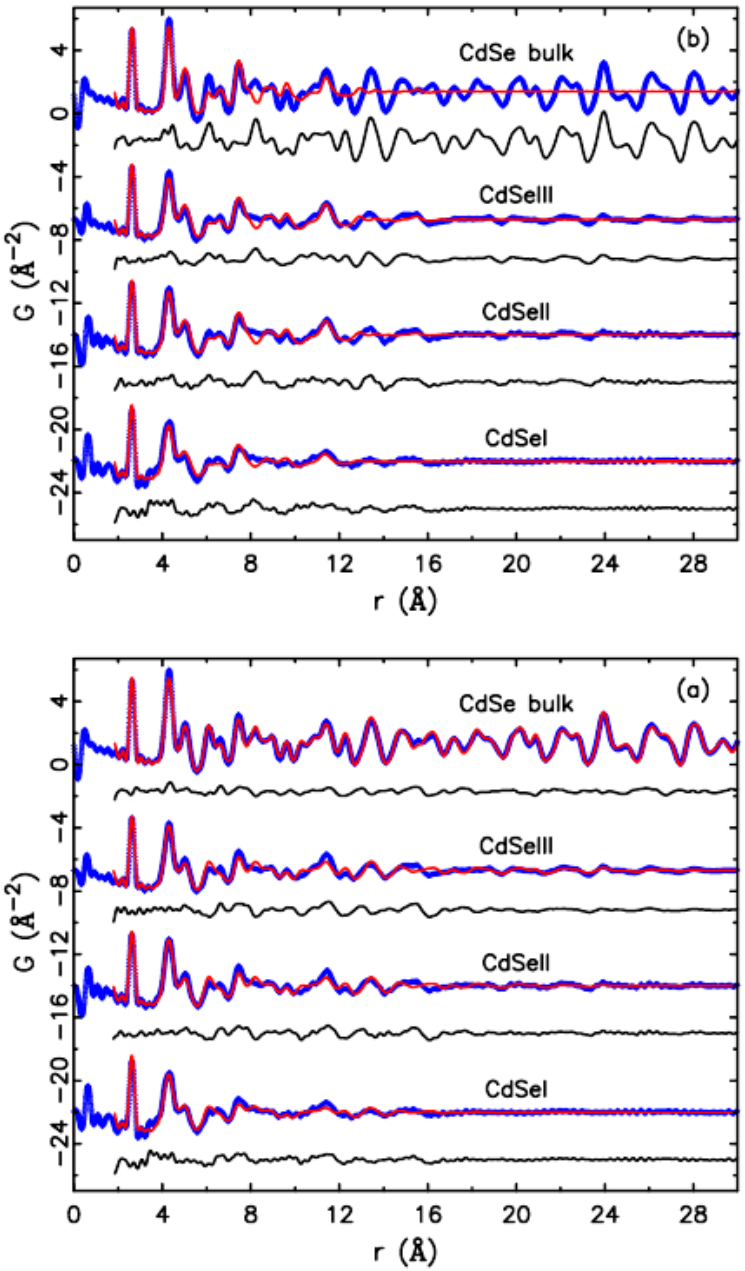

The top panel shows the fit to the data using the wurtzite structure which has ABAB stacking of hexagonal planes

"Quantitative size-dependent structure and strain determination of CdSe nanoparticles using atomic pair distribution function analysis," A.S. Masadeh, et al. *Phys. Rev. B* **76**, 115413 (2007).

Initial modeling

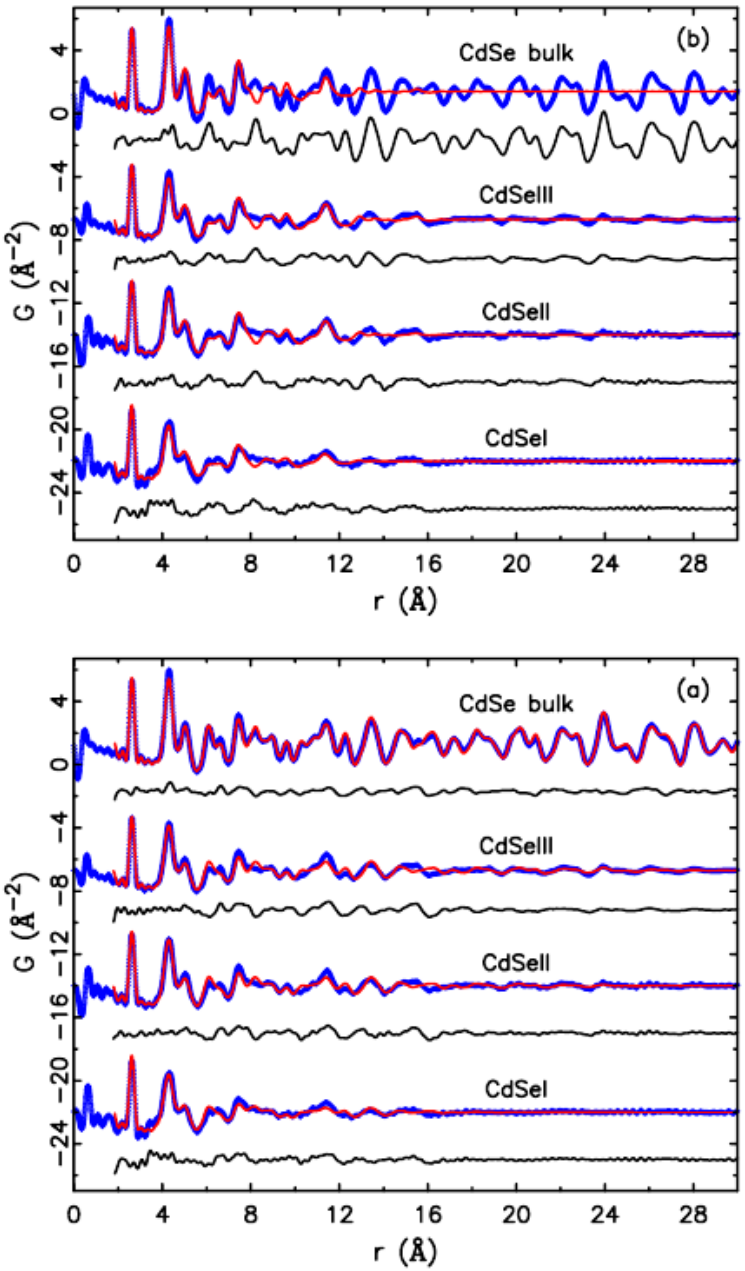

The top panel shows the fit to the data using the wurtzite structure which has ABAB stacking of hexagonal planes

The bottom panel shows the fit using the zinc blende structure with ABC stacking

"Quantitative size-dependent structure and strain determination of CdSe nanoparticles using atomic pair distribution function analysis," A.S. Masadeh, et al. *Phys. Rev. B* **76**, 115413 (2007).

Initial modeling

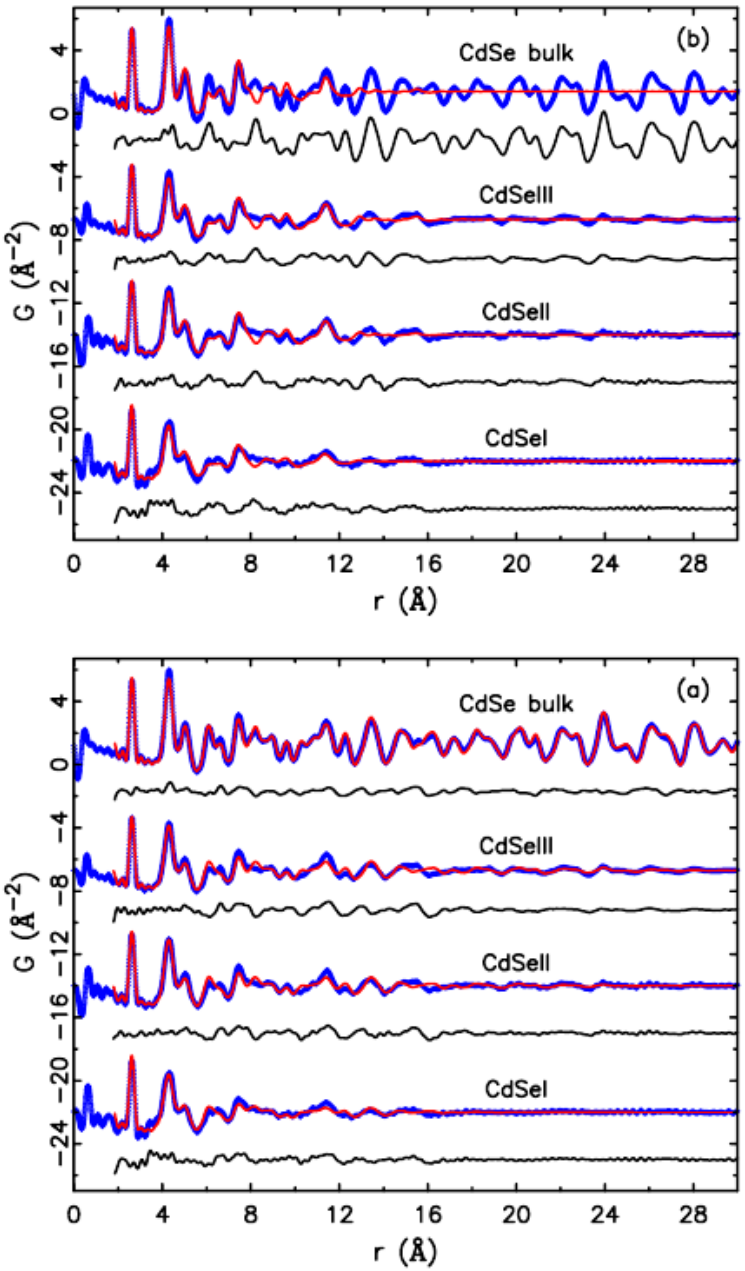

The top panel shows the fit to the data using the wurtzite structure which has ABAB stacking of hexagonal planes

The bottom panel shows the fit using the zinc blende structure with ABC stacking

While the zinc blende does slightly better at fitting the experimental data, it is clear that neither is perfect for the builk or the nanoparticles

"Quantitative size-dependent structure and strain determination of CdSe nanoparticles using atomic pair distribution function analysis," A.S. Masadeh, et al. *Phys. Rev. B* **76**, 115413 (2007).

Initial modeling

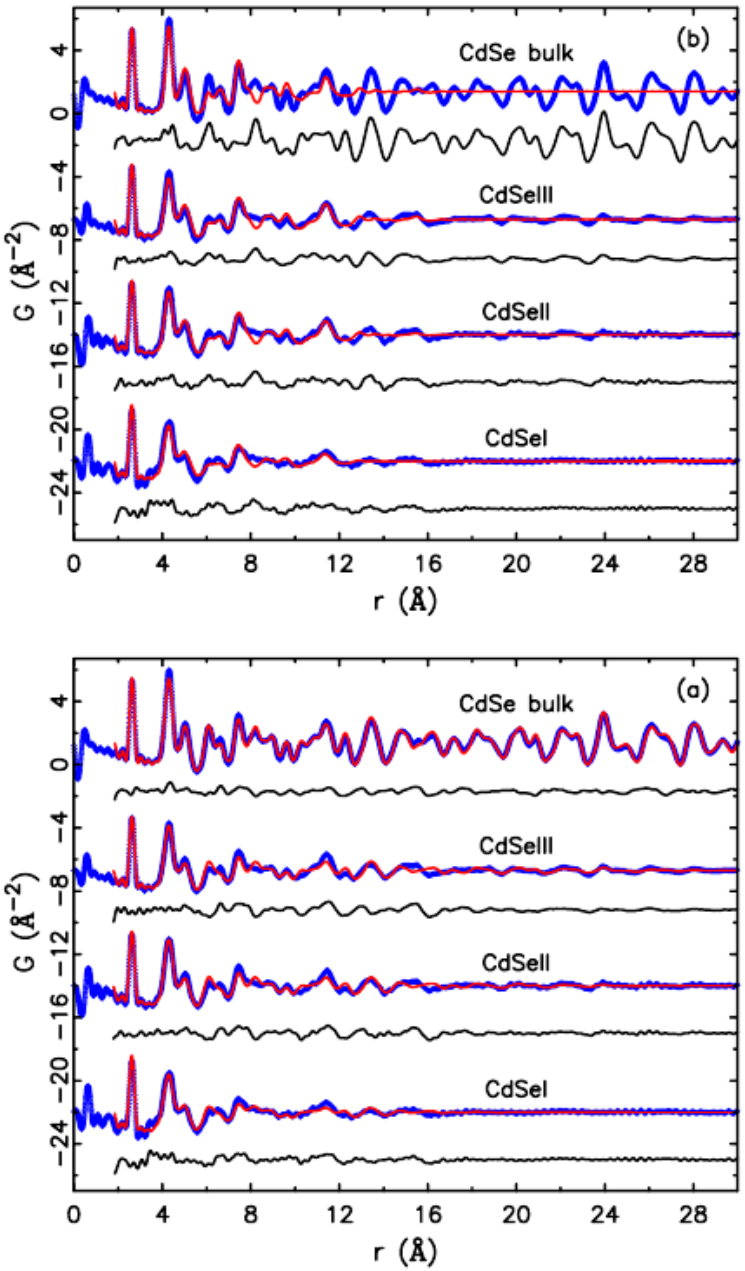

The top panel shows the fit to the data using the wurtzite structure which has ABAB stacking of hexagonal planes

The bottom panel shows the fit using the zinc blende structure with ABC stacking

While the zinc blende does slightly better at fitting the experimental data, it is clear that neither is perfect for the builk or the nanoparticles

It is likely that a better fit can be obtained using a mixture of the two stacking arrangements

"Quantitative size-dependent structure and strain determination of CdSe nanoparticles using atomic pair distribution function analysis," A.S. Masadeh, et al. *Phys. Rev. B* **76**, 115413 (2007).

Final structural models

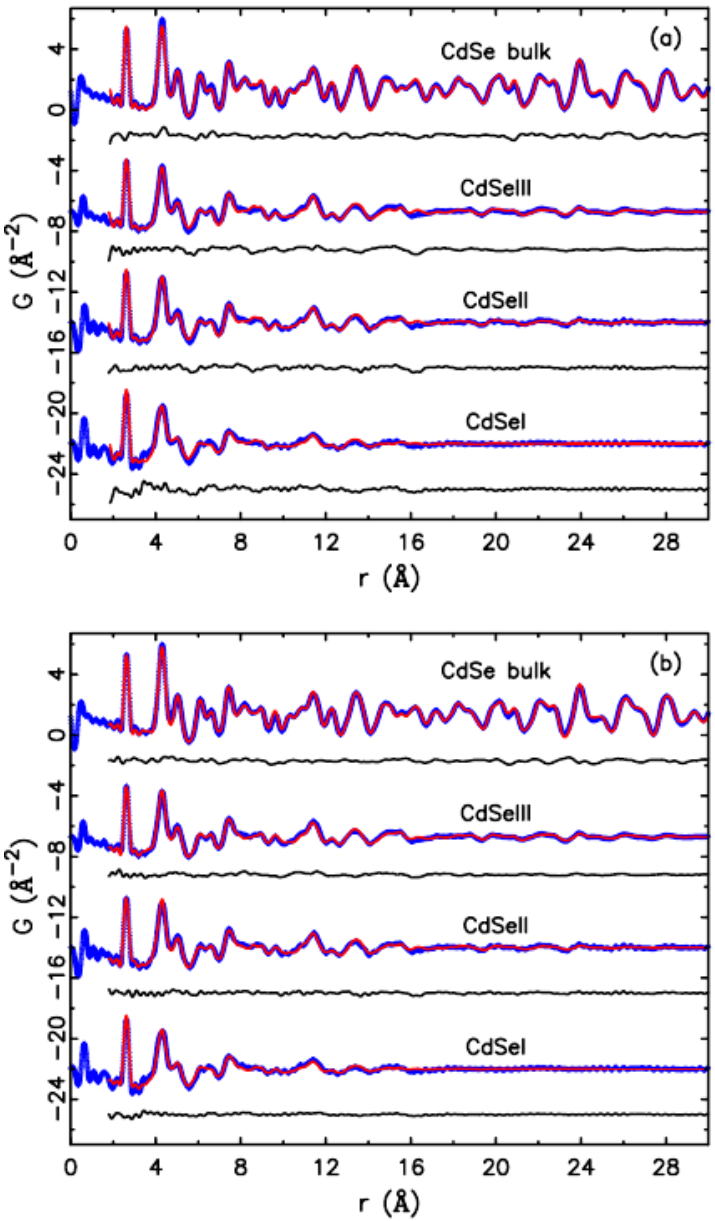

The top panel shows a fit using both wurtzite and zinc blende which fits much better for all particles

"Quantitative size-dependent structure and strain determination of CdSe nanoparticles using atomic pair distribution function analysis," A.S. Masadeh, et al. *Phys. Rev. B* **76**, 115413 (2007).

Final structural models

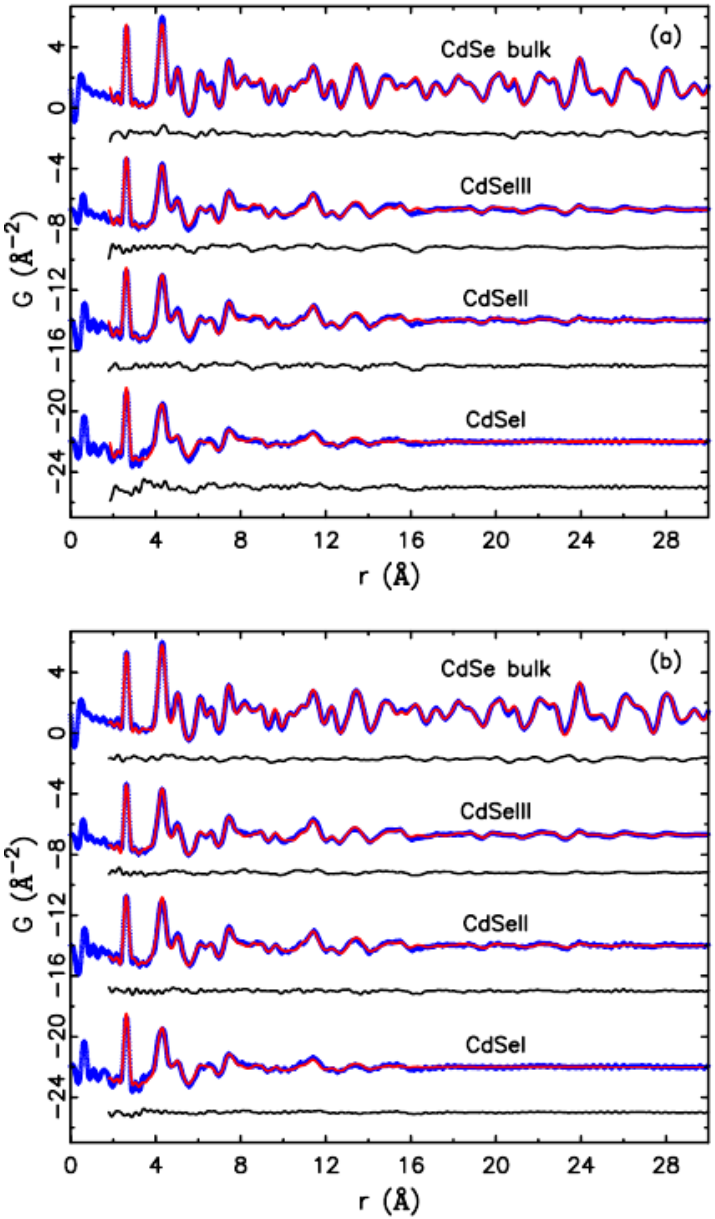

The top panel shows a fit using both wurtzite and zinc blende which fits much better for all particles

An even better fit is obtained by including a variable number of stacking faults in the model (i.e. transitions between wurtzite and zinc blende structures)

"Quantitative size-dependent structure and strain determination of CdSe nanoparticles using atomic pair distribution function analysis," A.S. Masadeh, et al. *Phys. Rev. B* **76**, 115413 (2007).

Final structural models

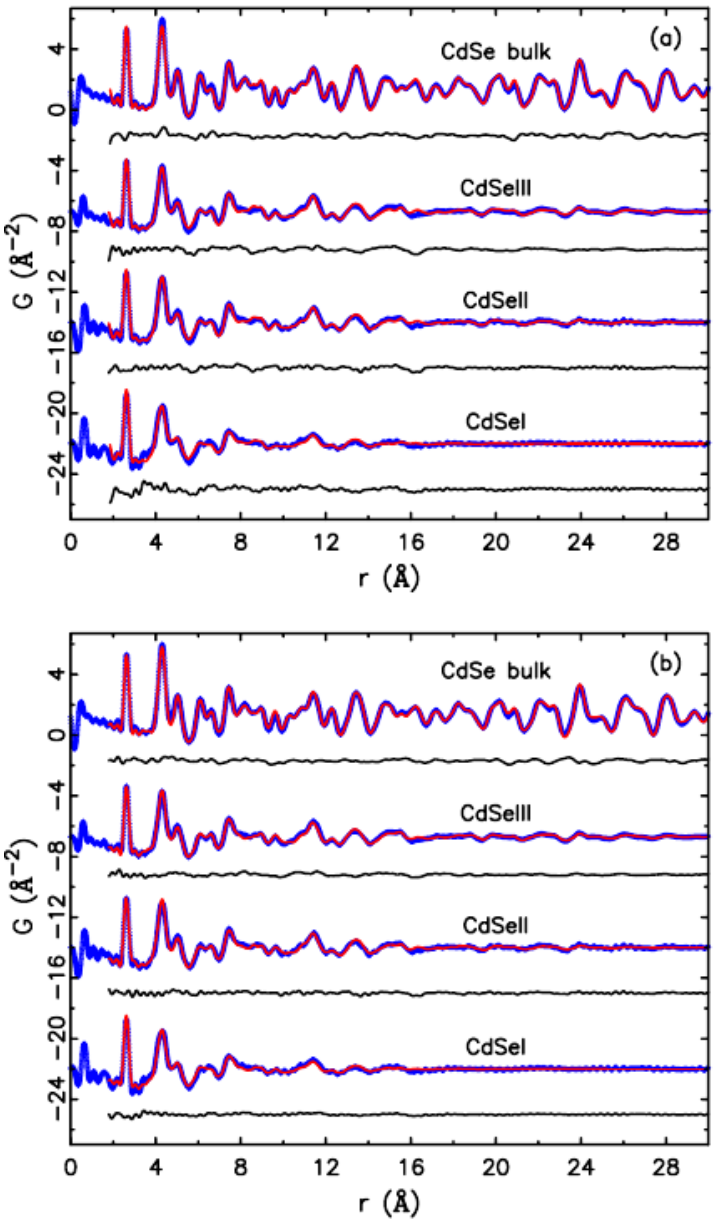

The top panel shows a fit using both wurtzite and zinc blende which fits much better for all particles

An even better fit is obtained by including a variable number of stacking faults in the model (i.e. transitions between wurtzite and zinc blende structures)

The final values obtained in the fitting give particle sizes consistent with TEM and optical measurements. The fits also show that the bulk sample has only about 33% stacking faults while the nanoparticles have 50%

"Quantitative size-dependent structure and strain determination of CdSe nanoparticles using atomic pair distribution function analysis," A.S. Masadeh, et al. *Phys. Rev. B* **76**, 115413 (2007).

Kinematical vs. dynamical diffraction

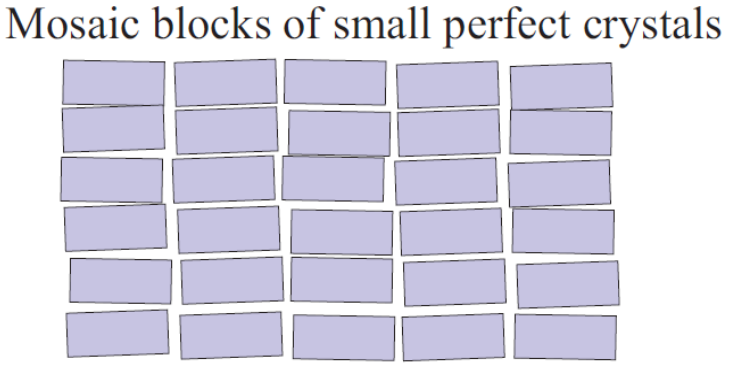

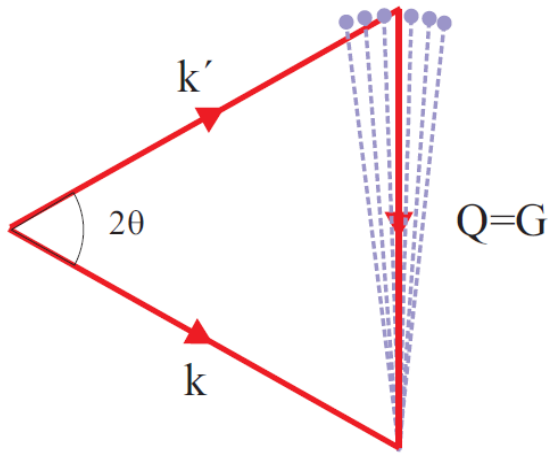

The kinematical approximation we have discussed so far applies to mosaic crystals. The size of the crystal is small enough that the wave field of the x-rays does not vary appreciably over the crystal.

Kinematical vs. dynamical diffraction

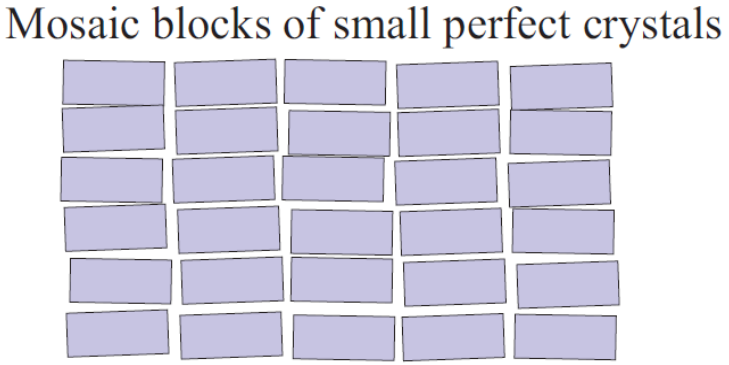

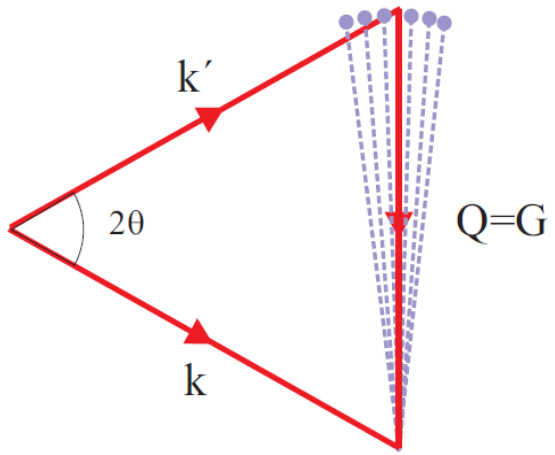

The kinematical approximation we have discussed so far applies to mosaic crystals. The size of the crystal is small enough that the wave field of the x-rays does not vary appreciably over the crystal.

For a perfect crystal, such as those used in monochromators, things are very different and we have to treat them specially using dynamical diffraction theory.

Kinematical vs. dynamical diffraction

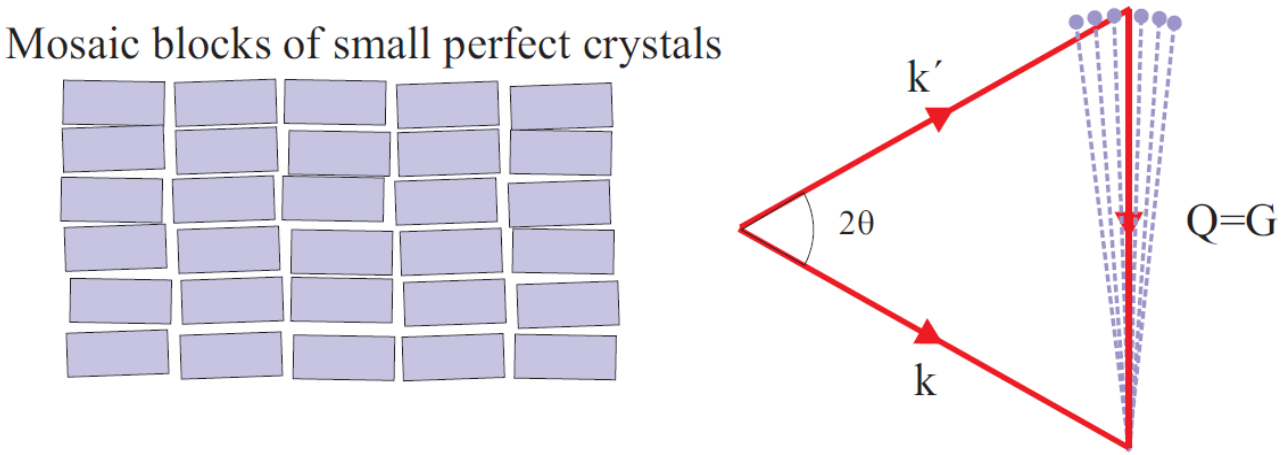

The kinematical approximation we have discussed so far applies to mosaic crystals. The size of the crystal is small enough that the wave field of the x-rays does not vary appreciably over the crystal.

For a perfect crystal, such as those used in monochromators, things are very different and we have to treat them specially using dynamical diffraction theory.

This theory takes into account multiple reflections, and attenuation of the x-ray beam as it propagates through the perfect crystal.

Bragg & Laue geometries

Bragg & Laue geometries

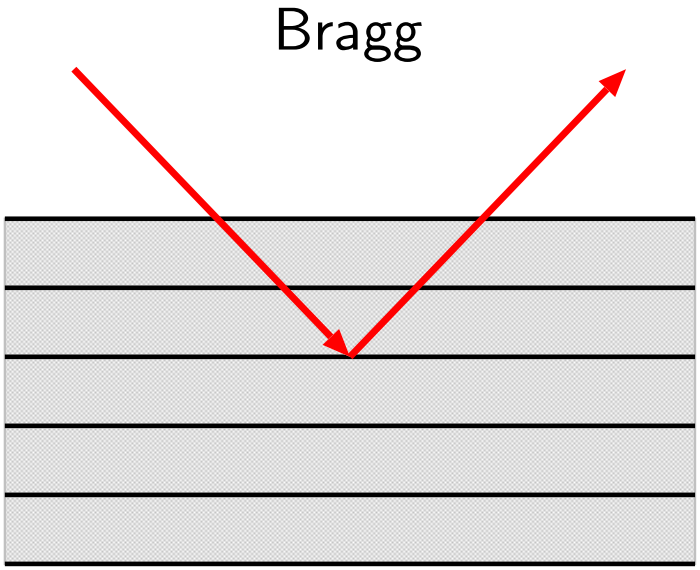

symmetric

Bragg & Laue geometries

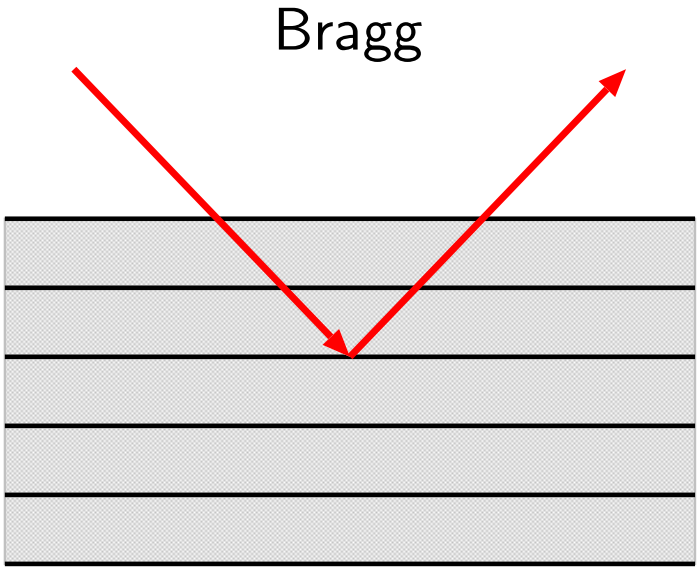

symmetric

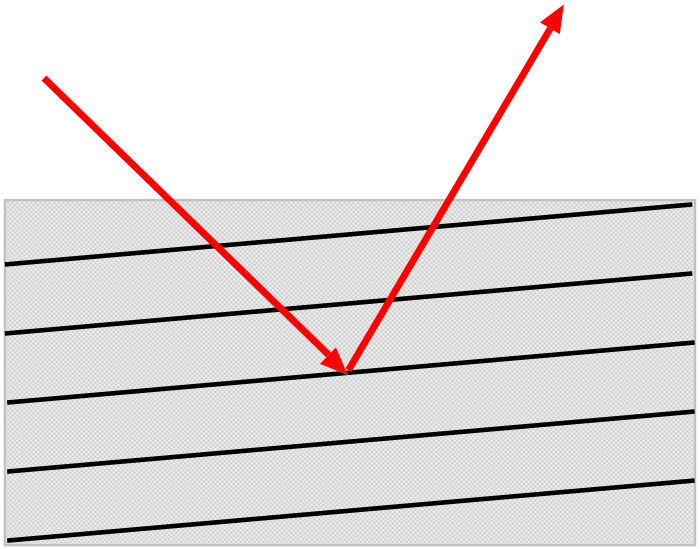

asymmetric

Bragg & Laue geometries

Bragg

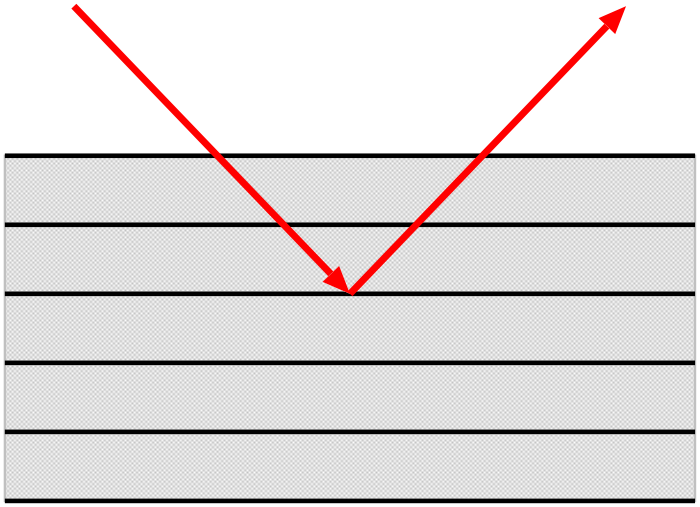

symmetric

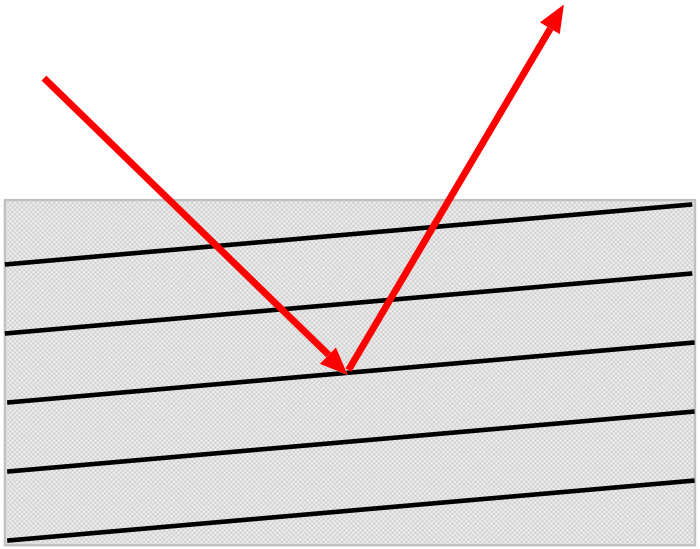

asymmetric

Laue

Bragg & Laue geometries

Bragg

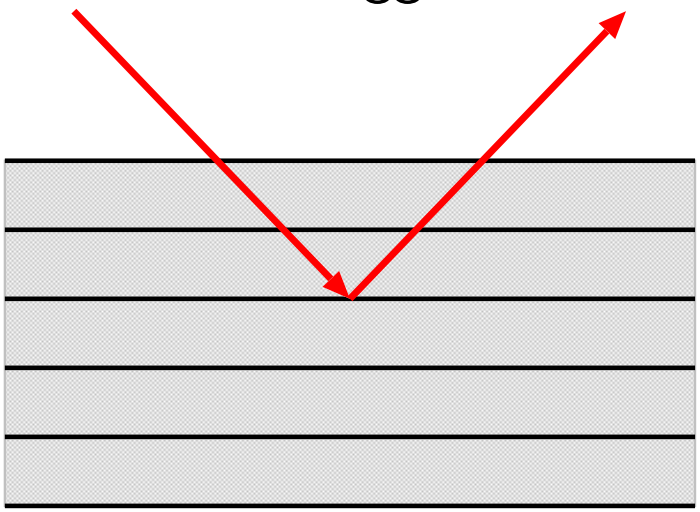

symmetric

Laue

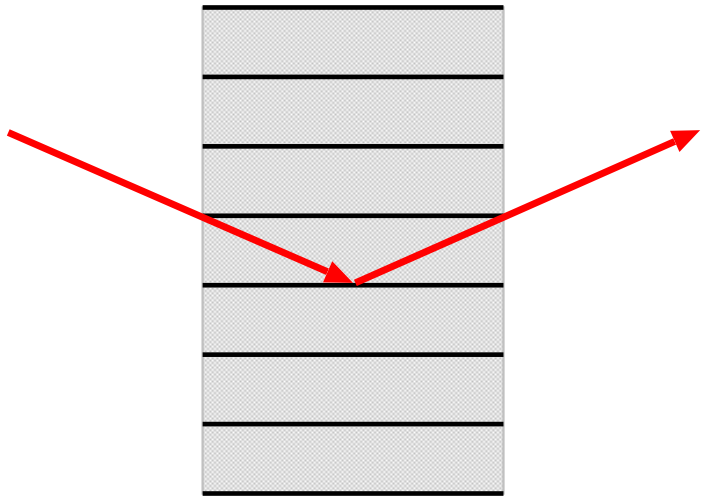

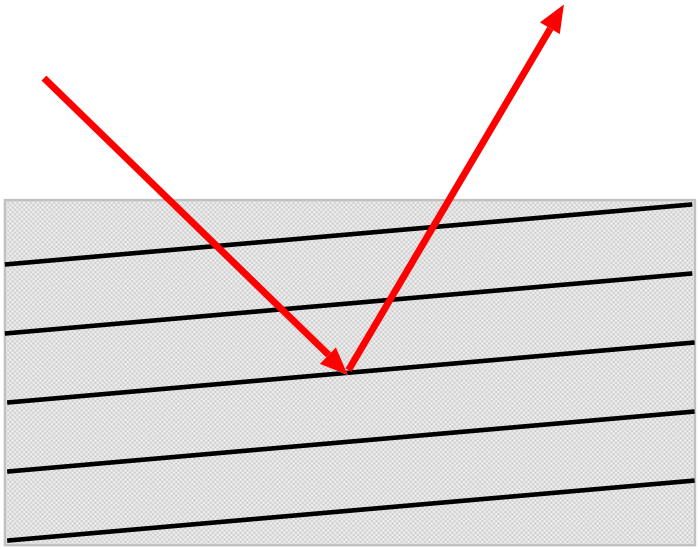

asymmetric

Bragg & Laue geometries

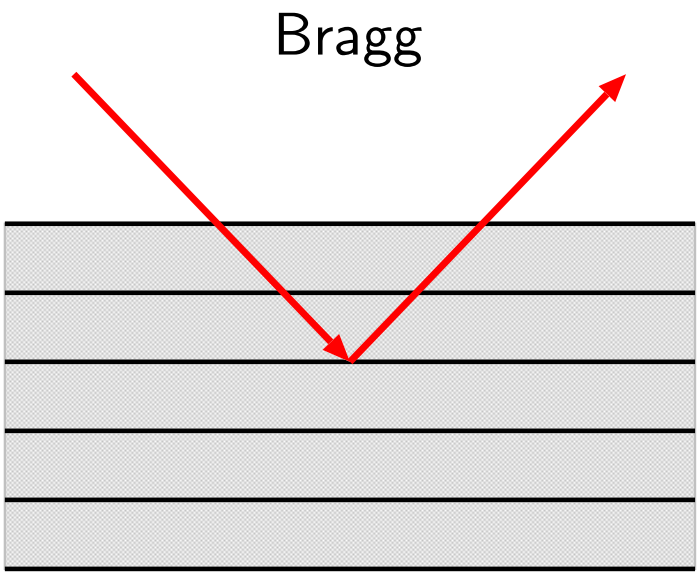

symmetric

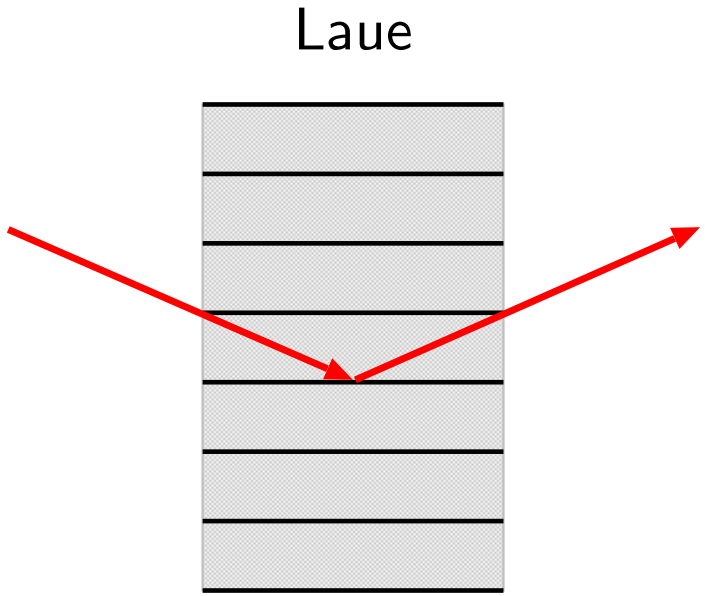

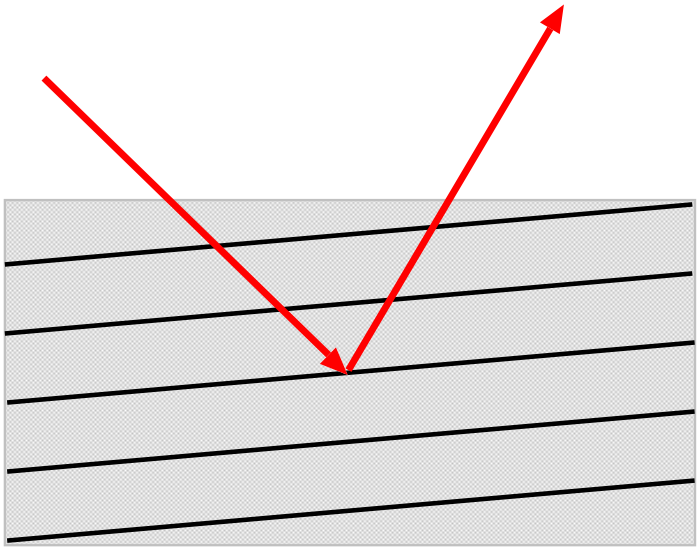

asymmetric

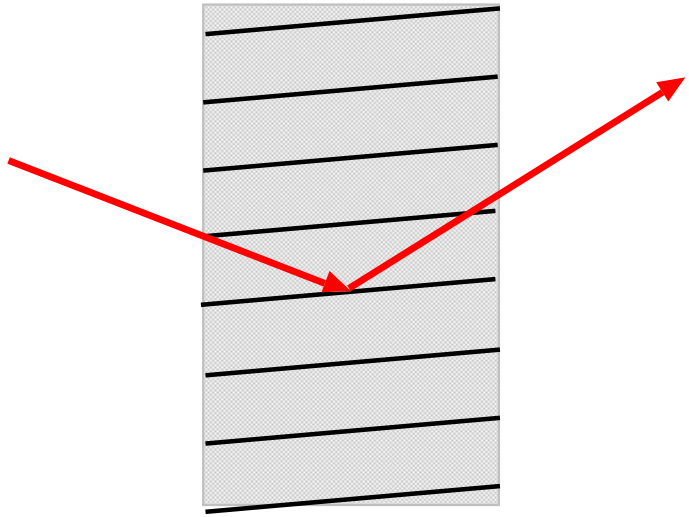

Scattering geometry

Consider symmetric Bragg geometry

Scattering geometry

Consider symmetric Bragg geometry

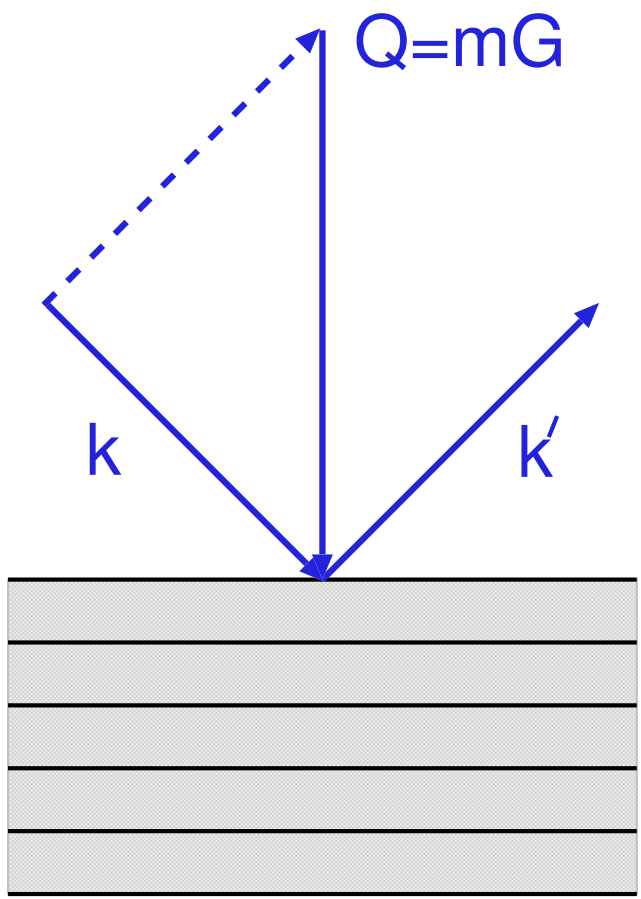

Scattering geometry

Consider symmetric Bragg geometry

We expect the crystal to diffract in an energy bandwidth defined by Δk

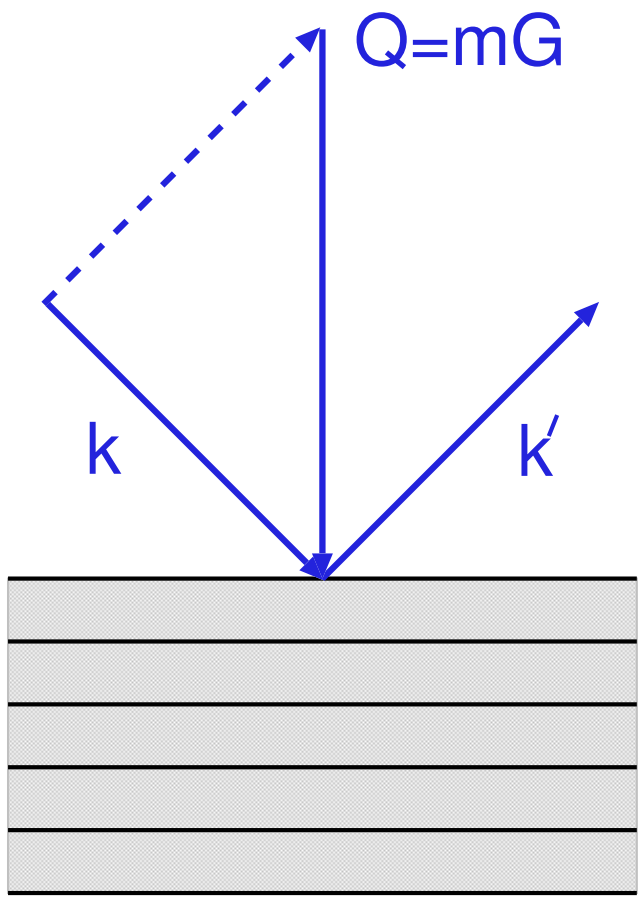

Scattering geometry

Consider symmetric Bragg geometry

We expect the crystal to diffract in an energy bandwidth defined by Δk

This defines a spread of scattering vectors such that

$$\zeta = \frac{\Delta Q}{Q} = \frac{\Delta k}{k}$$

called the relative energy or wavelength bandwidth

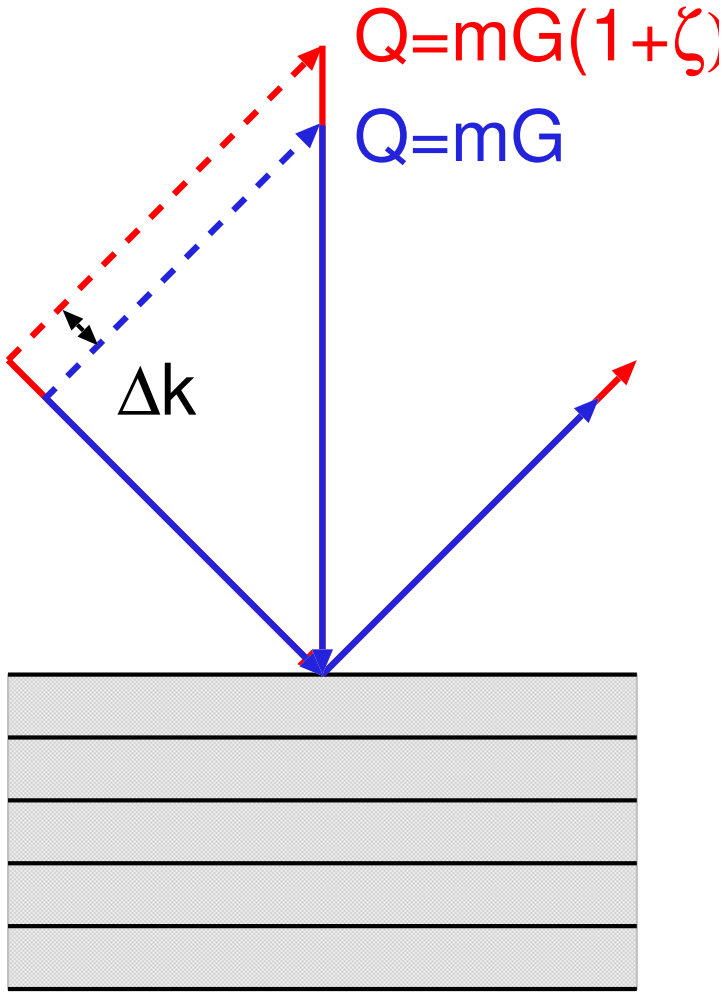

Dynamical diffraction - Darwin approach

The Darwin approach treats a perfect crystal as an infinite stack of atomic planes.

Dynamical diffraction - Darwin approach

The Darwin approach treats a perfect crystal as an infinite stack of atomic planes.

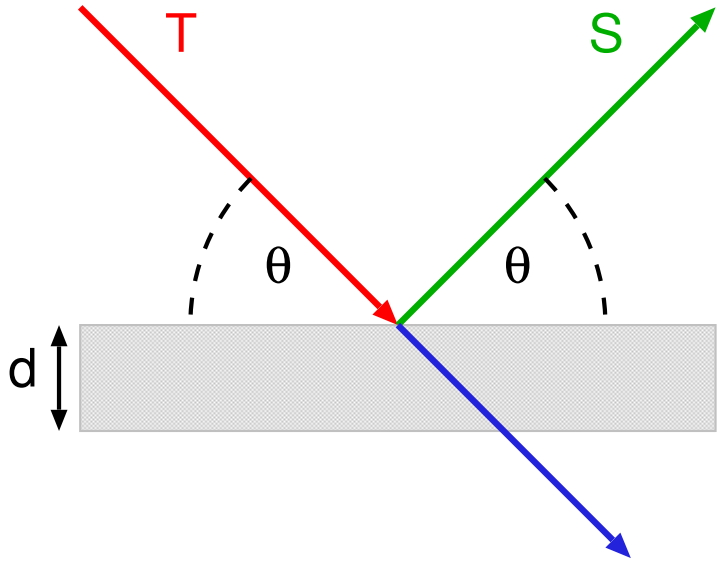

Dynamical diffraction - Darwin approach

The Darwin approach treats a perfect crystal as an infinite stack of atomic planes.

Considering a single thin slab with electron density ρ and thickness $d \ll \lambda$, the reflected and transmitted waves are

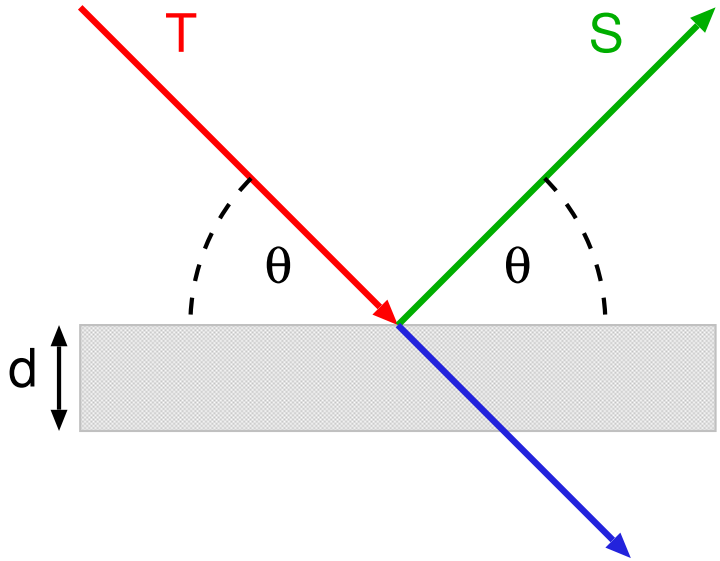

Dynamical diffraction - Darwin approach

The Darwin approach treats a perfect crystal as an infinite stack of atomic planes.

Considering a single thin slab with electron density ρ and thickness $d \ll \lambda$, the reflected and transmitted waves are

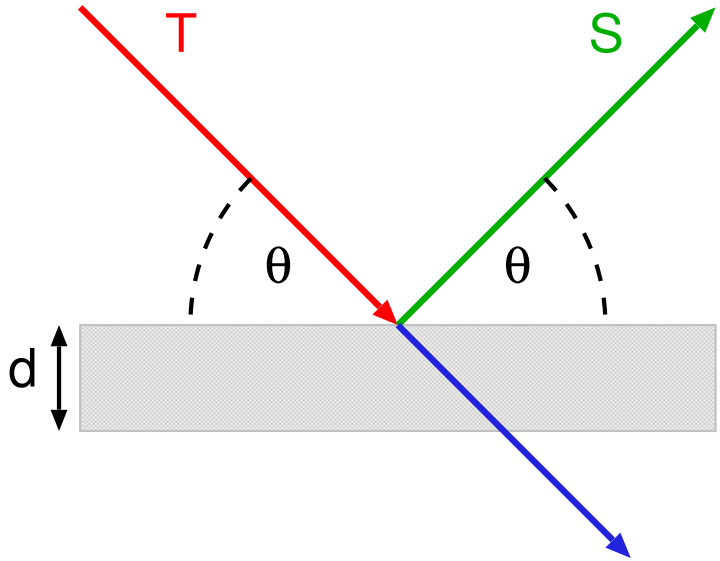

$$S = -igT$$

Dynamical diffraction - Darwin approach

The Darwin approach treats a perfect crystal as an infinite stack of atomic planes.

Considering a single thin slab with electron density ρ and thickness $d \ll \lambda$, the reflected and transmitted waves are

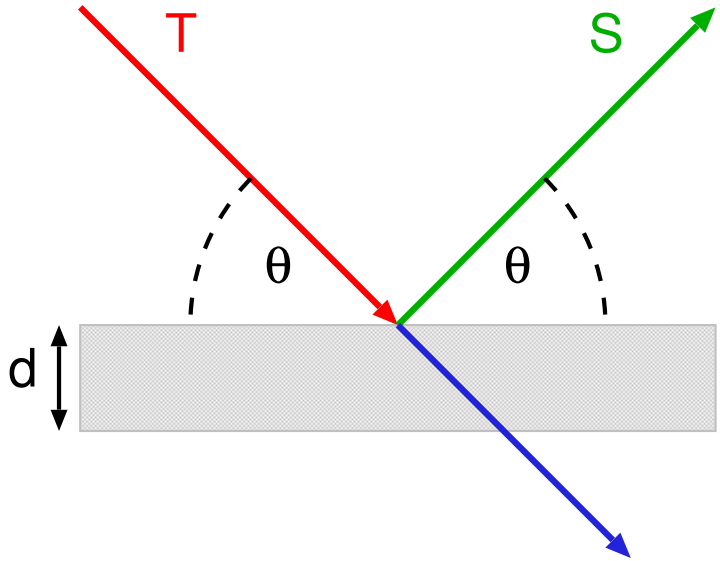

$$S = -igT$$

$$(1 - ig_0)T \approx e^{-ig_0}T$$

Dynamical diffraction - Darwin approach

The Darwin approach treats a perfect crystal as an infinite stack of atomic planes.

Considering a single thin slab with electron density ρ and thickness $d \ll \lambda$, the reflected and transmitted waves are

where

$$g = \frac{\lambda r_0 \rho d}{\sin\theta}$$

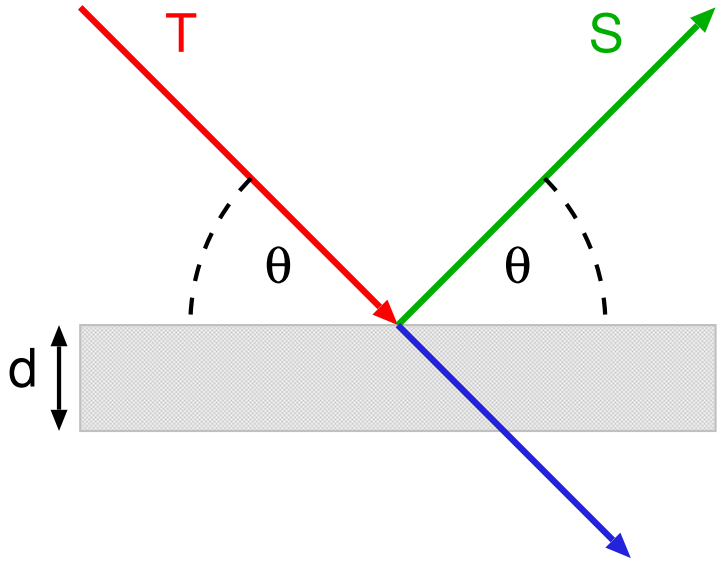

$$S = -igT$$

$$(1 - ig_0)T \approx e^{-ig_0}T$$

Dynamical diffraction - Darwin approach

The Darwin approach treats a perfect crystal as an infinite stack of atomic planes.

Considering a single thin slab with electron density ρ and thickness $d \ll \lambda$, the reflected and transmitted waves are

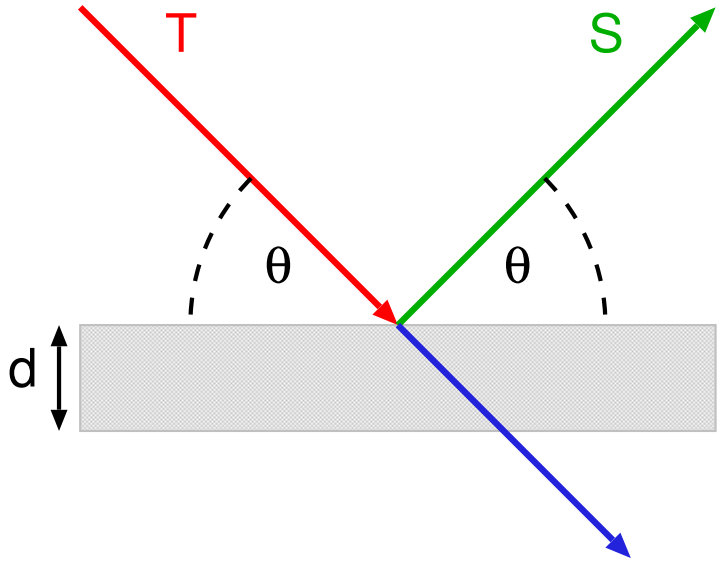

where

$$g = \frac{\lambda r_0 \rho d}{\sin\theta}$$

if the layer is made up of unit cells with volume v_c and structure factor $F \xrightarrow{Q=0} Z$, the electron density is $\rho = |F|/v_c$ and using the Bragg condition, we can rewrite g as

$$S = -igT$$

$$(1 - ig_0)T \approx e^{-ig_0}T$$

Dynamical diffraction - Darwin approach

The Darwin approach treats a perfect crystal as an infinite stack of atomic planes.

Considering a single thin slab with electron density ρ and thickness $d \ll \lambda$, the reflected and transmitted waves are

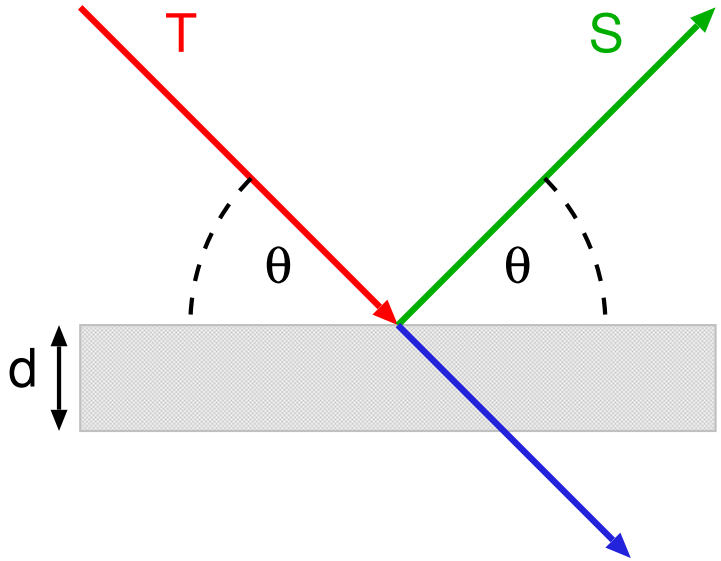

where

$$g = \frac{\lambda r_0 \rho d}{\sin\theta}$$

if the layer is made up of unit cells with volume v_c and structure factor $F \xrightarrow{Q=0} Z$, the electron density is $\rho = |F|/v_c$ and using the Bragg condition, we can rewrite g as

$$g = \frac{[2d\sin\theta/m] r_0 (|F|/v_c) d}{\sin\theta}$$

$$S = -igT$$

$$(1 - ig_0)T \approx e^{-ig_0}T$$

Dynamical diffraction - Darwin approach

The Darwin approach treats a perfect crystal as an infinite stack of atomic planes.

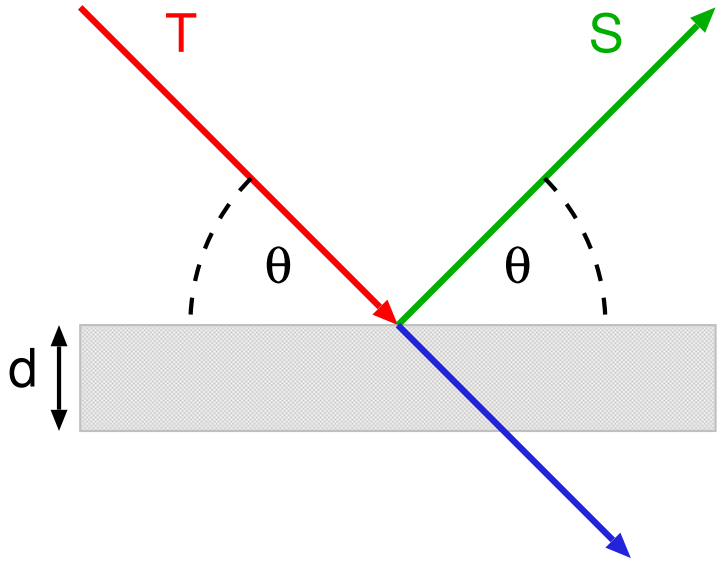

Considering a single thin slab with electron density ρ and thickness $d \ll \lambda$, the reflected and transmitted waves are

$$S = -igT$$

$$(1 - ig_0)T \approx e^{-ig_0}T$$

where

$$g = \frac{\lambda r_0 \rho d}{\sin\theta}$$

if the layer is made up of unit cells with volume v_c and structure factor $F \xrightarrow{Q=0} Z$, the electron density is $\rho = |F|/v_c$ and using the Bragg condition, we can rewrite g as

$$g = \frac{[2d\sin\theta/m]r_0(|F|/v_c)d}{\sin\theta} = \frac{1}{m}\frac{2d^2 r_0}{v_c}|F|$$

Dynamical diffraction - Darwin approach

$$g = \frac{1}{m}\frac{2d^2 r_0}{v_c}|F|$$

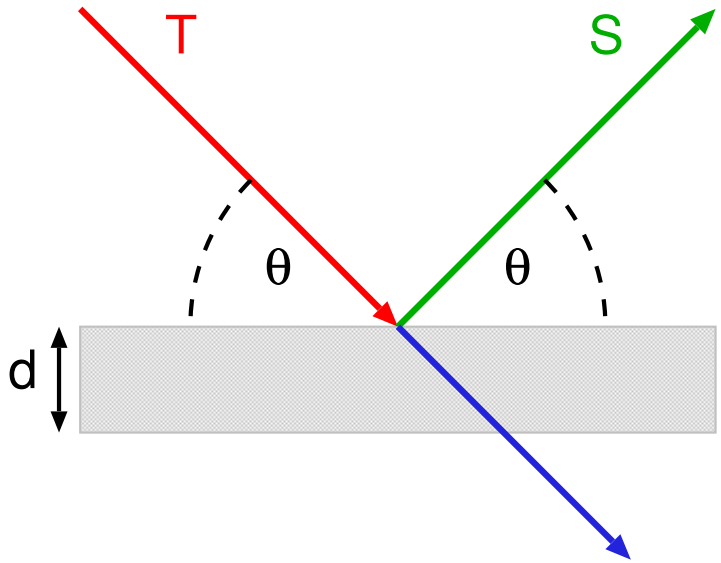

$$S = -igT$$

$$(1 - ig_0)T \approx e^{-ig_0}T$$

Dynamical diffraction - Darwin approach

$$g = \frac{1}{m}\frac{2d^2 r_0}{v_c}|F|$$

since $v_c \sim d^3$ then $g \sim r_0/d \approx 10^{-5}$

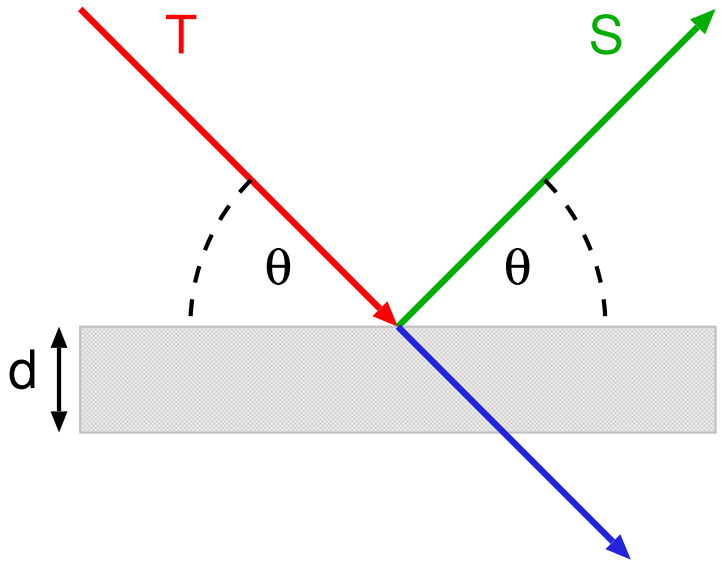

$$S = -igT$$

$$(1 - ig_0)T \approx e^{-ig_0}T$$

Dynamical diffraction - Darwin approach

$$g = \frac{1}{m}\frac{2d^2 r_0}{v_c}|F|$$

since $v_c \sim d^3$ then $g \sim r_0/d \approx 10^{-5}$

the transmitted beam depends on

$$g_0 = \frac{\lambda \rho_{at} f^0(0) r_0 \Delta}{\sin\theta}$$

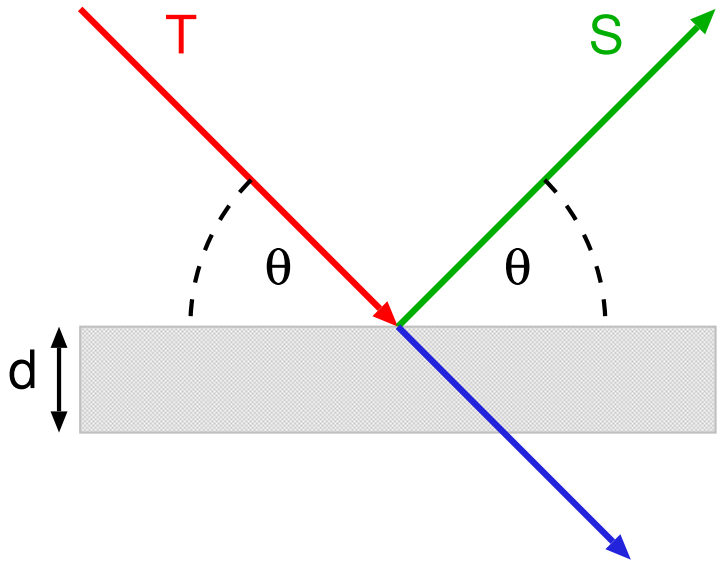

$$S = -igT$$

$$(1 - ig_0)T \approx e^{-ig_0}T$$

Dynamical diffraction - Darwin approach

$$g = \frac{1}{m}\frac{2d^2 r_0}{v_c}|F|$$

since $v_c \sim d^3$ then $g \sim r_0/d \approx 10^{-5}$

the transmitted beam depends on

$$g_0 = \frac{\lambda \rho_{at} f^0(0) r_0 \Delta}{\sin\theta}$$

which can be rewritten

$$g_0 = \frac{|F_0|}{|F|} g$$

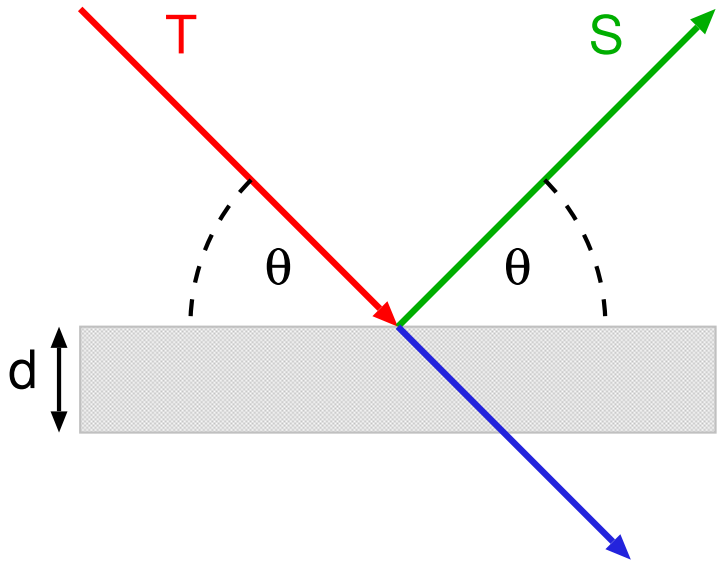

$$S = -igT$$

$$(1 - ig_0)T \approx e^{-ig_0}T$$

Dynamical diffraction - Darwin approach

$$g = \frac{1}{m}\frac{2d^2 r_0}{v_c}|F|$$

since $v_c \sim d^3$ then $g \sim r_0/d \approx 10^{-5}$

the transmitted beam depends on

$$g_0 = \frac{\lambda \rho_{at} f^0(0) r_0 \Delta}{\sin\theta}$$

which can be rewritten

$$g_0 = \frac{|F_0|}{|F|} g$$

where F_0 is the forward scattering factor at $Q = \theta = 0$

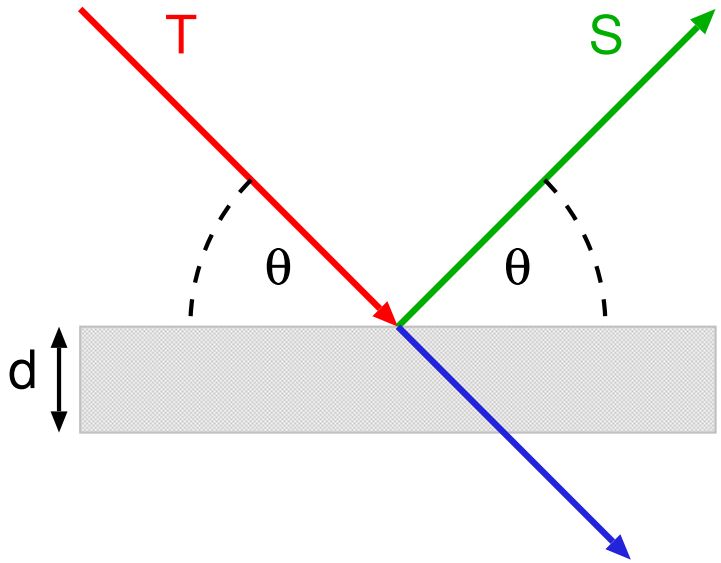

$$S = -igT$$

$$(1 - ig_0)T \approx e^{-ig_0}T$$